

HEATWAVES IN URBAN AREAS: ANALYSIS OF THE MAIN DRIVERS

Joke De Meester

Student number: 01405318

Promotor(s): Prof. Dr. Diego G. Miralles, Dr. Hendrik Wouters

Master's Dissertation submitted to Ghent University in partial fulfilment of the requirements for the degree of master in the direction Bio-engineering: Land & Water management.

Academic year: 2018 - 2019

De auteur en de promotoren geven de toelating deze masterproef voor consultatie beschikbaar te stellen en delen van de masterproef te kopiëren voor persoonlijk gebruik. Elk ander gebruik valt onder de beperkingen van het auteursrecht, in het bijzonder met betrekking tot de verplichting de bron uitdrukkelijk te vermelden bij het aanhalen van resultaten uit de masterproef.

The author and the promotors give permission to use this thesis for consultation and to copy parts of it for personal use. Every other use is subject to the copyright laws, more specifically the source must be extensively specified when using results from this thesis.

Ghent, June 6, 2019

The promotors,

The author,

Prof. Dr. Diego G. Miralles

Dr. Hendrik Wouters

Joke De Meester

THANK YOU

I am really happy that I took up the challenge to dive (and get lost from time to time) in the modelling world of CLASS, trying to adapt it to better cope with urban features. It was both the modelling part as well as the relevance to urban climate that attracted me to the subject. I want to thank my promoters for giving me the opportunity to learn so much.

I want to thank dr. Hendrik Wouters for his very effective and to the point help during the modelling and the interpretation of the results, giving much needed advice on where to focus on and on the structure of the thesis, and for always being available when needed. I also want to thank prof. dr. Diego Miralles for his good advice and openness for discussion during the delineation of the subject and his interest in my progress, and for his help with the interpretation of the results. I really appreciated it that both of you allowed me a lot of freedom to explore and to express my (probably naive) thoughts.

Also I would like to thank my fellow students and friends: Emma Tronquo, Laurence Bekaert, Barbara D'Hondt, Wissam Barhdadi, Wouter Van den Broeck, Aurélien Goubau, Sebastiaan Vermeersche, Axel Moerman, Astrid Francoys, Mathilde Depoortere, Hanne Criel, Janna Delfosse, Iris Bombeke, Eline Rasson, Wim de Schuyter, Klara bouwen, Isaac Lievevrouw, Floris Huyghe, Hannah van der Cruyssen, Jolien Wissaert, Maïté Coppens, Freke Hespeels for the support and enjoyable moments. Being available whenever needed and always ready to give some distraction and perspective. But also ready to give advice, help with problems and enjoy life! This last year was wonderful and I am very glad that I could spend it with such a great group of fellow students.

Finally, I want to thank my parents and my sister Iwut for their continuous support and for helping me by proofreading parts of my thesis.

Thank you!

Joke

CONTENTS

Thank you	i
Content	v
Abstract	vii
Nederlandse samenvatting	ix
1 Introduction	1
2 Scientific background	3
2.1 Heatwaves	3
2.2 The Atmospheric Boundary Layer	5
2.3 The urban climate	6
2.3.1 Urban Heat Island	7
2.3.2 Other characteristics of the urban environment	9
2.3.3 Local Climate Zones	11
2.4 Adaptation and mitigation	12
2.5 Case area: Moscow	13
2.5.1 Urban climate in Moscow	13
2.5.2 Heatwaves in Moscow	14
2.5.3 Local Climate Zone classification	14
3 Objectives	17
4 Methodology	19
4.1 CLASS and CLASS4GL	19
4.2 Urban software upgrade CLASS4GL_urban	23
4.2.1 Implementation of Microwave Temperature Profiles into CLASS4GL	26
4.3 Simulations	27
4.3.1 Set-up	28

4.3.2	Evaluation of model performance	34
4.3.3	Surface energy balance	37
4.3.4	General limitations	37
5	Results and Discussion	39
5.1	Initialisation with balloon profile data (batch 1)	39
5.1.1	Height profiles	39
5.1.2	Indicators of model performance	40
5.1.3	Diurnal changes in the mixed-layer features over time	42
5.1.4	Surface energy balance	42
5.2	Initialisation with MTP data and model validation (batch 2)	44
5.2.1	June 15 2015	44
5.2.2	June 1 2015	50
5.3	Perturbation experiment (batch 3)	55
6	Conclusion	59
7	Future research	61
	Bibliography	64
A	Appendix A	73
B	Appendix B	75
C	Appendix C	79
D	Appendix D	81
E	Appendix E	85
E.1	Data from the city Rjazan was used as input data in the original model CLASS (RJA_ORIG)	85
E.2	Data from the city Rjazan was used as input data in the urban parameterization of the model CLASS (RJA_URB)	87
E.3	Data from the rural area Suhinici was used as input data in the original model CLASS (SUH_ORIG)	88
E.4	Data from the rural area Suhinici was used as input data in the urban parameterization of the model CLASS (SUH_URB)	89
F	Appendix F	93

G Appendix G	95
H Appendix H	97
I Appendix I	103
J Appendix J	107

ABSTRACT

Urbanization is one of the most intensive human-induced land use changes and is predicted to rapidly increase in the coming decades. Urbanization leads to many biophysical changes, such as changes in albedo, soil moisture, evaporation or aerodynamic resistance. These changes affect how the land interacts with the atmospheric boundary layer, the lowest part of the atmosphere that is in direct contact with the land surface. As such, urbanization affects air temperature, atmospheric moisture, clouds and precipitation. In this thesis, the effect of urbanization on the atmospheric boundary layer is explored, with the focus on air temperature. To this end, an urban parametrisation that was recently developed for the model Chemistry Land-Surface Atmosphere Soil Slab model (CLASS) is implemented into the CLASS model for Global studies (CLASS4GL) software framework, which can simulate how feedbacks between land surface and atmospheric conditions lead to changes through a diurnal cycle of the mixed-layer features. CLASS enables to detect causal relationships between surface and atmospheric conditions because it is a mechanistic model that is initialised and constrained with observations. CLASS can be initialised by a wide range of global climate observations from satellite, remote sensing, balloon soundings and climate models. In this thesis, CLASS4GL was extended so that the high-resolution Microwave Temperature Profile (MTP) data can also be used to initialise the model. This extended version of CLASS4GL is then used to explore how the incorporation of urban features provides added value in understanding the behaviour of the atmospheric boundary layer in urban areas, using data of Moscow and surroundings as a case study. Heatwaves will occur more often and more intense in the future, especially in urban areas. Because of the negative health consequences of intense heatwaves, it is important that the processes intensifying heatwaves in urban areas are fully understood. The extensions of CLASS4GL implemented in this thesis and the results of the first exploratory simulations may in the future contribute to achieve better understanding and allow the development of improved management and planning strategies to mitigate the consequences of these events.

SAMENVATTING

Verstedelijking is één van de meest intensieve antropogene veranderingen in landgebruik, de verstedelijking zal in de komende decennia sterk stijgen. Verstedelijking heeft verschillende biofysische veranderingen als gevolg, zoals veranderingen in albedo, bodemvocht, evaporatie of aerodynamische weerstand. Deze veranderingen hebben een effect op hoe het land de atmosferische grenslaag, dit is de luchtslaag in contact met het oppervlak, beïnvloedt en omgekeerd. Als gevolg hiervan beïnvloedt verstedelijking de luchttemperatuur, het vochtgehalte in de atmosfeer, de neerslag, enz. In deze thesis wordt het effect van verstedelijking op de atmosferische grenslaag verkend, met de focus op luchttemperatuur. Om dit te kunnen doen werden de geparametriseerde stedelijke eigenschappen die recent ontwikkeld waren voor het model CLASS geïmplementeerd in het overkoepelend modelkader CLASS4GL. CLASS4GL kan aan de hand van verschillende terugkoppelingen tussen het landoppervlak en de atmosfeer de veranderingen over de dag simuleren van verschillende kenmerken van de atmosferische grenslaag. CLASS4GL bestaat uit een mechanistisch model, CLASS, dat volledig wordt geïnitieerd en begrensd door observaties, en laat daarom toe om oorzaak-gevolg relaties tussen het landoppervlak en de atmosfeer te bestuderen. CLASS kan geïnitieerd worden door een brede waaier van globale klimaatobservaties; verkregen door satellieten, remote sensing, ballonpeilingen en klimaatmodellen. In deze thesis werd CLASS4GL uitgebreid zodat het ook kan geïnitieerd worden met hoge-resolutie microgolf temperatuurprofiel data. Deze uitbreidingen worden dan gebruikt om te verkennen of de toevoeging van de stedelijke kenmerken een meerwaarde bieden bij het begrijpen van de atmosferische grenslaag in stedelijke gebieden. Hiertoe werden gegevens gebruikt van Moskou en omgeving om het model te initialiseren. Hittegolven zullen in de toekomst meer voorkomen en intenser zijn, dit vooral in stedelijke gebieden. Door de negatieve gevolgen van intense hittegolven op onder andere het gebied van gezondheid is het belangrijk dat de processen die verantwoordelijk zijn voor de intensifiëring van hittegolven in stedelijke gebieden volledig begrepen worden. De uitbreidingen van CLASS4GL die in deze thesis werden geïmplementeerd en de resultaten van de eerste verkennende simulaties zouden in de toekomst kunnen helpen om de interacties die gebeuren tussen de atmosfeer en het landoppervlak in stedelijke gebieden beter te begrijpen, en zo de ontwikkeling van aangepaste beheers- en planningstrategieën te faciliteren.

LIST OF ABBREVIATIONS

ABL Atmospheric Boundary Layer.

BLLAST Boundary Layer Late Afternoon and Sunset Turbulence.

CBL Convective Boundary Layer.

CLASS Chemistry Land-Surface Atmosphere Soil Slab Model.

CLASS4GL CLASS model for Global studies.

ERA European Centre for Medium-Range Weather Forecasts Re-Analysis.

GLEAM Global Land Evaporation Amsterdam Model.

HUMPPA-COPEC 2010 The summertime Boreal forest field measurement intensive.

IGRA Integrated Global Radiosonde Archive.

LCZ Local Climate Zone.

MAE Mean Absolute Error.

MBE Mean Bias Error.

MSU Moscow State University.

MSU_ORIG_01 Data from MSU on 01/06/2015 was used as input data in the original model CLASS.

MSU_ORIG_15 Data from MSU on 15/06/2015 was used as input data in the original model CLASS.

MSU_URB_01 Data from MSU on 01/06/2015 was used as input data in the urban parameterization of the model CLASS.

MSU_URB_15 Data from MSU on 15/06/2015 was used as input data in the urban parameterization of the model CLASS.

MTP Microwave Temperature Profiles.

MTP-5 Microwave Temperature Profiler 5.

NOAA National Oceanic and Atmospheric Administration.

OHM Objective Hysteresis Model.

RJA_ORIG Data from the city Rjazan was used as input data in the original model CLASS.

RJA_URB Data from the city Rjazan was used as input data in the urban parameterization of the model CLASS.

RMSE Root Mean Square Error.

SUH_ORIG Data from the rural area Suhinici was used as input data in the original model CLASS.

SUH_URB Data from the rural area Suhinici was used as input data in the urban parameterization of the model CLASS.

UCI Urban Cool Island.

UDI Urban Dry Island.

UHI Urban Heat Island.

UMI Urban Moist Island.

UN United Nations.

WRF Weather Research and Forecasting.

CHAPTER 1

INTRODUCTION

Heatwaves have several negative consequences on local ecosystems, economics and human health (Barriopedro et al., 2011; Wouters et al., 2013). The mega-heatwave of 2010 in Russia killed an estimated of 55,000 people (Barriopedro et al., 2011; Hoag, 2014). According to climate projections, heatwaves will become more frequent, more intense and longer lasting in the future (Meehl and Tebaldi, 2004; Barriopedro et al., 2011; Hoag, 2014; Murari et al., 2015; Russo et al., 2015). Heatwaves usually happen over large areas (Miralles et al., 2014). Their intensity, however, varies with the local characteristics of the land (Tan et al., 2010). In urban areas, heatwaves last longer and the temperatures during these heatwaves are higher, especially at night. This increases the risk of morbidity and mortality (Tan et al., 2010; Fischer et al., 2012). The main reason for the differences between urban and rural climate is the Urban Heat Island (UHI) effect (see Chapter 2.3). Cities are characterized by large percentages of impervious surfaces, buildings trapping heat, reduction in evaporation, and additional anthropogenic sources of heat, e.g. burning of fuels. According to the United Nations (UN), 68 % of the world population will live in urban areas by 2050 (UN, 2018). There is a need to obtain more insight in the dynamics of the urban atmosphere, so that more precise adaptation strategies can be developed to minimise the effects of heatwaves, especially given the context of ongoing climate change.

A better understanding of the interactions between land surface and the Atmospheric Boundary Layer (ABL) provides insight into the causes and dynamics of heatwaves. The ABL, which is the layer between the surface and the free atmosphere, plays a key role in the accumulation of heat and is key to the escalation of temperatures during heatwaves (Fischer, 2014). That is why it is important to simulate the ABL layer in an accurate way. By doing this, the main drivers behind extreme temperatures can be determined. Earlier observational studies and urban climate models already revealed several features that are caused by urbanization, such as the UHI, the Urban Dry Island (UDI), the Urban Moist Island (UMI), the cross-over effect where warm air is trapped under a cold layer, and the urban breeze circulation (Lokoshchenko, 2014; Theeuwes et al., 2015; Varentsov et al., 2018). But these earlier models have important limitations, their complexity turns them essentially into black box models when

it comes to interpreting their simulations. These models can represent the processes that are observed but are difficult to apply when aiming to differentiate among individual causal relationships. Often the models are poorly constrained by observations, the computational cost is high, and results depend on the model being applied. To overcome this problem, simpler mechanistic models are needed. Some studies in this direction have been done on the urban climate, but mechanistic studies on the UHI are rare (Theeuwes et al., 2015; Droste et al., 2018). Recently the framework Chemistry Land-Surface Atmosphere Soil Slab Model (CLASS) for Global studies (CLASS4GL) was developed. This framework fully automatizes ABL model experiments on the basis of multiple data sources including radio soundings, and satellite data, and reanalysis data to assess the effects of land and atmospheric conditions on the ABL evolution (Wouters et al., 2019). It is based on a mechanistic model of the ABL, called CLASS. CLASS4GL allows the physical interpretation of the diurnal evolution of the ABL and enables to determine the main drivers of heatwaves. Unfortunately, this framework has not yet been adapted to urban environments.

In this thesis CLASS4GL_urban is developed, an extension of CLASS4GL so that it can also take into account urban characteristics such as anthropogenic heat and the thermal characteristics of buildings. This makes it possible to explore the ABL drivers of excessive heatwave temperatures in cities, and particularly the role of land characteristics typically linked to urbanization. Such analyses can point to specific adaptation and mitigation strategies to counteract the problems linked to extensive heatwaves in urban areas. Moscow will be used as a compelling case area (see chapter 2.5) to explore the new framework CLASS4GL_urban. In order to be able to use the detailed information about the urban boundary layer of Moscow, CLASS4GL_urban is in this thesis further extended to employ Microwave Temperature Profiles (MTP) data. This allows to test whether it is possible to use an ABL model in combination with boundary layer profiles derived from Microwave Temperature Profiler 5 (MTP-5) remote sensing technology, to identify the drivers of exacerbated heatwaves in cities.

The next sections provide some scientific background on heatwaves (Chapter 2.1), the ABL (Chapter 2.2) and urban climate (Chapter 2.3). Then the region of Moscow and its surroundings is introduced as a case area (Chapter 2.5). In Chapter 4, the model, the extension to incorporate urban dynamics performed in this thesis, and the various simulations and validation steps are introduced. The results of the simulations are presented and discussed in Chapter 5.

CHAPTER 2

SCIENTIFIC BACKGROUND

2.1 Heatwaves

There exist several definitions of heatwaves, depending on whether the focus is on the intensity and/or duration of either daytime maxima or night-time minima (Meehl and Tebaldi, 2004). This divergence is amongst others caused by the fact that the relation of health problems and mortality rates with temperatures is region dependent (Baccini et al., 2008). In studies on heatwaves, often percentile based thresholds are applied to identify extreme temperatures (Meehl and Tebaldi, 2004; Fischer et al., 2012; Tong et al., 2015; Bador et al., 2017; Wouters et al., 2017). In Belgium, for instance, a heatwave is defined by a period of at least three consecutive days with a maximum temperature above 29.6 °C and a minimum temperature higher than 18.2 °C (Wouters et al., 2017). Heatwaves have several important consequences such as reduced human wellbeing, increased mortality, water scarcity, air pollution, degradation of natural ecosystems, crop losses, loss of labour productivity, transport disruptions, and many other (Meehl and Tebaldi, 2004; Barriopedro et al., 2011; Miralles et al., 2014; Russo et al., 2015; Wouters et al., 2017). Especially the occurrence of consecutive nights with high night time temperatures cause severe health problems (Meehl and Tebaldi, 2004).

Several mega-heatwaves have been recorded over the past years; they are called mega-heatwaves because they broke all previous temperature records (Fischer, 2014). Heatwave of 1972 in Finland caused 840 deaths (Näyhä, 2007). The heatwave of 2003 in Europe had a death toll of 20,000-70,000 people (Robine et al., 2008; Barriopedro et al., 2011). In the summer of 2010, an even stronger heatwave hit Russia and Eastern Europe (Barriopedro et al., 2011; Fischer, 2014; Hoag, 2014; Miralles et al., 2014; Russo et al., 2015). And more recently, in 2017 a heatwave occurred in central and western Europe, its intensity, persistence and extension was comparable to previous mega-heatwaves in Europe (Sánchez-Benítez et al., 2018).

Heatwaves occur when a high pressure system persists for several days over an area and traps warm air near the ground. This in combination with atmospheric blocking

patterns brings little rain, clear skies and advection of warm air (Meehl and Tebaldi, 2004; Fischer, 2014; Miralles et al., 2014). These long lasting large-scale conditions induce a soil moisture-temperature feedback, because the local energy balance becomes the major driver of temperature change (Miralles et al., 2012, 2014). The high atmospheric water demand depletes soil moisture, which results in less evaporative cooling and leads to a larger surface heat flux (Miralles et al., 2012, 2014). Because of this, the ABL increases in depth. When the ABL grows, air with a higher potential temperature is entrained into the ABL. As a result of the advection of warm air, the entrainment of heat, and an increase in sensible heat, the ABL becomes deeper and warmer (Figure 2.1) (Fischer, 2014; Miralles et al., 2014). At night there is formation of a warm and deep nocturnal residual layer several meters above the surface. This allows in the following days a re-entering of heat into the mixed layer. When the night ground inversion is broken by the diurnal convection, this leads to a further increase in temperature in the consecutive days. This multi-day memory of the ABL and the land surface plays a key role in the accumulation of heat during heatwaves (Miralles et al., 2014). Nonetheless, the duration and location of heatwaves is determined by large-scale weather patterns (Fischer, 2014).

Anthropogenic warming has doubled the risk of mega-heatwaves (Fischer, 2014). According to current climate projections, heatwaves will become more frequent, more intense and longer lasting in the future (Meehl and Tebaldi, 2004; Hoag, 2014; Murari et al., 2015; Russo et al., 2015). The intensity and magnitude of heatwaves depends on the emission scenario (Fischer, 2014; Hoag, 2014; Russo et al., 2015). In the next 40 years, the probability of deadly mega-heatwaves will increase by a factor 5-10 (Barriopedro et al., 2011). Heatwaves will not only occur more frequently and will be

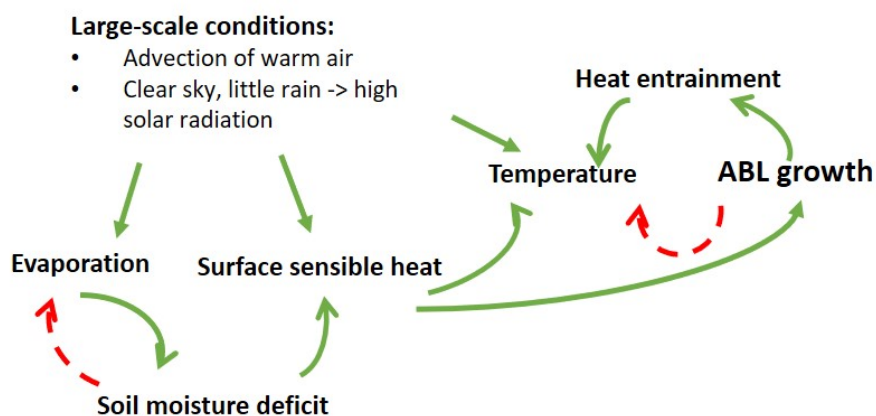


Figure 2.1: Land-atmospheric interactions and feedbacks that are relevant with respect to the built up of heatwaves. The green full lines indicate positive feedbacks, the dashed red lines indicate negative feedbacks. Based on Figure 4 in Miralles et al. (2014).

come more intense in the coming years (Meehl and Tebaldi, 2004; Barriopedro et al., 2011), but are also disproportionately more intense in urban areas (see 2.3). In addition, it is especially in urban areas where heatwaves can have the most profound consequences.

2.2 The Atmospheric Boundary Layer

The ABL is the lower part of the atmosphere and is in direct contact with the land surface. Four regions can be distinguished in the ABL, namely the surface layer, the mixed layer, the inversion layer and residual layer (Figure 2.2) (Vilà-Guerau de Arellano et al., 2015). The ABL shows strong diurnal variation. In the early morning the layer is about a few meters deep, while in the afternoon it can grow up several km, especially during clear sky conditions (Figure 2.2). The conditions of the nocturnal ABL have a strong influence on the weather conditions and processes that happen during the day (Vilà-Guerau de Arellano et al., 2015). In the ABL buoyancy of warm air results in an upward force and drives turbulent flow. From the surface, air is rising in the form of eddies or thermal plumes, which may reach to the top of the boundary layer and can have a diameter of up to one km. Moisture is transported upwards by these thermal plumes and is surrounded by dry air that is going down. This dry air is entrained from the free troposphere. Because these plumes mix air from the top of the ABL, where air enters the ABL, to the surface, a well-mixed layer tends to be created. In this mixed layer, moisture, potential temperature and atmospheric constituents do not change with height (Vilà-Guerau de Arellano et al., 2015). This mixed-layer that forms during the day is often referred to as the Convective Boundary Layer (CBL) (Figure 2.2). The surface layer is usually characterised by a decrease in moisture and

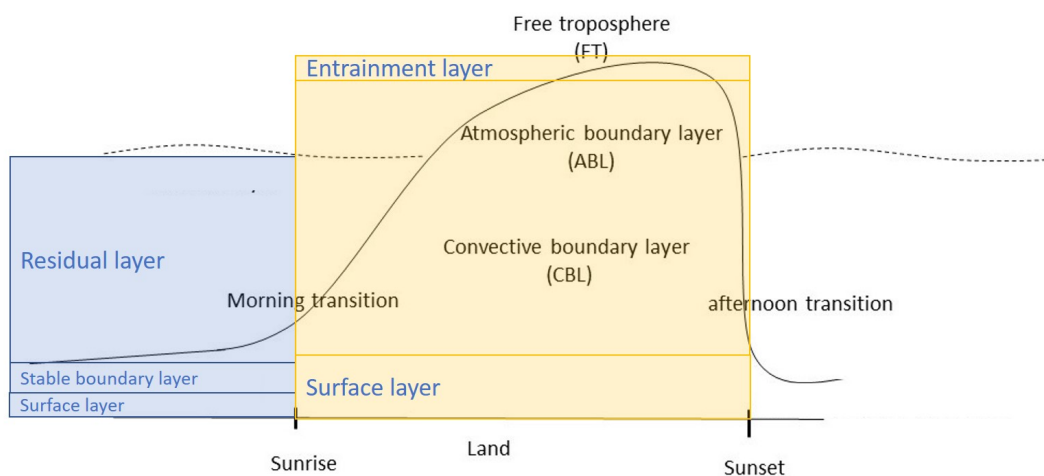


Figure 2.2: The diurnal evolution of the ABL. Based on Figure 2.1 in Vilà-Guerau de Arellano et al. (2015).

potential temperature with height, and the occurrence of wind shear. As a result, the surface layer is unstably stratified. The latent and surface-sensible heat fluxes mainly drive the surface layer. These generate turbulent eddies that transport moisture and heat into the well-mixed layer from the land surface. Hence, the well-mixed layer is moistened and heated from below. Inside the well-mixed layer the eddies transform into thermal plumes. The inversion layer is also called entrainment zone. This region is stably stratified, with the potential temperature increasing with height in the free atmosphere. The thermal plumes that reach this zone are often unable to penetrate this stable layer (Vilà-Guerau de Arellano et al., 2015).

The ABL is the atmospheric layer in which all the processes occur that are directly influenced by the biosphere. For this reason it is important that this layer and its interaction with its boundaries is fully understood and accurately represented in weather and climate models.

2.3 The urban climate

There is a rapidly increasing proportion of the global population that lives in cities, and the area of urbanized land rapidly increases (Seto et al., 2012). Rural and urban areas have a different response to climate change. It is therefore important to consider (1) the distinct elements of the urban environment, (2) their effect on the urban climate, and (3) the influence they have on the surrounding areas (Oleson, 2012; Lokoshchenko, 2014; Varentsov et al., 2018). The phenomena that originate from urban features are mostly seen as negative because they tend to accelerate climate warming in urban areas, increase heat stress, and intensify heatwaves, with negative effects on human health and wellbeing (Ward et al., 2016; Varentsov et al., 2017, 2018).

The characteristics of the landscape and land surface processes strongly influence the weather and climate phenomena (Pielke, 2005). For the development of extreme weather events like convective thunderstorms and heatwaves, the coupling between atmosphere, vegetation and soil are particularly important (Sillmann et al., 2017; Miralles et al., 2019). Therefore the processes shaping the dynamics of the ABL, such as the land-atmospheric feedbacks, need to be better understood (Wouters et al., 2019) in order to be able to make better climate projections, identify early warning signals and develop more effective climate adaptation actions (Wouters et al., 2013; Sillmann et al., 2017; Varentsov et al., 2018).

In the following sections first some characteristics of the urban climate will be discussed and both the UHI and the Urban Cool Island (UCI) will be briefly explained.

Next the classification system of Local Climate Zones (LCZ) will be introduced. Finally some adaptation strategies that are already present to reduce urban warming are briefly addressed.

2.3.1 Urban Heat Island

Description

The UHI is a phenomenon that is already known for a long time. It was first discovered by Luke Howard in 1820 (Oleson, 2012) and first defined in the 1940s. It refers to the higher temperatures in city centres compared to the countryside (Balchin and Pye, 1947). In almost every city the phenomenon of UHI exists (Lokoshchenko, 2014; Theeuwes et al., 2015). In hot climates, the UHI can increase heat stress and mortality of humans (Stewart and Oke, 2012). In some areas, cities do not create a UHI but create a cooling effect (see section 2.3.2). This is for instance the case in the arid tropics, where towns are often characterised by a lot of vegetation and multiple sources of open water as a result there is a high intensity of evapotranspiration (Lokoshchenko, 2014). Often the intensity of the UHI is described as the difference in temperature between the rural zone and the city centre, averaged over time (Lokoshchenko, 2014; Varentsov et al., 2017). An important parameter of the UHI is the maximal observed difference in temperature. These maxima occur when there is strong anticyclonic weather, clear sky and low wind velocity (Lokoshchenko, 2014). These conditions occur during heatwaves, so the UHI intensities are enhanced when a heatwave is happening (Wouters et al., 2017). When looking at the diurnal changes in the UHI, the most intense UHI effect can be found at late evening, night and early morning (Lokoshchenko, 2014). This maximum of UHI occurs downwind of the centre along the prevailing wind direction (Wouters et al., 2013). In the afternoon, the heat island intensity in winter is higher than in the summer, but at night the heat island intensity in the summer is higher than in the winter (Lokoshchenko, 2014). The UHI effect is nearly zero in the middle of the day; sometimes even a UCI can occur (see Section 2.3.2). The shape of the UHI is ellipsoidal and is characterised by a stretch along the prevailing wind direction (Wouters et al., 2013). During the night the UHI persists at approximately the same intensity until sunrise (Wouters et al., 2013).

The UHI can become stronger by an increase in the size of the population inhabiting a city, by a growth of the city area, and by climate change (Lokoshchenko, 2014; Varentsov et al., 2017). Despite the fact that city expansions and land use change mainly take place at the edges of cities, these developments lead to an intensification of the UHI in the city centre as well (Varentsov et al., 2017). The UHI intensity

asymptotically reaches an upper limit. This happens when in the city centre the density of the buildings is maximal and the city only grows by extension to the periphery. An estimation of this urban saturation can be made by looking at the density of the population (Lokoshchenko, 2014). The UHI is a three-dimensional phenomenon and affects thermal stratification and the extent of the ABL. In comparison with rural areas, unstable stratification happens more often and surface inversions less often in urban areas (Lokoshchenko, 2014). Also the UHI reduces condensation, so there is less fog and haze in cities during the summer nights in comparison with rural areas (Varentsov et al., 2018).

Causes of UHI

The land cover and structural differences between rural and urban areas are the main causes of the UHI. These differences create changes in the radiation balance and surface energy balance (Stewart and Oke, 2012). The absorption of solar radiation in urban areas is often higher, due to the trapping of radiation and multiple reflection of radiation caused by vertical surfaces and building walls. When the buildings are more compact and taller, the sky view decreases. This results in an increase in retention of infrared radiation, especially in street canyons. In the urban canopy layer, the convective losses are reduced because the airflow is reduced. In combination with the trap of infrared and solar radiation and the thermal properties of the materials used for the buildings and paved surfaces, the uptake of heat is increased. Often the albedo is lower in urban areas compared to rural areas. Moreover, the waterproofed surfaces and impermeable grounds cause a reduction in surface evaporation. As a result, more absorbed solar radiation is converted to sensible heat (leading to an increase in temperature) instead of latent heat (energy transfer that does not lead to an increase in temperature) (Fischer et al., 2012; Stewart and Oke, 2012; Lokoshchenko, 2014; Wouters et al., 2017). Also, there are less green areas in urban areas compared to rural areas, so transpiration is reduced (Lokoshchenko, 2014; Wouters et al., 2017). In addition, there are direct anthropogenic heat and moisture releases, such as those linked to the combustion of fuels, industrial processes, etc., but this is only a relatively small contribution of the total heat that is entrapped by urban centres (Oleson, 2012; Stewart and Oke, 2012; Lokoshchenko, 2014; Wouters et al., 2017).

The main cause for the creation of the maximum UHI at night is the increase in storage heat during the day, which can be released at the night as sensible heat. The storage of heat during the day is caused by the heat capacity characteristics of building materials, reduced evapotranspiration and small thermal roughness lengths in urban areas. These smaller thermal roughness lengths lead to a reduction of turbulent heat

transfer from the surface during the day. For the surface sensible heat flux, the anthropogenic heat release also plays a role (Theeuwes et al., 2015; Wouters et al., 2013). When there is an urban expansion, there is an excess accumulation of heat in the peri-urban areas around the centre. During the night the air in the direction of the city centre cools less and accumulates more heat because of the increase in stored heat in the periphery. All of this leads to a more intense UHI in the city centres (Wouters et al., 2017).

Link to the ABL

The formation of the UHI is influenced by radiative cooling, boundary layer stability, boundary layer radiation, interactions with orographic forcing, the nocturnal low level jet, and shear mixing (Wouters et al., 2013). The sensible heat release in the afternoon has a relatively small impact on the surface temperature because the unstable stratification and the large volume of the ABL. At night, the sensible heat flux, which is caused by the stored heat during the day and to a lesser extent by the anthropogenic heat flux, is smaller than during daytime. Despite this, the sensible heat flux has a much bigger influence than during daytime because the ABL is less thick (Wouters et al., 2013). Above the shallow mixed layer at night in urban areas, the cross-over effect can be observed, also called "cold lens", where a cold layer is located on top of a warmer layer (Varentsov et al., 2018). Due to the heat stored during the day and the release of this heat at night, there is a mixed layer above urban areas during the night. This leads to less radiative cooling. In addition, the adiabatic vertical cooling has less influence in comparison with rural areas, where a stable stratification takes place. This reduction in radiative cooling also intensifies the UHI over city areas (Theeuwes et al., 2015; Wouters et al., 2013).

2.3.2 Other characteristics of the urban environment

As mentioned before, land modification by urbanization leads to changes in the radiation and heat balance at the surface (Lokoshchenko, 2014). This changes the urban climate and weather (Theeuwes et al., 2015). The urban land interacts with the ABL, creating various feedbacks leading to typical urban climatic features (Varentsov et al., 2018). In a megacity urban climatic features become mesoscale (1-100 km) phenomena (Varentsov et al., 2018). Urban features influence the UHI, UDI/UMI, the cross-over effect and the urban breeze circulation (Lokoshchenko, 2014; Varentsov et al., 2018). Also the chemical composition of air in urban areas is different, with a higher concentration of carbon oxide and nitrogen oxides than in rural areas due to, amongst others, the combustion by vehicles and industries. These add to the natural

aerosols (Lokoshchenko et al., 2006; Oke et al., 2017). The effects of these higher concentrations in aerosols are complicated, and climate and location specific (Oke et al., 2017). Above urban areas there is an increase in cloud nuclei. This leads to an increase in the amount of clouds (Changnon, 1989). Another typical feature of the urban climate is industrial haze (Lokoshchenko, 2014). In megacities these effects persist in the lower troposphere not only during favourable conditions but also across the season (Varentsov et al., 2018). Urbanization does not only influence the climate in the city area itself but also in the surrounding areas. There is, for example, an enhanced stable stratification in rural areas at night caused by the urban heat plumes downwind of the city centre (Varentsov et al., 2018).

Besides the well-known UHI effect, urbanization has other consequences on the local climate such as a decrease in wind speed by the higher roughness (Varentsov et al., 2018). Also the moisture budget is influenced by urban characteristics (Varentsov et al., 2018). The UDI reflects that the relative humidity in cities tends to be lower than in rural areas (Fischer et al., 2012; Lokoshchenko, 2014). An explanation for this can be that reaching the dew point in warm air happens less often and later (Varentsov et al., 2018). In general the thermal stratification is less stable over urban areas. This is due to the fact that the air in urban areas is warmer and thus has a higher buoyancy (Varentsov et al., 2018). The urban breeze is another urban induced mesoscale phenomenon. These are circulations caused by the effects of urbanization on upward motions and stratification. The urban breeze can increase the near surface wind speed in urban areas (Varentsov et al., 2018). Urban heat plumes can also be observed downwind of the city centre. The warm urban air is transported by the wind, interacts with the more stable, colder boundary layer from the suburbs, and gets pushed upwards (Varentsov et al., 2018). The diverse dimension and placement of buildings creates a deep roughness surface layer. In this layer the mechanical turbulence dominates. In addition, air is forced to move up or around the sides of the buildings (Oke et al., 2017).

Sometimes in the morning and early afternoon, the air temperature in cities is lower than in rural areas. This is called the UCI effect and occurs when there are low wind speed conditions and the sky is clear. Under these conditions, the depth of the mixed-layer profile in the morning is deeper over urban areas than over rural ones (Theeuwes et al., 2015). The nocturnal ABL in urban areas remains deeper (~400m) in comparison with the rural ABL because in urban areas the air cools down slower. This difference in thickness of ABL causes a difference in warming in the early morning. As the ABL in rural areas is thinner, it warms up faster (Theeuwes et al., 2015). Around sunrise, the ABL is only heated by the surface heat flux. While this flux is higher in urban than in rural areas, the ABL layer heating rate in cities is less than in rural areas, as a

larger volume has to be heated. This UCI occurs until 2 hours after sunrise, and peaks with a maximum value 2K about 4 hours after sunrise (Theeuwes et al., 2015). After the UCI, a second heating and growing phase of the ABL happens. This is caused by entrainment of warm air from the free troposphere into the ABL. In urban areas the temperature then increases faster than in rural areas because the surface sensible heat flux is higher in the city than in rural areas. As a result the urban temperature exceeds the rural one after some time and the UCI changes to an UHI (Theeuwes et al., 2015). When the initial height of the ABL in urban areas is less than twice the height of the ABL in rural ones, an UCI is not necessarily formed. This is because the surface sensible heat flux in urban areas is larger and as such compensates for the larger volume (Theeuwes et al., 2015).

2.3.3 Local Climate Zones

For studies on urban climate, a research framework is offered by the classification system Local Climate Zone (LCZ). The Local Climate Zone (LCZ) is a climate-based classification for temperature studies of rural and urban areas that can be applied worldwide (Stewart and Oke, 2012). It can be used by urban planners to tackle the negative effects of extreme weather events (Verdonck et al., 2018). This classification system couples the typical characteristics of land use to the local climate (Theeuwes et al., 2015). In general, rural areas are defined as less populated, with more natural space and less buildings than urban areas (Stewart and Oke, 2012).

The LCZ classification is based on surface cover and structure. Both of these influence the screen-height (1-2m) temperature, they are non-specific in time and space, and measurable (Stewart and Oke, 2012). The surface structure consists of the spacing and height of trees and buildings that affect airflow, shortwave and longwave radiation balance, and atmospheric heat transport. The surface cover (impervious/pervious) affects the heating and cooling potential, the albedo and the moisture availability (Stewart and Oke, 2012).

Stewart and Oke (2012) defined 17 standard LCZs, of which 15 are defined by surface cover and structure and two are defined by anthropogenic heat emissions and construction materials. This standard set of 17 LCZs is divided in 10 built types and 7 land cover types. The land cover types consist of seasonal and ephemeral properties, and can be pervious or impervious. The built types consist of constructed features. The different LCZ can be found in Figure A.1 in Appendix A. Every LCZ has its own characteristic values for parameters such as emissivity and imperviousness (Theeuwes et al., 2015). To reduce errors due to edge effects each LCZ should span at least a few hundred off metres to km in horizontal scale, and are assumed to be uniform in

surface structure, cover, human activity and material. Each LCZ has its characteristic screen-height temperature regime, which is most probable during clear, calm nights over dry surfaces in areas with a simple relief (Stewart and Oke, 2012). This is because under these circumstances, the land cover and building geometry largely drive the thermal contrasts (Stewart and Oke, 2012). Every classification system is a simplification of reality. In the real world, the assumed internal homogeneity is unlikely to be observed. Also the thermal climate is not spatially discontinuous at the boundaries (Stewart and Oke, 2012). When using LCZ the UHI magnitude can be studied by comparing differences in temperature between different LCZ instead of engaging in urban-rural comparisons. This approach allows mechanistic explanations can be provided because one can objectively compare the characteristics of the landscape (Stewart and Oke, 2012).

2.4 Adaptation and mitigation

Some management and urban planning approaches have already been proposed to reduce the UHI effect. These include installing white and green roofs on buildings, afforestation, and the installation of fountains (Lokoshchenko, 2014; Oleson, 2012; Zhao et al., 2018).

Green areas can reduce the UHI because of increased evapotranspiration. The available energy for sensible heat release is reduced because there is a higher release of latent heat, which has a cooling effect (Ward et al., 2016). But the cooling effect depends on the amount of water that is available to the vegetation (Kleerekoper et al., 2012; Zhao et al., 2018). The thermal load during the day can also be reduced by increasing the number and surface area of water bodies, because of their high thermal inertia and evaporation rates (Kleerekoper et al., 2012; Liu and Weng, 2008). Flowing water bodies or water that is dispersed have a larger cooling effect than stagnant water bodies because they can transport heat away from the area (Kleerekoper et al., 2012).

Some side notes can be made about these strategies. During a heatwave, there are indications that the increase in magnitude of the UHI is linked to the presence of inner city water bodies. An explanation of this can be found in the thermal inertia of water. The rate of cooling of water bodies is less during the night, so they retain more heat (Ward et al., 2016). In the case of long lasting heatwaves water bodies might increase the magnitude of the UHI (Ward et al., 2016). Droughts can reduce the benefits of green areas, as the water supply is reduced and plants transpire less under the same solar radiation; also the albedo can change during droughts (Ward

et al., 2016). Some studies also show that inter spacing green area into urban areas has a larger effect than one large green zone (Dugord et al., 2014).

2.5 Case area: Moscow

Moscow is a megacity with about 16,855,000 people living within an area of 5,698 km². This gives a population density of approximately 3,000 people/km² (Cox, 2018). Because of its building structure, location in a continental climate, and size, Moscow generates an intensive UHI (Varentsov et al., 2017). The UHI has a mean intensity of 2°C, and a maximum of up to 12–13°C. These maxima can occur at night when there is strong anticyclonic weather, the wind velocity is low and the sky is clear (Lokoshchenko, 2014). These values are high compared to several other megacities such as London (Wilby, 2003) and Shanghai (Longxun et al., 2003). Based on observations from nine rural stations over the period 1981-2010, the mean annual rural temperature in the area is 5.1°C, the mean winter temperature is –7.2°C, and the mean summer temperature is 17.2°C. The mean annual precipitation is about 700 mm and has a typical summer maximum (Varentsov et al., 2018).

2.5.1 Urban climate in Moscow

The interference of mesoscale features from non-urban surface properties is minimized in Moscow, because Moscow is located in a flat and homogeneous terrain, far away from mountains and large waterbodies. This in combination with the relatively symmetric and compact shape of the city makes Moscow an interesting area for investigating pure urban-atmospheric interactions (Varentsov et al., 2018).

The rate of climate warming in the 20th century was higher in big cities compared to smaller urban centers or rural areas (Lokoshchenko, 2014). In Moscow, the air temperature in the 20th century increased with 2.3 °C, whereas on average the global air temperature increased about 0.6-0.7 °C in the last hundred years (Lokoshchenko, 2014). Urbanization leads to an enhancement of climate warming (Varentsov et al., 2017). Also the UHI intensifies with climate change. The mean UHI intensity of Moscow has grown with 0.4 °C since 1970. This was caused by climate change, population growth (the population has doubles since 1970) and city expansion (Varentsov et al., 2017; Lokoshchenko, 2014).

The average daytime UHI of Moscow is about 0.5K with a vertical extent of around 1.5 km. At night the UHI is larger than 3K. The vertical extent of intense UHI in Moscow is, however, shallower during the night than during the day. This is caused by the

cross-over effect, with a cold layer found at a height from 150m onwards (Varentsov et al., 2018). In Moscow the UDI follows the same pattern as the UHI both in space and time. So its vertical extent is up to 1.5 km during daytime and the maximal intensity is reached in the evening. This maximal intensity is located near the surface, and during night-time the intensity weakens (Varentsov et al., 2018). Sometimes at night an UMI can be observed. Downwind of Moscow, urban heat plumes can be observed. These are most clear in the early morning hours (between 0 and 4 UTC) and they stretch for tens of km (Varentsov et al., 2018).

2.5.2 Heatwaves in Moscow

Russia was struck by a mega-heatwave in 2010. This mega-heatwave was the worst of its kind in the past decades (Barriopedro et al., 2011; Fischer, 2014; Hoag, 2014; Russo et al., 2015). It broke all previous records—the night time records as well as the day time records in average, peak, duration and spatial extent (Russo et al., 2015). It killed an estimated 55,000 people (Barriopedro et al., 2011; Hoag, 2014). The heatwave also created the deadliest wildfires recorded in Russia since 1972. These wildfires had a major impact on wheat crops and left 3,500 people homeless in Western Russia. It has been estimated that the heatwave caused 15 billion US dollars of economical loss; this is 1% of the gross domestic product of Russia (Barriopedro et al., 2011; Sánchez-Benítez et al., 2018). The average daily temperature at the beginning of August 2010 was about 15 °C above average (36 °C instead of 21 °C) (NOAA, 2010). In the city of Moscow the daytime temperature reached 38.2 °C, which is extremely high for this region (Barriopedro et al., 2011). The ABL in Voronez, a city located about 470 km south of Moscow, reached almost four km during the afternoon, whereas under normal conditions the ABL height is less than two km (Miralles et al., 2014).

2.5.3 Local Climate Zone classification

As can be seen in Figure 2.3, Moscow is dominated by three LCZs. In the center of the city the main LCZ is “compact mid-rise” (LCZ 2) (Samsonov and Trigub, 2017), which means a paved land cover with almost no trees, and midrise buildings (3-9 stories) close together (Stewart and Oke, 2012). The other two most widespread LCZs are “open high-rise” (LCZ 4) and “open midrise” (LCZ 5) (Samsonov and Trigub, 2017), which indicate some pervious land cover (scattered trees, low plants) with tall or midrise buildings in an open arrangement, respectively (Stewart and Oke, 2012). The characteristics of the main LCZs represented in Moscow can be found in Appendix B (Stewart and Oke, 2012).

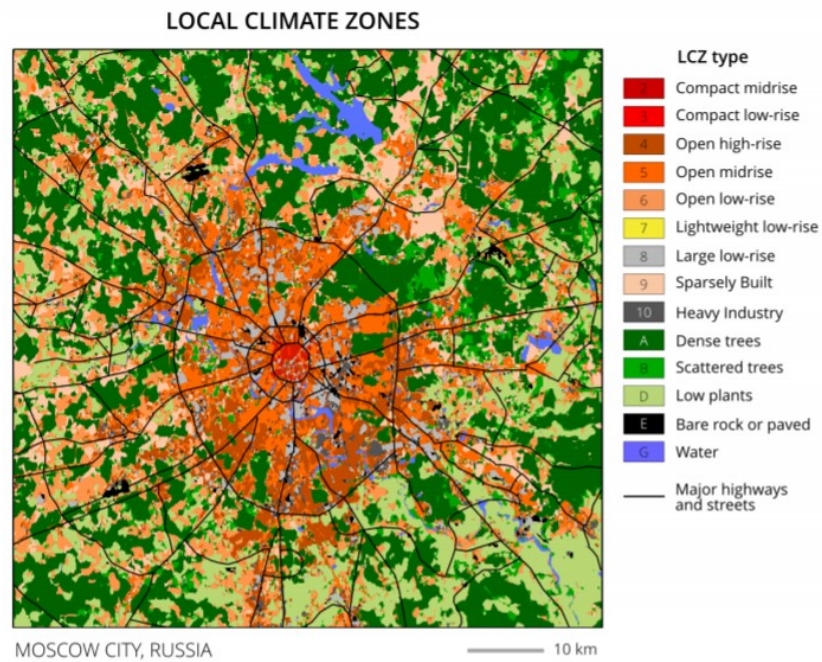


Figure 2.3: The local climate zones of Moscow (Samsonov and Trigub, 2017).

CHAPTER 3

OBJECTIVES

The general aim of this thesis is to provide a new software framework, called CLASS4GL_urban, to study urban boundary layer dynamics and its drivers. The basis is a conceptual mixed-layer model constrained with among others continuous remotely sensed high-resolution MTP data. CLASS4GL_urban aims to foster a better understanding of the development of extreme weather associated to urban areas, and the development of more precise urban adaptation strategies. More specifically, the thesis studies how urban features impact the changes in characteristics of the mixed layer during the course of the day for the city of Moscow. This is highly relevant for a better understanding of the development and the effects of heatwaves in cities.

There are four specific objectives. The first two are technical objectives that involve implementing extensions to an existing framework, called CLASS4GL, to model the diurnal evolution of the mixed layer. The third and fourth objective involve validating these extensions and an exploration of the resulting simulations.

1. Implement a recently developed urban module (Boeke et al., 2018) in CLASS4GL.
2. Adapt CLASS4GL to enable the use of MTP as initialisation data.
3. Use data from Moscow to test the hypothesis that incorporating of urban features in the framework CLASS4GL improves the accuracy of the simulations of the dynamics of the mixed layer during the course of the day in urban areas.
4. Use data from the case area Moscow to test the hypothesis that the high resolution MTP data can be used to obtain reliable simulations of the dynamics of the mixed layer during the course of the day in urban areas.



CHAPTER 4

METHODOLOGY

For investigating the climate in urban areas, often regional or mesoscale climate models (Wouters et al., 2013, 2017; Varentsov et al., 2017, 2018; Sparks and Toumi, 2015; Oleson, 2012) or even global climate models (Fischer et al., 2012) are used. The disadvantage of these models is that it is difficult to determine causal relationships because they are poorly constrained by observations and they represent a very large number of processes. In addition, the complexity of these models hampers a more focussed analysis of individual feedback processes (Wouters et al., 2019). The amount of studies that involve urban-induced phenomena in the lower troposphere is small compared to the amount of studies that only focus on near-surface features (Varentsov et al., 2018). A mechanistic column, observation based model such as CLASS can simulate the diurnal evolution of the ABL as it is influenced by local land-atmospheric feedbacks. Observations of the urban climate are sparse, and mostly limited to ground-level observations (Voogt and Oke, 2003). Microwave temperature profile data, obtained using a mobile remote sensing device, can give observations of the urban climate until a height of 1000m. These data are used in this thesis to understand the temporal changes of the mixed-layer features in urban climate.

4.1 CLASS and CLASS4GL

A new software framework CLASS for global studies (CLASS4GL) has been developed recently to constrain and initialise CLASS with balloon sounding measurements, satellite and re-analysis data (Wouters et al., 2019). It automatizes multiple ABL model simulations over large areas and climatological time spans, in response to different surface and atmospheric forcings and feedbacks in different regions over the world (Wouters et al., 2019). CLASS4GL aims to foster a better understanding of the drivers behind changes in the ABL through a diurnal cycle, especially during the amplification and the onset of extremes such as heatwaves (Wouters et al., 2019). Cause-effect relationships can be investigated as well as the local land-atmospheric feedbacks (Wouters et al., 2019).

The core of CLASS4GL is the conceptual bulk ABL model CLASS, based on a series of differential equations (Figure 4.1). The assumption is made that the ABL consists of a well-mixed layer so that the specific humidity (q), potential temperature (θ) and wind components are homogeneous within this layer. Under convective conditions there is efficient turbulent mixing, which supports this assumption. So by using mixed layer equations the turbulence inside the ABL is not explicitly solved. The entrainment of moisture and heat happens at the inversion layer which is characterized by a discontinuous jump (Δ) of specific humidity (q), potential temperature (θ) and the wind components over an infinitesimally small height at the top of the mixed layer (see Figure 4.1). The jumps are initialised by the changing parameters over height in the free atmosphere, which is modelled as a constant lapse rate (γ). However, CLASS4GL provides a representation of the upper-air atmospheric profile that also evolves according to the external large-scale dynamic forcing of advection and subsidence and as such accounts for varying (instead of constant) lapse rates of the capping inversion during the growth of the mixed layer (Wouters et al., 2019). The boundary layer growth is further determined in the model by the entrainment flux ($\overline{(w'\theta')_e}$) and the large scale subsidence velocity (w_s). CLASS4GL also offers a representation of advection as an additional atmospheric dynamic forcing (see below). The large scale subsidence velocity is a function of the wind divergence in horizontal direction and the inversion jump of potential temperature ($\Delta\theta_h$). This jump is a function of the lapse rate (γ_θ) and limits the growth of the mixed-layer because it represents a stratified layer. The variables w_s and γ_θ represent the conditions of the free troposphere at synoptic-scale (Vilà-Guerau de Arellano et al., 2015). Figure 4.1 gives a representation of the ABL layer in CLASS. CLASS has a resolution of 1° by 1° , over which the parameters are averaged (Wouters et al., 2019). Under assumption of a mixed-layer ABL, the diurnal changes of the atmospheric conditions and thermodynamic variables can be solved by three equations: equations 4.1, 4.2 and 4.3, which are used in the model. ψ is a generic variable; this can for example represent the specific humidity or the potential temperature. γ is the gradient of the generic variable in the free troposphere just above the top of the mixed layer, w represents the wind velocity, t represents time and h is the height of the mixed-layer. The subscripts s and e represent the surface and the entrainment air, respectively (Vilà-Guerau de Arellano et al., 2015).

$$\frac{\partial\langle\psi\rangle}{\partial t} = 1/h[\overline{(w'\psi')_s} - \overline{(w'\psi')_e}] \quad (4.1)$$

$$\overline{(w'\psi')_e} = -\Delta\psi_h\left(\frac{\partial h}{\partial t} - w_s\right) \quad (4.2)$$

$$\frac{\partial\Delta\psi_h}{\partial t} = \gamma_\psi\left(\frac{\partial h}{\partial t} - w_s\right) - \frac{\partial\langle\psi\rangle}{\partial t} \quad (4.3)$$

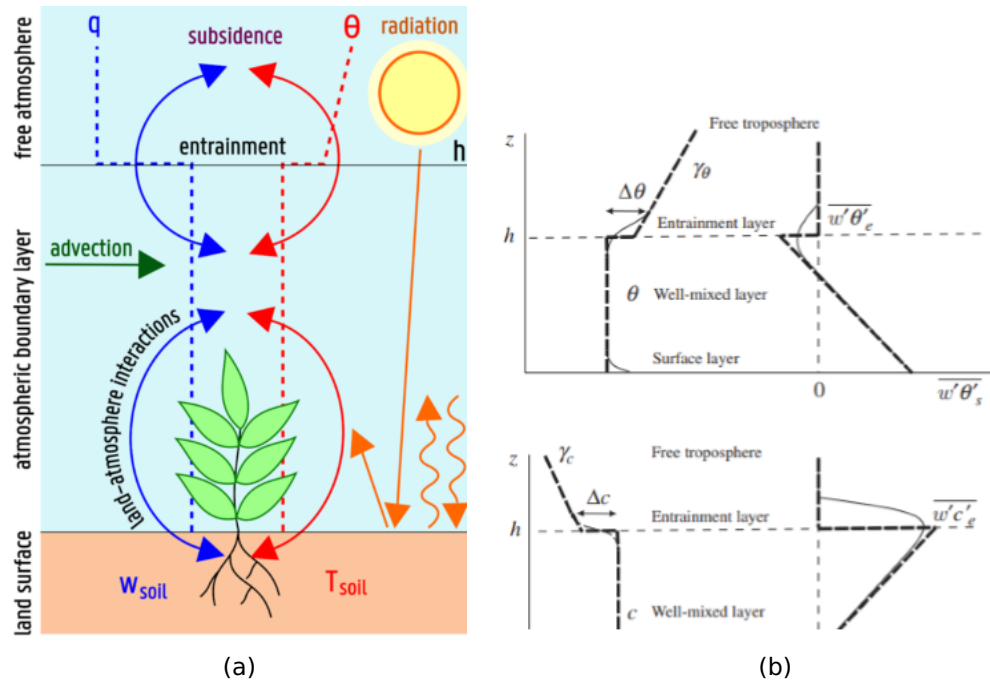


Figure 4.1: (a): The ABL representation in CLASS. The dashed lines represent the ABL state implementation, the full lines display the fluxes that occur. w_{soil} represents the volumetric water content in the soil layer and T_{soil} is the temperature of the soil; for explanation of the other symbols see text (Wouters et al., 2019). (b): The different layers that form the convective boundary layer are displayed. The Dashed lines represent the mixed-layer theory for the mean (left) and flux (right) profiles. The upper figure gives the model representation of the parameter potential temperature (θ), whereas the lower figure shows the model representation of c , which is a generic scalar such as specific humidity (q). For both the lower and the higher figure the left graph shows the mixed-layer theory for the mean profiles of the parameter, whereas the right graph shows the mixed-layer theory for the flux profiles of the parameter (Vilà-Guerau de Arellano et al., 2015). The explanation of the symbols can be found in the text, whereas the subscript e represents entrainment and the subscript s means surface.

The model needs as input detailed observations of the ABL. It needs to be initialised with morning soundings and it needs afternoon soundings for model validation. Beside balloon observations, gridded data of the atmospheric state on a large spatial scale and of the land state are used to further constrain and initialise CLASS simulations. These data provide additional context about the atmospheric (e.g., advection, cloud cover) and land (e.g., soil temperature, soil moisture, vegetation leaf-area index) conditions when the measurements took place (Wouters et al., 2019). The vertical atmospheric profile data used to initialise and validate the model are obtained by intensive research campaigns such as Boundary Layer Late Afternoon and Sunset Turbulence (BLLAST) (Pietersen et al., 2015) and The summertime Boreal forest field measurement intensive (HUMPPA-COPEC 2010) (Williams et al., 2011), and weather balloon soundings worldwide. The weather balloon soundings are taken from the Integrated Global Radiosonde Archive (IGRA) (Durre et al., 2006), under protection of the National Oceanic and Atmospheric Administration (NOAA). These balloon soundings

delivers also the vertical profiles of specific humidity and wind. Four satellite based datasets, one re-analysis and two survey datasets are used to represent the atmospheric forcing on a large scale and the soil-vegetation conditions (Wouters et al., 2019). The initial land cover parameters (e.g. albedo, fraction of vegetation) and soil properties are described by static datasets. The vegetation cover and albedo are described by the Moderate Resolution Imaging Spectroradiometer vegetation continuous field product (MODIS MOD44B) (Hansen et al., 2005). The Global Land Evaporation Amsterdam Model (GLEAM) version 3.2a is used to get values of the initial root-zone and surface soil moisture (Wouters et al., 2019). The atmospheric forcing data (cloud cover, subsidence, advection) and the initial temperature of the soil are used from the European Centre for Medium-Range Weather Forecasts Re-Analysis (ERA)-Interim dataset (Dee et al., 2011). For the datasets that are used to represent some other parameters such as wilting point, radiation and soil porosity, see Wouters et al. (2019). The explicit formulations and more details of the coupled land-atmosphere system used in CLASS can be consulted in Van Heerwaarden et al. (2010), van Heerwaarden and Teuling (2014) and Vilà-Guerau de Arellano et al. (2015). In Figure 4.2 a schematic overview of CLASS4GL_urban is displayed as well as the components where adaptations were made during this thesis. So in this thesis the model was complemented with (1) a switch that allows to include urban characteristics, such as the thermal properties of buildings and anthropogenic heat. (2) An additional input data source, namely microwave temperature profile data. These changes are further explained in the following paragraphs.

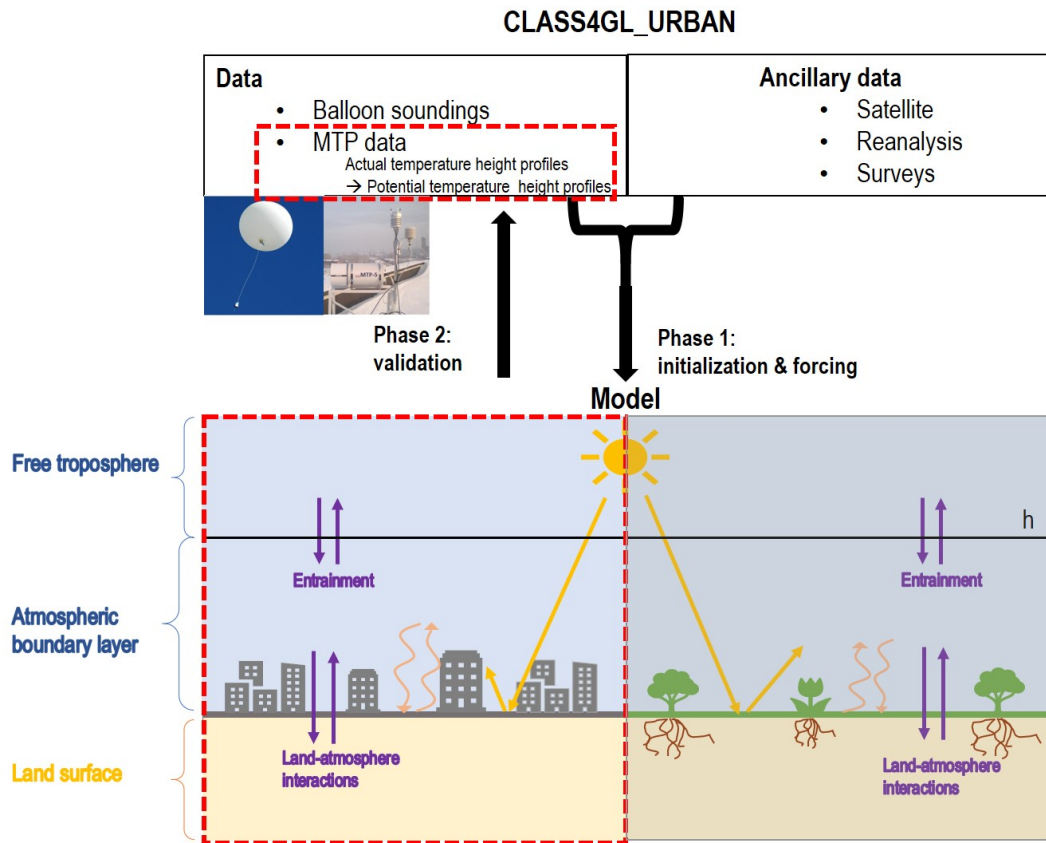


Figure 4.2: A schematic overview of CLASS4GL_urban. Height profiles obtained by balloon measurements or using a Microwave Temperature Profiler device can be used as input data. This in combination with ancillary data that delivers additional surface conditions and larger-scale atmospheric variables is used by the model to simulate the diurnal changes of the mixed-layer features. These changes over a diurnal cycle are caused by land-atmospheric feedbacks and entrainment from the free troposphere (purple arrows). The model is amongst others driven by the shortwave radiation (yellow) and longwave radiation (orange). The components encircled by red dashed lines are implemented during this thesis.

4.2 Urban software upgrade CLASS4GL_urban

The original CLASS4GL code does not have an urban parametrisation. In order to include urban effects, the urban land-surface scheme needs to be upgraded with urban physics and parameters. In this thesis, an urban parametrisation that was recently developed for CLASS (Boeke et al., 2018), has been implemented into the CLASS4GL software framework, so as to generate CLASS4GL_urban. Below, a short description of this urban extension is given. Three major changes have been implemented in this extension: (1) the storage heat flux is predicted by the Objective Hysteresis Model (OHM), (2) the anthropogenic moisture and heat fluxes are calculated and added, and (3) the advection of rural air is calculated using knowledge of the UHI, while in the original model this value is obtained from an external dataset. All these changes are

integrated in a new energy balance equation developed by Boeke et al. (2018). To make the changes possible the urban parametrisation developed by Boeke et al. (2018) had to be compared with the original model CLASS to detect the differences. Afterwards the code of CLASS4GL was changed to add an urban switch. When this switch is on, parameters representing the urban characteristics are activated and the changes in the energy balance caused by the urban characteristics is be taken into account. These parameters (e.g. anthropogenic heat flux, impervious surface, UHI, . . .) were implemented as well as the additional changes in the energy balances. If CLASS_urban is run, a local climate zone can be specified in the input and then the model uses average values for the urban parameters from the ranges delivered by Stewart and Oke (2012). One typical characteristic of urban areas is the heat that is stored. This stored heat flux density (equal to the net uptake of energy) is calculated by the OHM and is function of the radiation (Eq.4.4, Eq. 4.5, Eq. 4.6, Eq. 4.7). As different land uses (buildings, impervious surfaces, vegetation and urban canyons) have different properties with respect to heat storage a weighted average of land use is used to calculate the total amount of stored heat. For every LCZ, the relative cover of the different land use types is based on empirical data from multiple cities. The constants can be changed if enough information about the surface cover is available (Grimmond et al., 1991). A physical reason why a hysteresis model should be used is that in the morning the boundary layer has to break through the inversion layer. Because of this, it is easier to have transportation of heat into the ground than into the atmosphere. Yet, because there is more turbulence in the afternoon, transportation of heat into the atmosphere becomes easier, while transportation of heat into the ground is then limited (Boeke et al., 2018).

$$\Delta Q_s = a_1 Q^* + a_2 \left(\frac{\partial Q^*}{\partial t} \right) + a_3 \quad (4.4)$$

$$a_1 = 0.145 * f_{veg} + 0.039 * f_{built} + 0.064 * f_{imp} + 0.106 * (1 - f_{veg} + f_{built} + f_{imp}) \quad (4.5)$$

$$a_2 = 0.161 * f_{veg} + 0.044 * f_{built} + 0.039 * f_{imp} + 0.005 * (1 - f_{veg} + f_{built} + f_{imp}) \quad (4.6)$$

$$a_3 = -11.8 * f_{veg} - 2.98 * f_{built} - 5.46 * f_{imp} - 9.14 * (1 - f_{veg} + f_{built} + f_{imp}) \quad (4.7)$$

In urban areas there is an extra energy source, which is the anthropogenic heat flux. The anthropogenic heat flux is described by equation 4.8. This formula was chosen because it does not require additional information (Boeke et al., 2018). Human activity shows a diurnal variation, so the maximum values of the anthropogenic fluxes are prescribed and multiplied with a factor depending on the hour of the day. The factors used are derived from the Weather Research and Forecasting (WRF) model (Appendix C) (Skamarock et al., 2008) .

$$Q_{ant, LE}(t) = Q_{ant, H}(t)/\beta \quad (4.8)$$

A new energy balance was made, which included the adaptations listed above. In this new energy balance a tile approach is used to represent the heterogeneity of urban areas. By doing this, natural and urbanized parts can coexist (Figure: 4.3). The urban tile consists of urban latent heat, urban sensible heat flux and heat storage, which is calculated using the OHM approach. The vegetation part uses the original CLASS equations, but with the assumption that the entire tile consist only of grass. There is no bare soil. The net radiation (Q^*) is different for the rural and the urban tile

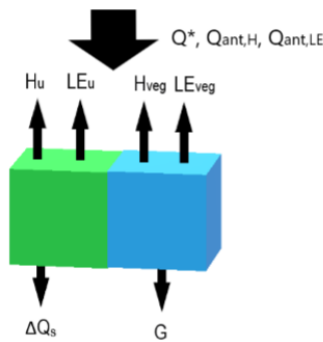


Figure 4.3: Representation of the urban tile approach. Q^* is the net energy available, $Q_{ant,h}$ represents the anthropogenic sensible heat, while $Q_{ant,LE}$ represents the anthropogenic latent heat. H represents in every case the surface sensible heat flux and LE is the latent heat flux, where u stands for urban and veg for vegetation. The storage of heat is represented by ΔQ_s , and G is the ground flux. From Boeke et al. (2018).

and is calculated by taking the weighted average of surface temperatures above the rural and urban tile, respectively, and this for every time step. From these surface temperatures the fluxes are calculated using equation 4.9 (Boeke et al., 2018).

$$Q^* + (1 - f_{veg}) * (Q_{anth, H} + Q_{anth, LE}) = (1 - f_{veg}) * (H_{urban} + LE_{urban} + \Delta Q_s) + f_{veg} * (H_{veg} + LE_{veg} + G) \quad (4.9)$$

The advection of rural air can be calculated from the UHI intensity, the average diameter of a city (set to be 15,000m), and the wind speed (u) using equation 4.10. The maximum value of the UHI is necessary in this formula. This is prescribed for each LCZ but can also be set by the user (Boeke et al., 2018). The magnitude of the advection of rural air for each hour of the day is calculated based on the intensity of

the UHI (see Appendix C), based on idealised diurnal changes in UHI (Oke, 1982).

$$\theta_{adv} = \frac{UHI}{(15000/u)} \quad (4.10)$$

By having the urban characteristics included in CLASS4GL_urban it is possible to investigate the main drivers of extreme events such as heatwaves in urban areas, and investigate why heatwaves are often more intense than in rural areas.

4.2.1 Implementation of Microwave Temperature Profiles into CLASS4GL

In addition to the implementation of the urban characteristics in CLASS, the framework CLASS model for Global studies (CLASS4GL) was also complemented with the option to use an additional kind of initialisation data, namely microwave temperature profiles data (MTP data). This made it possible to also use these temperature profiles, which have a higher resolution, to initialise simulations. The use of MTP data has two crucial advantages, first MTP data can be measured at a very local scale (high flexibility of the site of which the profiles are measured). Second their high vertical resolution is important because in the cities there is a high variation in vertical profiles within and among nights that has important consequences for the dynamics of the mixed-layer during the day.

MTP is a passive remote sensing instrument that consists of radiometers that operate in the 5mm wave band (Kadygrov et al., 2009). Every 5 minutes there is a temperature profile shown. Typically the temperature is shown at 50 m height intervals. It scans in angular steps from horizontal to vertical. To measure the temperature profile, a very sensitive instrument is required because the changes in emission of radiation due to differences temperature are small (ATTEX, 2013). The data used in this thesis is part of the TRIADA-2 experiment, this data is obtained using MTP-5HE and provided by Moscow State University. The accuracy of the temperature is about 0.2°C to 1.2 °C (ATTEX, 2013) and depends on the duration, place and time of the measurements, and the presence of inconvenient conditions such as breezes (Yushkov, 2014).

The temperature profiles were measured at four sites: two places in the suburbs (Kosino and CAO), one at a rural site (Zvenigorod), and one at Moscow State University (MSU), which is located in an urban park about 8 km Southwest of the centre of Moscow city (Varentsov et al., 2017). The profiles obtained in Kosino, CAO and MSU go up until 1000m, the profile obtained in Zvenigorod goes until 600m. In this thesis the profiles obtained in MSU will be used, because these represent an urban area and

have a height up to 1000m. The actual temperature height profiles are obtained by a MTP device.

A script was added to CLASS4GL_urban that fits an initial potential temperature height profile from the actual temperature height profile at a certain time step, obtained using an MTP device. This fitted potential temperature height profile can be used by the model to simulate the diurnal changes of the mixed-layer features. The actual temperature height profiles have to be entered as input data as an excel file together with the date. Then CLASS4GL_urban determines the timing of the sunrise and gets data out of ERA-Interim at sunrise. The resolution of the profiles obtained using an MTP device is 50m, this is higher than the resolution of ERA-Interim data. To solve this inconsistency ERA-Interim data is interpolated, as a result a value was obtained for every 50m over height. As initial profile the model needs potential temperature height profiles, so the actual temperatures are converted to potential temperatures. This is done using eq 4.11. θ represents the potential temperature, T represents the actual temperature, R is the gas constant of air and is calculated using Eq. 4.12, where q is set equal to zero. R_v is the gas constant for dry air and is set to $287 \frac{J}{kgK}$. R_d is the gas constant for moist air and is set to $461.5 \frac{J}{kgK}$. c_p is the specific heat of dry air and is set to $1005 \frac{J}{kgK}$. P_0 is the reference pressure and is set equal to 10 000 Pa. P is the pressure and is calculated using the hydrostatic equilibrium (Eq. 4.13). g is the gravitational constant and is equal to 9.81. ρ is set to 1.293, which is the value at sea level. Afterwards these observations of potential temperature and the ancillary data with the same vertical grid were used to fit an initial profile that later is used as start point to simulate the temporal change of the mixed-layer features.

$$\theta = T \left(\frac{P_0}{P} \right)^{\frac{R}{c_p}} \quad (4.11)$$

$$R = R_d * (1 - q) + R_v * q \quad (4.12)$$

$$P(z) = P(z - 1) - \rho * g * (h(z) - h(z - 1)) \quad (4.13)$$

4.3 Simulations

In the following section the set-up of the several batches of simulations will be discussed as well as the methods used to evaluate the model.

4.3.1 Set-up

Overview

Several simulations have been done to evaluate and investigate the characteristics of the urban parametrisation of the model and using MTP data to initialise the model. They can be grouped under three batches (see Figure 4.4). (1) In the first batch of simulations balloon soundings were used to initialise the model. Two locations were examined, namely Rjazan (urban) and Suhinichi (rural). This batch of simulations was used to evaluate the model and to investigate if the urban parametrisation can deliver an added value to predicting weather in an urban area (Rjazan). These simulations can also be used to look at the differences in characteristics between an urban (Rjazan) and a rural (Suhinichi) area. (2) In the second batch of simulations, observations obtained using an MTP-5 device were used. These observations were obtained in MSU, located in the city center of Moscow and thus representing an urban area. First, the raw observations were used to initialise the model. Afterwards the input data of MTP was bias-corrected using ERA-Interim data. (3) In the third batch of simulations, a perturbation experiment was performed on five parameters. The balloon profiles at August 6, 1984 in Rjazan and the bias-corrected MTP data of MSU at the 15th of June 2015 were used as input data.

Initialisation with balloon profile data (batch 1)

Two stations were selected, namely Suhinichi (27707) and Rjazan (27730). Suhinichi represents a rural area and is located 234 km SW of Moscow. Rjazan is a city located 200 km SE of Moscow. It has a population of 520,173 (Population, 2019). For both stations, simulations were made for the 6th of August in 1994, once with the original model and once with the urban parametrisation of the model. This date was chosen because observations are available for the two stations, and this date is in summer, so the chances on optimal weather for the model, i.e. clear sky, are higher. When using the urban parametrisation of the model, the parameters of the most probable LCZ was used, which in this case is LCZ five ('open mid rise'). This LCZ was chosen based on a visual analysis of Google Earth images. Table 4.1 gives the parameter values that were used to describe LCZ five in CLASS4GL_urban, following (Boeke et al., 2018).

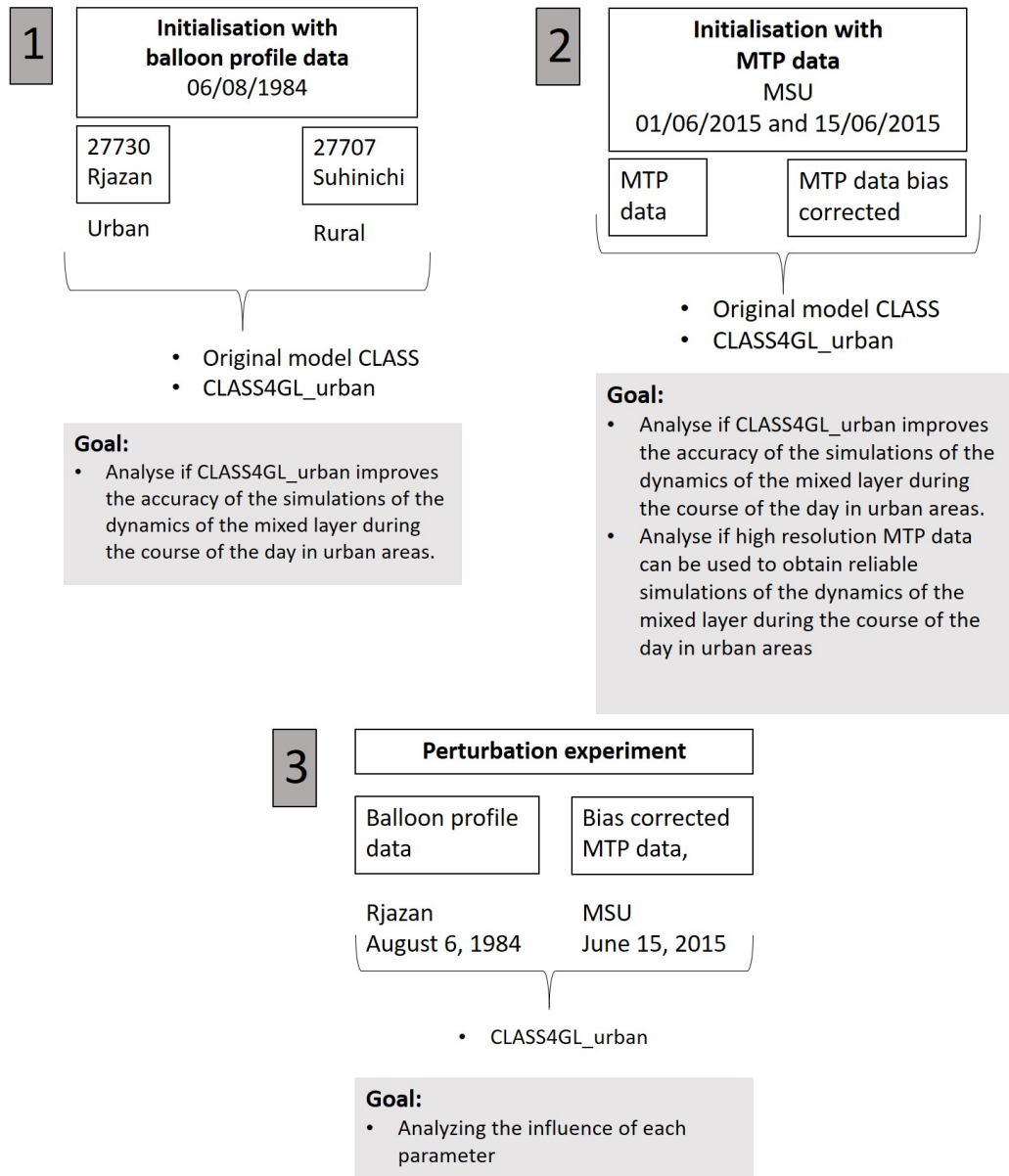


Figure 4.4: An overview of the different batches of simulations applied in this thesis. For each batch of simulations the used dates, which type of input data, which model and the intended goal is given. MSU: Moscow State University, represents an urban area. MTP: Microwave Temperature Profiles, vertical profiles obtained using a remote sensing device.

For both stations balloon sounding observations of the temperature height profiles and the specific humidity height profiles are available in early morning (around 2.30am) and in the afternoon (around 2.30pm). The early morning profile needed to initialise CLASS is actually an observation obtained at night, but the assumption is made that during the night the ABL is stable and does not change a lot, so that the profile at sunrise is expected to be similar.

Table 4.2 summarizes the simulations for both stations. As can be derived from above a total of four simulations were run: SUH_ORIG; SUH_URB; RJA_ORIG; RJA_URB.

Limitations

- The determination of the LCZ should ideally be done using a three step process. First metadata should be collected, such as relief, land cover, population density. Second the thermal source areas should be determined from where the temperature sensor receive data. And last the local climate zone should be selected (Stewart and Oke, 2012). In my study, the decision to take LCZ 5 is only based on visual inspection of Google Earth images. So it is possible that the parameters that are used are not ideal for this region.
- As a second limitation the profiles to initialise the model are obtained at 2.30am. This is still at night so these might not exactly represent the conditions at sunrise. Normally the ABL does not change much over night because it is stable, but it could be that the conditions are slightly different at sunrise than here assumed.

Initialisation with MTP data (batch 2)

For this set of simulations the observations obtained by the MTP-5 device are used to initialise the model. These observations are obtained in MSU. MSU is located in the city center of Moscow, so it represents an urban area. The observations have been bias-corrected using ERA-interim data and these new values have also been used to initialise the model. The bias correction using ERA-interim data has been applied because the observations obtained by MTP-5 have uncertainties. These deviations could be noticed when the observations were plotted over time. MTP is a remote sensing instrument (see 4.2.1). These instruments are sensitive, which makes them vulnerable to small local deviations.

The simulations are performed for two days, namely the 1st and 15th of June 2015. Two dates were analysed to have a first idea on the variation in weather between

days. The two dates are chosen in summer because the chances of optimal weather conditions for the model (clear sky, no precipitation) are higher. It is also most interesting to investigate the urban characteristics under these conditions and they are most relevant in obtaining insights on the urban effects during heatwaves. Heatwaves are typically characterized by clear sky and no precipitation.

MTP data from MSU First the MTP data obtained in MSU was used to initialise the model. Both the urban parametrisation and the original model were used to investigate the diurnal evolution of the mixed-layer. So it could be investigated whether the urban parametrisation of the model has an added value compared to the original model in an urban area such as MSU.

The observations at 4am were used as input data to the model because the sunrise occurred at 4am. Only observations until a height of 1000m are available, so the model is not able to run the entire day. When the mixed-layer height becomes higher than 1000m, the model stops. When using the urban parametrisation the local climate zone is set to five, which is equal to 'open mid rise' (figure 2.3). For parameter values associated with LCZ five see Table 4.1.

MTP data from MSU, bias-corrected with ERA-Interim data As said before the temperature profiles obtained by the MTP device are uncertain. ERA-interim data was used to bias-correct them. First the initial profiles of MTP data were compared with the initial profiles of the ERA-Interim data. By using ERA-Interim data as initialisation data, it was made sure that the model started the simulation at the same time as MTP data, which is at 4am. By doing this the MTP data and the ERA-Interim data can be compared and the ERA-Interim data can be used to bias-correct the MTP data. As a result the errors made while obtaining the observations using the MTP-5 device can be minimised. Between the heights of 600m-1000m, the difference is being taken between the ERA-Interim data and MTP data. The average of these differences were added to the MTP data. This generates a new initial profile, now bias-corrected. So the profile is now shifted along the axis of potential temperature, so that the average potential temperature between 600m-1000m is identical to the ERA-Interim data. The resulting data was transferred to an excel file and given as input for the model. The mean difference between the two datasets is taken over a height of 600m-1000m because the assumption was made that the urban characteristics do not have an influence at those heights, especially not at sunrise. And when looking at results obtained by Varentsov et al. (2018) at night, the main effects of urban characteristics in Moscow only go up to a height of about 500m. Above this height the effects are small.

Table 4.2 summarizes the simulations for MSU. As can be derived from above a total of four simulations were run: Data from MSU on 01/06/2015 was used as input data in the original model CLASS (MSU_ORIG_01); Data from MSU on 15/06/2015 was used as input data in the original model CLASS (MSU_ORIG_15); Data from MSU on 01/06/2015 was used as input data in the urban parameterization of the model CLASS (MSU_URB_01), Data from MSU on 15/06/2015 was used as input data in the urban parameterization of the model CLASS (MSU_URB_15).

Limitations

- The LCZ is set to 5 based on a study done by Samsonov and Trigub (2017). But as can be seen on Figure 2.3 this LCZ is not uniform in the area of MSU. According to the guidelines to use LCZs as a classification scheme, the minimum diameter of the LCZ should be between 400-1000m (Stewart and Oke, 2012). This is not the case in our situation. So there could be influences of other LCZs and the parameters used are not necessarily the optimal ones. There is also no knowledge on how the device was placed to see if the data obtained came from an area characterized by LCZ 5.
- For the conversion of the actual temperatures to the potential temperatures, the specific humidity is set equal to zero. This is a simplification and it would be more precise to measure the specific humidity over height or use this information from other datasets. Moreover, for applying the bias correction the assumption is made that urban characteristics do not influence the atmosphere between the height 600m and 1000m in the early morning.

Table 4.1: The parameter values used to describe LCZ 5 in CLASS4GL_urban, following Boeke et al. (2018).

PARAMETER	SYMBOL	VALUE
Albedo	α	0.185
Anthropogenic heat flux	$Q_{anthheat}$	12.5 W/m ²
Fraction of buildings	$cbuilt$	0.30
Fraction of impervious surface	$cimper$	0.40
Fraction of vegetation	$cveg$	0.3
Roughness length for momentum	$z0m$	1.25 m
Bowen ratio	bowen	2.0
Strength Urban Heat Island	UHI	0.2 K
Height of roughness elements	d	18 m

Table 4.2: This table shows an overview of the different simulations. First the different study sites, areas where the measurements were obtained are given as well as the land use on this site. Then the code used in the following sections is displayed. In the following columns, the characteristics of these simulations are explained; which model was used, the original one (CLASS) or the version which was extended in this thesis with an urban parametrisation (CLASS_Urban), also which input data was used, what date was run and, last, what type of LCZ was entered in the model.

Study site	Land use	Code	Model	Input data	Date	LCZ
Rjazan	Urban	RJA_ORIG	CLASS	Balloon profiles	06/08/1994	/
	Urban	RJA_URB	CLASS_urban	Balloon profiles	06/08/1994	5
Suhinici	Rural	SUH_ORIG	CLASS	Balloon profiles	06/08/1994	/
	Rural	SUH_URB	CLASS_urban	Balloon profiles	06/08/1994	5
MSU	Urban	MSU_ORIG_01	CLASS	MTP profiles	01/06/2015	/
	Urban	MSU_URB_01	CLASS_Urban	MTP profiles	01/06/2015	5
MSU	Urban	MSU_ORIG_15	CLASS	MTP profiles	15/06/2015	/
	Urban	MSU_URB_15	CLASS_urban	MTP profiles	15/06/2015	5

Perturbation experiment (batch 3)

A perturbation experiment was performed. The urban parametrisation of the model was used. As initialisation data two data sets were used: the balloon soundings from Rjazan on the 6th of August and the MTP data from MSU on the 15th of June 2015 bias-corrected with ERA-interim data. The date for the bias-corrected MTP data was chosen because earlier simulations indicated that the 15th of June was a day with no or few clouds and that the model represents the observations on this day most accurately. A script was made to be able to run sensitivity analyses using the urban parametrisation of the model. The same initial profile was used for every scenario.

For this perturbation experiment three parameters were adjusted: the anthropogenic heat, the roughness length, and the deviation of fraction between buildings, vegetation and impervious surface (see table 4.3.1).

In the model each grid of the soil consists of a certain fraction of buildings, impervious surface, vegetation and urban canyon. The sum of all these fractions should be equal to one. In local climate zone five, urban canyons are not considered. As a result, the sum of the fraction of buildings, impervious surface and vegetation is equal to one. In the perturbation experiment three scenarios were looked at to investigate the importance of the division of the surface in fractions. (1) The fraction of buildings was increased while the fraction of vegetation remained constant. Intuitively this can be seen as replacing impervious surface by buildings while the amount of vegetation re-

mains the same. (2) In a second scenario the fraction of buildings was increased while the fraction of impervious surface remained constant. Intuitively this can be seen as replacing vegetation by buildings. (3) In a third scenario the fraction of impervious surface was increased while the fraction of buildings remained constant. Intuitively this can be seen as replacing vegetation by impervious surfaces such as a parking spaces. We note that the categories of buildings and impervious surfaces are both, in fact, impervious surface.

The minimum and maximum values used for this perturbation experiment can be found in table 4.3.1. These values are based on literature for different LCZs (Stewart and Oke, 2012). When changing one parameter, all the other parameters remain the same, namely the parameters used in local climate zone 5, 'open mid rise'. By doing this, the importance of each parameter is investigated as well as the effect of every parameter on the diurnal evolution of the mixed-layer.

When using the bias corrected MTP data the model is run for 7,5 hours, so until 11.30am, which is the maximum amount of time possible, because only observations upon a height of 1000m are available. In some cases, this runtime created errors because the mixed-layer got to high. There, the runtime was lowered until simulations were obtained and usually 30 minutes less was simulated.

Table 4.3: A perturbation experiment was performed on three different parameters. The minimum and maximum value are given, as step size. C_{built} , C_{veg} and C_{imper} represent the fraction of total cover that is buildings, vegetation and impervious surface respectively. Impervious surface is here defined as a category and includes all impervious surfaces except for buildings.

	min	max	stepsize
anthropogenic heat flux	5	280	25
roughness length	3	25	2
C_{built} ($C_{veg} = cte$)	0.15	0.7	0.05
C_{built} ($C_{imper} = cte$)	0.15	0.7	0.05
C_{imper} ($C_{built} = cte$)	0.15	0.7	0.05

4.3.2 Evaluation of model performance

The results of the first and second batch of simulations were analysed using qualitative and quantitative methods. In this evaluation the accuracy of the initialisation was not taken into account. This evaluation for urban areas was done for both CLASS4GL and CLASS4GL_urban.

Height profiles of θ and q were plotted as well as time series of q , θ , mixed-layer height (h) and the different components of the energy balance. The time series are

used to investigate the effect of urbanization on the evolution of the mixed-layer. For the first batch of simulations, observations are available of the height profiles of θ and q in the morning and afternoon. These profiles were used to evaluate the model qualitatively. The vertical profiles are evaluated up to a height of 5000 m, since this coarsely represents the height of the troposphere.

For a more quantitative validation, several metrics of model performance were calculated: Mean Absolute Error (MAE), Root Mean Square Error (RMSE), correlation and Mean Bias Error (MBE). Validation metrics should always be looked at in combination, because every validation metric focusses on a different characteristic. It is by combining them and analysing them together that a total view of the error or performance of the model can be obtained (Chai and Draxler, 2014).

The mean absolute error (MAE). Equation 4.14 was used to calculate the mean absolute error where n represents the number of observations, P is equal to the predictions and O represents the observations. The MAE gives insight in the average error of the model. If the value is close to zero than the model accurately predicts the observations. While this measure quantifies the average magnitude of the error it does not indicate whether the model over- or underestimates the values.

$$MAE = \frac{1}{n} \sum_{i=1}^n |P_i - O_i| \quad (4.14)$$

The root mean square error (RMSE). The RMSE is calculated using equation 4.15. This validation measure will give more weight to outliers in terms of errors than the MAE. It is influenced by several factors such as the total error, the variation of the magnitudes of the errors, and the amount of observation points (Willmott and Matsuura, 2005).

$$RMSE = \sqrt{\frac{1}{n} \sum_{i=1}^n (P_i - O_i)^2} \quad (4.15)$$

Correlation. The correlation is calculated by calculating the Pearson correlation coefficient between the observed and predicted values (see equation 4.16). C represents the covariance matrix (Eq. 4.17). The correlation coefficient gives information of the linear association between observations and predictions (Taylor, 1990) .

$$R_{OP} = \frac{C_{OP}}{\sqrt{C_{OO}C_{PP}}} \quad (4.16)$$

$$C_{AB} = \sum_{i=1}^n (A_i B_i) - \frac{\sum_{i=1}^n (A_i) \sum_{i=1}^n (B_i)}{n} \quad (4.17)$$

The mean bias error (MBE). Equation 4.18 was used to calculate the MBE. This gives an idea whether the model in general over- or underestimates the observations. If the mean bias is positive this means that in general the model overestimates the observations, while when it is negative the model in general underestimates the observations (Willmott and Matsuura, 2005). It should be kept in mind that it is highly sensitive to outliers, just like the RMSE.

$$MBE = \frac{1}{n}(P_i - O_i) \quad (4.18)$$

All these validation measures were calculated using one of the following two methods: (1) In a first method—referred thereafter as "height profile method"—the difference between θ height profile at the end of the day and θ height profile used to initialise the model were compared between the observations and the model. This says something about the increment in θ over the day, but no conclusion can be made about the absolute values or the time evolution of θ . This was used to validate the first batch of simulations.

(2) For the second batch of simulations, using the MTP-data, the height profile method is not ideal because the model assumes a constant θ in the mixed-layer, while θ in the MTP-data increases with height within the mixed-layer. For this reason another method was used to calculate the validation measures using MTP data. In this method—called "time series method" in further sections—the difference in θ at a height of 1000m and θ in the mixed-layer was calculated for every 30 minutes for both the observations as well as the simulations. For the observations the average was taken of θ between a height of zero and the height of the mixed-layer given by the framework (CLASS4GL/CLASS4GL_urban). Because the mixed-layer height, at any given time step, can differ regarding which framework was used (CLASS4GL or CLASS4GL_urban), the average of the observations which are used to validate, at any time step, differ depending on which framework was used (CLASS4GL or CLASS4GL_urban). The time series method gives information on the temporal evolution of the range of temperatures over height but does not inform us on the distribution of the temperature over height, the absolute values of θ over height, or the absolute value of θ over time. Another possibility would be to initialise the model with the observations at several time steps and use the θ that the model gives for the mixed layer. By doing this, the model performance would be calculated based on what the model is made for.

4.3.3 Surface energy balance

The general energy balance of an ecosystem is represented by Eq. 4.19 (Chapin et al., 2002). Q represents the net radiative energy. In a natural ecosystem the storage of energy, through an increase in temperature and photosynthesis, is usually small (less than 10 %). Throughout a day, the energy loss approximately equals the energy input received at the surface (Chapin et al., 2002). In the model the heat storage is not taken into account (see Eq. 4.20). The surface sensible heat in combination with the latent heat is often called the available energy because these fluxes are responsible for the turbulent exchange with the atmosphere (Chapin et al., 2002). Equation 4.21 displays surface energy balance used in urban areas (Grimmond et al., 2010) and is a simplified version of the one used in the urban parametrisation of the model, $Q_{anthheat}$ represents the anthropogenic heat source in urban areas.

$$Q = H + LE + G + \Delta S \quad (4.19)$$

$$Q = H + LE + G \quad (4.20)$$

$$Q + Q_{anthheat} = H + LE + \Delta S \quad (4.21)$$

4.3.4 General limitations

Besides the limitations already mentioned for each batch of simulations, there are some shortcomings which apply to each simulation:

- The first hours that are simulated should be seen as a spin-up period due to the inaccuracy/uncertainty of the initial height of the mixed-layer.
- In the batches of simulations only one or two days are examined. However, there is a lot of weather variation from day to day. The choice to only simulate a limited number of days was inspired by the fact that a lot of time was invested in the implementation of the urban parametrisation of the model and the adaptation of the model to be able to work with MTP data.
- The switch of advection from the free troposphere is turned off, so that the atmosphere above the mixed layer will not change over time. This is a simplification of reality.
- ERA-Interim delivers several weather variables and has a spatial resolution of 80 km (Dee et al., 2011). This is larger than the diameter of Moscow, which is about 40km. So the parameters obtained using ERA interim data are probably not entirely representative of the area that is investigated.

- The model stops running when the mixed-layer height gets higher than 1000m. Usually this happens around 11am, so the results are most often limited to the first half of the day.

CHAPTER 5

RESULTS AND DISCUSSION

5.1 Initialisation with balloon profile data (batch 1)

Suhinici is a rural area, so the expectation is that when using this data to initialise the model the original model will perform better than the urban parametrisation of the model. While for Rjazan, which is a city, the expectation is that the urban parametrisation of the model will represent better the observations than the original model.

5.1.1 Height profiles

Figure 5.1 displays the potential temperature height profiles of the initialisation (2am) and the observations as well as the modelled profiles in the afternoon (2.30pm) for each station. Both the original model and the urban parametrisation of the model were used to simulate the profiles. The initial estimated profiles fit accurately on the observations. Above the mixed layer the original model and the urban parametrisation of the model follow the same line. Because the advection is switched off, the air above the mixed layer is not predicted by the model to change over time; as a result this line remains equal to the initialisation.

Because it is known that the predictions of the specific humidity are more uncertain (Wouters et al., 2019), the focus of our comparison of the models will be on the height profiles of potential temperature. For both stations one could argue that the urban parametrisation of the model represents better the observations than the original model. This is was expected for Rjazan but not for Suhinici. But the differences in predictions between the urban parametrisation and the original model are small and it should be kept in mind that only the 2-3 lowest data points of the observations provide insight in how the model performs because these are the only data points that are situated in the mixed-layer.

It is noticeable that when the urban parametrisation of the model was run the mixed layer grows higher (see figure 5.2). This is in agreement to what is known on the effects of urban features on the height of the mixed-layer (Dupont et al., 1999;

Theeuwes et al., 2015) (see Section 2.2). When looking at the specific humidity height profiles at 2.30pm (Figure 5.2), it can be seen that the profile of Rjazan (urban area) has lower values for the specific humidity. This indicates that the mixed layer is drier in comparison with the profiles of Suhinici. This is in line with earlier studies comparing rural and urban areas (Moriwaki et al., 2013; Lokoshchenko, 2014). Figure 5.1 shows that both areas have a similar initialisation profile. This implies that it is valid to interpret the afternoon differences in light of changes in the diurnal evolution of the ABL, although they are located 290km away from each other.

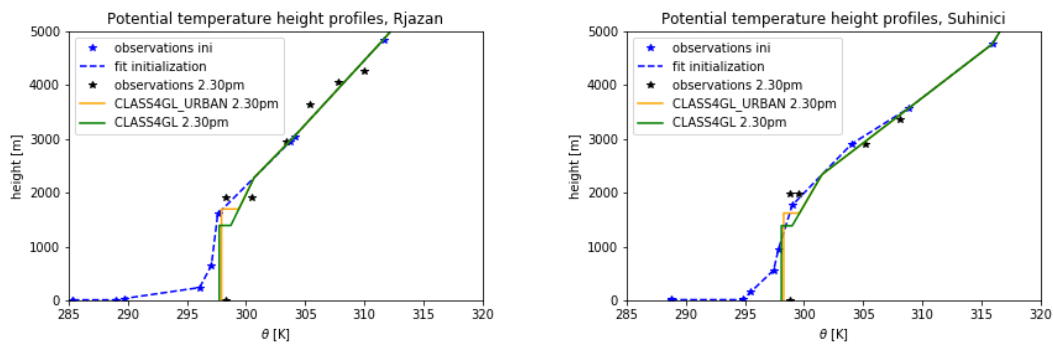


Figure 5.1: The profile used to initialise the model (blue) and the simulations and observations (*) around 2.30pm are displayed for Rjazan (left) and Suhinici (right). For both stations, the urban parametrisation of the model (orange) was used as well as the original model (green)

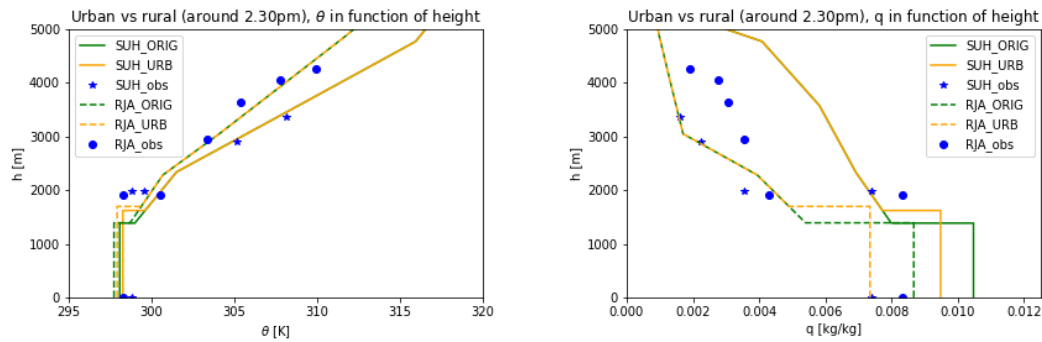


Figure 5.2: Left: Height profiles of the potential temperature (θ) for Rjazan (urban) and Suhinici (rural), for the original model (green) and the urban parametrisation of the model (orange). Right: Height profiles of the specific humidity (q) for both stations, with the original model (green) and the urban parametrisation of the model (orange). The blue stars and circles are the observations for Suhinici and Rjazan, respectively. The dashed lines are Rjazan (urban) and the full lines are Suhinici (rural).

5.1.2 Indicators of model performance

The height profile method (Method (1) in Section 4.3.2) for calculating the validation metrics was used. So first the difference was taken between the potential temperature height profiles at the end of the day and the beginning of the day for both

observations and predicted data. Table 5.1 shows the values for the validation metrics on these differences. The graphs plotting the differences in potential temperature height profiles and specific humidity height profiles between the end of the day and the beginning of the day for both the observations and the simulations can be found in Appendix E. Also the scatterplots of the observations against the simulations can be found in Appendix E.

Table 5.1: The scores of the comparison between the observations and the simulations for the original and the urban parametrisation of the model, by looking at the difference in profile at the end of the day and the beginning of the day. To calculate the bias, the simulated values are subtracted from the observations. The values in red indicate which model has the best performance. 50 data points were used for these calculations.

Potential temperature height profiles				
Suhinici				
	MAE	RMSE	CORR	BIAS
urban	0.90 K	1.18 K	0.85	0.30 K
original	0.94 K	1.21 K	0.84	0.29 K
Rjazan				
	MAE	RMSE	CORR	BIAS
urban	0.64 K	0.72 K	0.94	-0.21 K
original	0.71 K	0.77 K	0.93	-0.20 K
Specific humidity height profiles				
Suhinici				
	MAE	RMSE	CORR	BIAS
urban	0.0029 kg/kg	0.0031 kg/kg	0.41	0.0029 kg/kg
original	0.0031 kg/kg	0.0033 kg/kg	0.46	0.0031 kg/kg
Rjazan				
	MAE	RMSE	CORR	BIAS
urban	0.0010 kg/kg	0.0012 kg/kg	0.47	$-9.8 * 10^{-4}$ kg/kg
original	0.0011 kg/kg	0.0014 kg/kg	0.13	$-8 * 10^{-4}$ kg/kg

Table 5.1 indicates that there is not much difference in performance between the original model and the urban parametrisation of the model with respect to the predictions of the potential temperature height profile at the end relative to the beginning of the day. Yet, while values are similar, the urban parametrisation of the model tends to score better in seven out of the eight metrics of Rjazan. There was a quite high cloud cover on the day of analysis (43 % in Suhinici and 55 % in Rjazan) which might provide an explanation for the fact that the model is not able to predict accurately the height-dependent difference between the end of the day and the beginning of the day.

The values of the validation metrics tend to be worse for the specific humidity height profiles than for the potential temperature height profiles. In general, the specific humidity is more difficult to predict than the potential temperature (Wouters et al., 2019). One reason for this is that the values for specific humidity are low and there is a large variability in both space and time (Miralles et al., 2014).

5.1.3 Diurnal changes in the mixed-layer features over time

To generate the figures of the time series (Figure 5.3, and Figure 5.4) only the simulations of the CLASS4GL_urban were used for Rjazan (RJA_URB) and of the original model for Suhinici (SUH_ORIG). Plots showing all the combinations (SUH_ORIG, SUH_URB, RJA_ORIG, RJA_URB) are given in Appendix F. There are no observations of the changes in the mixed layer during the course of the day so it is not possible to evaluate performances of the model against observations. Instead, differences between the urban and rural areas are discussed. When looking at the time series of the mixed-layer height, specific humidity and potential temperature (Figure 5.3), it can be observed that the mixed layer of the urban area is higher than in the rural area. This is what can be expected from literature (Theeuwes et al., 2015). The specific humidity is higher in rural areas than in urban ones; in the literature urban areas are often described as UDI (Lokoshchenko, 2014). When looking closely at the potential temperature, just after sunrise the potential temperature is higher in rural areas than in urban areas. This seems at first sight odd because one might expect that either the potential temperature in urban areas is higher than in rural areas or that the mixed-layer height is higher in urban than in rural areas so that a larger volume of air is taken into account (Theeuwes et al., 2015). A possible explanation for the observed pattern might be that in the urban area first heat is stored. Because the thermal properties in urban areas are different, it is possible that the energy is not directly released as sensible heat, resulting in a time lag. Another explanation could be that the period up to 6am should also be seen as a spin-up period of the model. The ABL is stable until this moment.

5.1.4 Surface energy balance

Figure 5.4 shows the time series of the surface sensible heat and latent heat. The difference between sensible heat and latent heat is much higher in rural than in urban areas. In general this figure agrees with the expectation that the fraction of sensible heat in urban areas is higher and the fraction of latent heat is lower than in rural areas. In Appendix F the comparison is made between the two stations, both run with

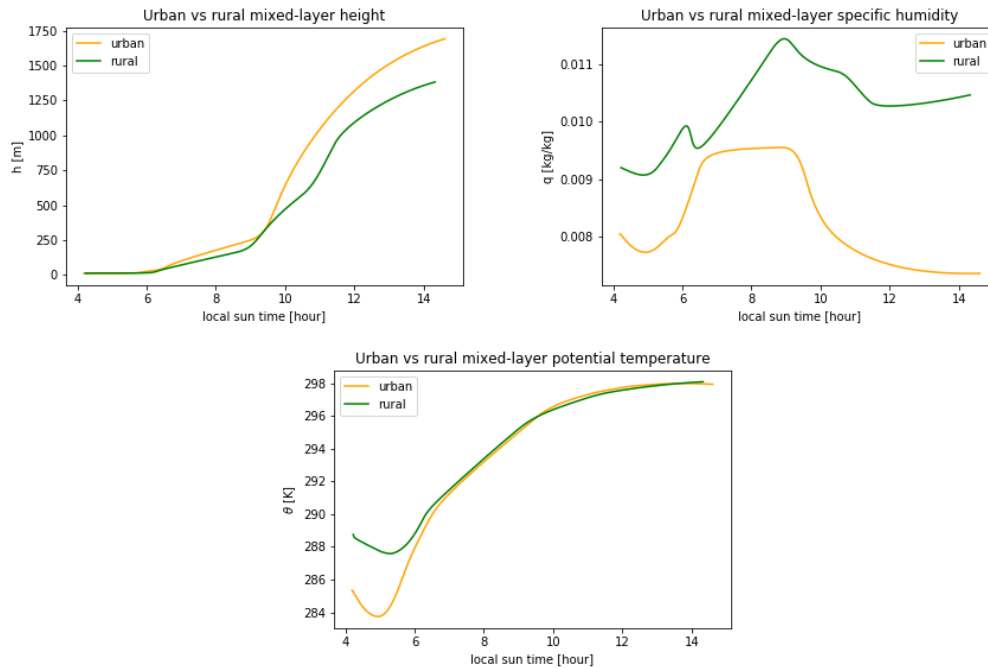


Figure 5.3: Time series of the mixed-layer height (h), specific humidity (q) and potential temperature (θ) simulated by CLASS4GL_urban for Rjazan (RJA_URB, orange) and by the original model for Suhinici (SUH_ORIG, green).

both the original model and the urban parametrisation of the model. This was done to check whether the initial conditions of the model result in the observed difference in time series. It is noticeable that for the parameters h , θ and q , the trend is caused by the initial profile. When looking at the energy balance, however, the urban parametrisation is largely responsible for the trend in the decrease of latent heat in urban areas and the increase in sensible heat, because all the lines generated using the urban parametrisation of the model are located in the middle, close to each other (surface sensible heat flux (H) and latent heat flux (LE)).

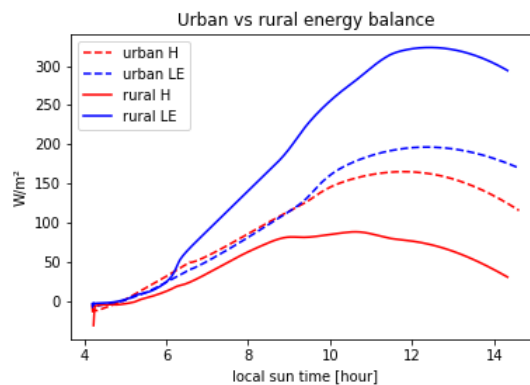


Figure 5.4: Time series of the surface sensible heat flux (H) and latent heat flux (LE) simulated by CLASS4GL_urban for Rjazan (RJA_URB, dashed lines) and by the original model for Suhinici (SUH_ORIG, full lines).

5.2 Initialisation with MTP data and model validation (batch 2)

Simulations were run for two days (June 1 and June 15 2015), which will be described separately. June 15 2015 was a day with only 35% of cloud cover, so this can be seen as a day with near-optimal conditions, as the model performs generally better under clear sky conditions with no precipitation (Wouters et al., 2019). June 1 2015 was a cloudy day, with a sky cloud cover of 51 %. Cloud cover estimates were obtained from ERA-interim data. The focus will be on the results obtained using the bias-corrected MTP data. The corrected data led to better model performances than the non-corrected data (see Appendix G). For both days a quantitative and a qualitative validation will be discussed. For the quantitative validation the calculation was done using the time series method (see Method (2) in Section 4.3.2). This means that the difference of potential temperature between a height of 1000m and the mixed layer is calculated for every 30 minutes and a comparison is then made between the observations and the simulations of both the CLASS4GL_urban and CLASS4GL. Values for validation metrics and scatterplots are shown. The values obtained in these validation analyses do not allow to say anything about the profile itself or the absolute values predicted by the model, but it does inform on whether the change in the profile of potential temperature over time reflects the observations. The height profiles of the potential temperature and the specific humidity across the day, with a resolution of 30 minutes, can be found in Appendix H for both June 1 and June 15 2015.

5.2.1 June 15 2015

Height profiles

In Figure 5.5a the bias-corrected MTP data can be seen that were used to initialise the model. As can be seen, bias correction of the MTP data leads to a shift of the potential temperature height profile to lower temperatures. The difference between the original initialisation data and the bias-corrected initialisation data are small, namely 0.50K. Figure 5.5b shows the beginning and end profile obtained using both CLASS4GL_urban and CLASS4GL when initialised with the bias-corrected MTP data. In this figure the bias was also added to the observations as to facilitate comparison. The initial fit is certainly not ideal; some improvements need to be implemented. For example, in the current initialisation fit the specific humidity is assumed zero but this is a simplification. One can obtain specific humidity data from the ERA-interim data. But when these data were used the initial fit was worse, perhaps because of the coarse

resolution of the ERA-interim data (see Section 4.3.4). Second, the initial mixed-layer height is now based on the calculation of the Richardson bulk number exceeding a critical value $RiBc$ (Wouters et al., 2019), which among others is calculated from the specific humidity and wind data obtained by ERA-interim. Because of the coarse resolution, the data might not well represent the urban area. A possibility would be to calculate the initial mixed layer height in a different way when using MTP data as initialisation, but further research is needed on this. When looking at the profiles at the end of the simulations (11.30am; Figure 5.5b), it is clear that those do not fit the observations accurately, at least not in absolute values. Specific validation metrics are described below to investigate whether the trend of potential temperature over height is correctly represented by the model.

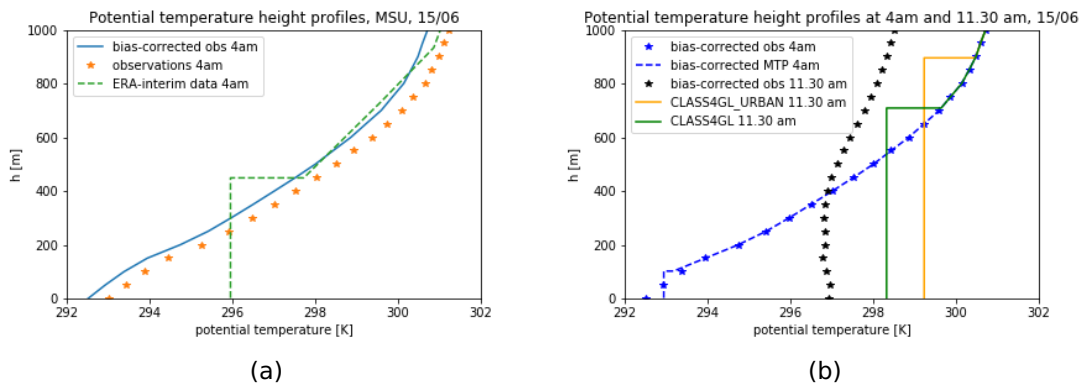


Figure 5.5: (a): The height profiles of potential temperature at 4am on 15/06/2015 obtained in MSU using the MTP device (orange), the ERA-interim data for MSU (green) and the bias-corrected observations (blue) that were used to initialise the model. (b): The potential temperature height profiles of the bias-corrected observations obtained in MSU using the MTP device that were used as initial data (blue). The initial profiles generated by the model (identical for MSU_ORIG_15 and MSU_URB_15, dashed blue lines), the observations at the end of the simulations (black; bias-corrected with ERA-interim data), and the height profile generated by MSU_ORIG_15 (green) and by MSU_URB_15 (orange) at the end of the simulations (11.30am) on the 15th of June.

When looking at the position of the height profiles relative to each other over time, the profiles are located as would be expected. More specifically, when looking at the potential temperature the profiles generated by MSU_URB_15 show a higher mixed layer and higher values of potential temperature than the profile generated by MSU_ORIG_15. The trends for the specific humidity on this day (Appendix H) are also as expected, with the profiles of MSU_URB_15 having lower values of specific humidity than the profiles of the simulations MSU_ORIG_15, which is in agreement with earlier studies that have indicated UDI effects during daytime over Moscow (Varentsov et al., 2018).

Indicators of model performance

In Figure 5.6 the time series of the difference in potential temperature between a height of 1000m and the mixed layer is displayed. The data obtained by MTP is uncertain, and for this reason it is recommended to look at differences instead of absolute values. When looking qualitatively at these graphs one could argue that the urban parametrisation of the model approximates better the observations than the original model. It makes sense that the difference of potential temperature between a height of 1000m and the mixed layer has a decreasing trend over time because the mixed layer grows over the day and as a result the difference will be lower, given that the above layers remain on the same position as the advection is turned off in the model. It should be kept in mind that taking the average of the observations over the predicted mixed-layer height can result in an error because it assumes that the mixed-layer height predicted by the model is representative for the observations. Looking at the profiles (see Appendix H) this is not necessarily the case.

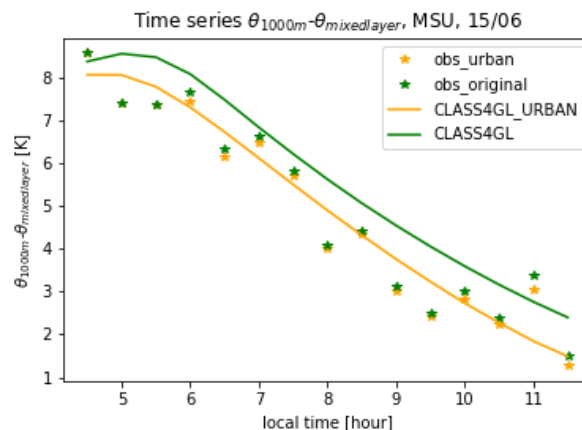


Figure 5.6: Time series of the difference in potential temperature between the height of 1000m and the mixed layer on the 15th of June at MSU for the observations (*) and simulations generated by MSU_ORIG_15 (green) and MSU_URB_15 (orange). For the observations in orange the mean was calculated between height zero and the mixed-layer height obtained using CLASS4GL_urban. For the observations in green the mean was calculated between height zero and the mixed-layer height obtained using CLASS44GL.

Table 5.2 gives an overview of the obtained values when calculating several validation metrics for the simulation results obtained using the urban parametrisation of the model and the original model based on the data plotted in Figure 5.6. As can be seen, scores from the urban parametrisation of the model are better for all validation measures than the original model. MSU is located in the city center of Moscow, so in an urban area. Our results are thus in line with the expectation that the characteristics of the diurnal evolution of the mixed layer in an urban area would be better predicted by the urban parametrisation of the model than the original model.

The mean bias is positive. This implies that both models in general overestimate the differences in potential temperature between a height of 1000m and the mixed layer. Thus the model will underestimate the mixed-layer height and potential temperature. The urban parametrisation of the model, however, performs much better than the original model (Table 5.2 and Figure 5.7). The average magnitude of the error is 0.50K, while the range of observed values is 8K. The urban parametrisation of the model is able to represent the change in height of the potential temperature over time on this day relatively well. Qualitatively, however, the profiles (see appendix H) do not fit well the observations. We can conclude that the trend over height of potential temperature is predicted by the urban parametrisation of the model but the location of the profile is not.

Table 5.2: The values for the different validation metrics when the model is initialised with bias-corrected MTP data for MSU from the 15th of June 2015. For each validation metric the performance of the urban parametrisation of the model (urban) as well as the performance of the original model are given. The values in red indicate which model has the best performance. 14 data points were used for these calculations.

15/06/2015 MSU				
	MAE	RMSE	CORR	BIAS
urban	0.50 K	0.57 K	0.97	0.13 K
original	0.85 K	0.96 K	0.96	0.74 K

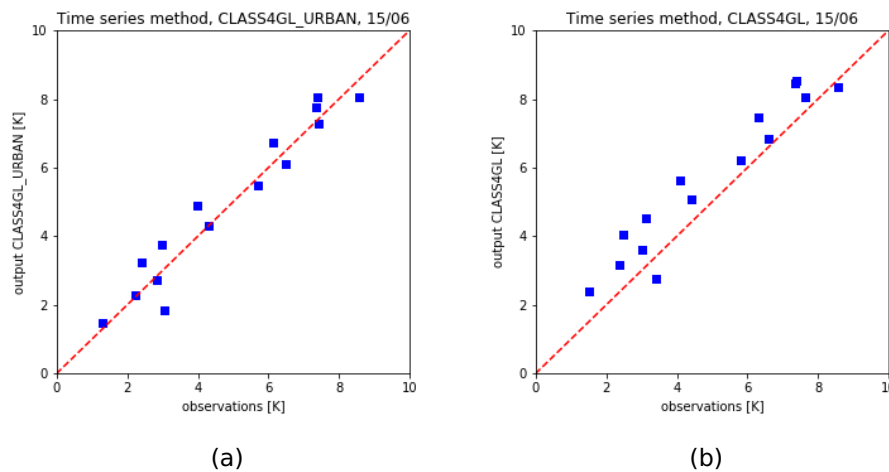


Figure 5.7: Scatterplots of the observations and the simulations of the differences in potential temperature between 1000m and the mixed layer for the MSU data on the 15th of June 2015. Every dot is a datapoint in time (every 30 min) of the differences in potential temperature between 1000m and the mixed layer for the MSU data on the 15th of June. (a) shows the results obtained with MSU_URB_15, while (b) shows the results obtained with MSU_ORIG_15.

Diurnal changes in the mixed layer features

Figure 5.8a shows the dynamics of the mixed-layer characteristics. Both models follow the same trend when looking at the potential temperature and mixed layer height. In both cases the urban parametrisation of the models delivers slightly higher values than the original model. This is in line with expectations, as it is often the case that in urban areas the mixed-layer height and the potential temperature are higher than in rural areas (Theeuwes et al., 2015). When looking at the specific humidity both models have a different trend. When the urban parametrisation of the model is applied the specific humidity is lower. This is in agreement to earlier studies that indicate that urban areas are usually drier than rural areas (Sisterson and Dirks, 1978; Varentsov et al., 2018). In addition, in urban areas the specific humidity often shows a stronger decrease in the morning than in rural areas. This can be due to two interacting factors: the vertical entrainment of dry air and a drier surface. Impervious surface obstruct evaporation, which leads to higher surface temperatures and thus to a higher surface sensible heat flux. This in combination with the roughness in urban areas leads to intense mixing. As a result, the mixed layer deepens and drier air is entrained from above. This leads to a reduction in the specific humidity, even though the total moisture is kept constant (Sisterson and Dirks, 1978). When the urban parametrisation of the model is applied, the specific humidity decreases stronger than the original model. In combination with a slightly higher potential temperature, a slightly larger mixed layer and lower specific humidity, this can indicate that the urban parametrisation of the model better represents the typical urban climate characteristics.

The temperature of the soil at initialisation was equal to 292.86K. This value is used in the model and is obtained from ERA-interim data. The initial temperature of the mixed layer from the initialisation profile at 4am is 292.94K, which is slightly higher than the temperature of the soil. So the expectation would be that in the first hours heat is transferred from the atmosphere to the soil. Figure 5.8b shows that in the early morning heat is indeed lost from the mixed layer either transferred to the ground or stored. This implies that the potential temperature of the mixed layer would decrease in these first hours, but when looking at the changes through a diurnal cycle of the potential temperature in the mixed layer (Figure 5.8a) the potential temperature remains quite stable for the urban parametrisation in the first hours. The soil temperature and the air temperature data are from different sources. It should be kept in mind that the period until about 6am might have to be viewed as a spin-up period for the model. After 6am the sensible heat transfer increases (Figure 5.8b) and this agrees with the increase in potential temperature and mixed-layer height after 6am (Figure 5.8a).

Surface energy balance

Looking at the sensible and latent heat flux (Figure 5.8b) shows that the latent heat flux is lower and the sensible heat flux is higher when the urban parametrisation of the model is used compared to when the original model is used. This is in line with expectations, amongst others, because impervious surfaces evaporate at lower rates. It is remarkable that the main flux is still the latent heat flux. During the day the latent and sensible heat flux increases for both models. This can be expected because of an increase in incoming solar radiation. It is remarkable that when the original model is used the net incoming available radiative energy is higher than when the urban parametrisation of the model is used. This could be because urban areas emit more longwave radiation at the surface as the temperatures are higher, and this is better captured by the urban parametrisation of the model. Also the albedo is different in the two models because in the original model this value is obtained from ERA-interim data ($\alpha = 0.210$), while in the urban parametrisation of the model this value comes from the literature and is a typical value for LCZ 5 ($\alpha = 0.185$).

Figure 5.9 plots the left and right part of the energy equation over time. Because of the law of energy conservation, one expects that the two lines always lie on each other. This is the case for the original model, but not for the urban parametrisation of the model. This could reflect that there is somewhere an inconsistency in the accounting for energy. Detailed inspection of Boeke et al. (2018) revealed that in the urban module the ground heat flux is not taken into account. This likely causes the mismatch observed in Figure 5.9 and should be looked at in the future.

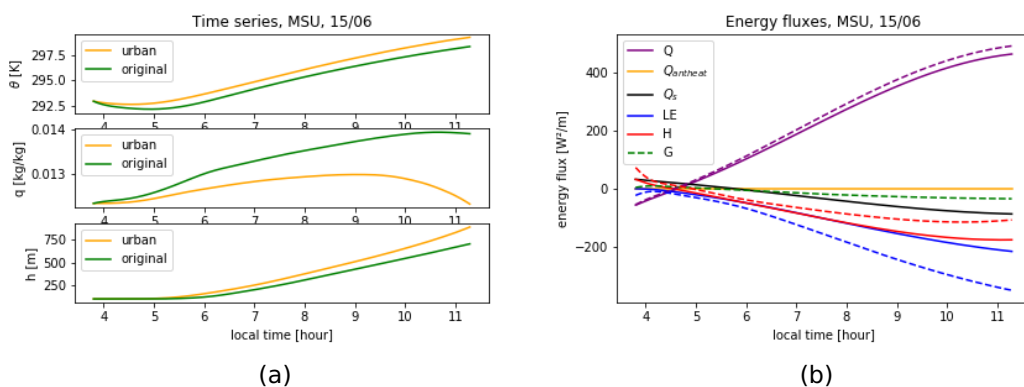


Figure 5.8: (a) The changes through a diurnal cycle of potential temperature (θ), specific humidity (q), and the mixed-layer height as generated by simulations MSU_ORIG_15 (dashed lines) and MSU_URB_15 (full lines). (b) The changes through a diurnal cycle of the different components of the energy balance from simulations MSU_ORIG_15 and MSU_URB_15. The dashed lines are the results of MSU_ORIG_15, while the full lines represent the results of MSU_URB_15. Q : net available radiative energy, $Q_{anthreat}$: anthropogenic heat; Q_s : storage heat; LE : latent heat flux; H : surface sensible heat flux; G : ground heat flux.

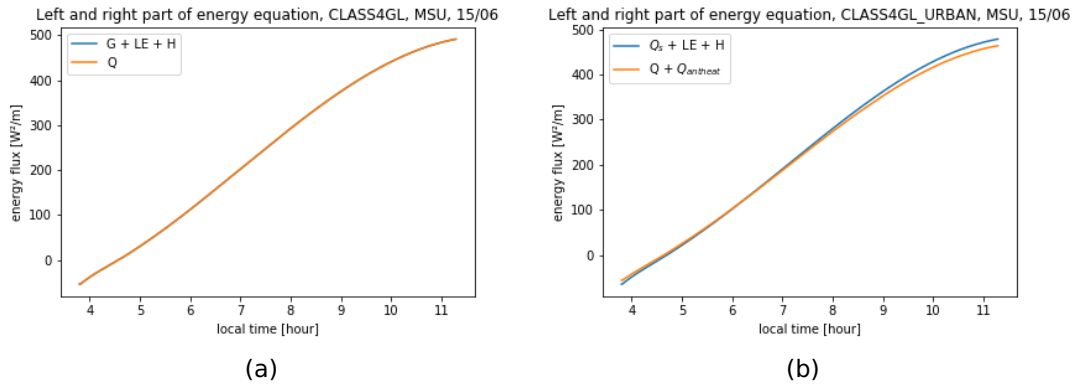


Figure 5.9: (a) The left part of the energy balance, which consists of the latent heat flux (LE), the sensible heat flux (H) and the ground heat flux (G), and the right part of the energy balance, the net radiation (Q) for the original model (MSU_ORIG_15). (b) The left part of the energy balance, which consists of the latent heat flux (LE), the sensible heat flux (H) and the storage energy (Q_s), and the right part of the energy balance, which consists of the net radiation (Q) and the anthropogenic heat (Q_{anthreat}) for CLASS4GL_urban (MSU_URB_15).

5.2.2 June 1 2015

The first of June 2015 was a cloudy day. Several explanations will be given for the deviations between the simulations and observations, but it should be kept in mind that at this stage, these are largely speculative.

Height profiles

Figure 5.10 shows the bias-corrected MTP data that was used to initialise the model. Bias correction of the MTP data results in a shift of the potential temperature height profile to higher temperatures. The differences between the original initialisation data and the bias-corrected initialisation data is small, namely 0.38K. Figure 5.10 shows the begin and end profile obtained using both models when initialised with the bias-corrected MTP data. For ease of comparing, the bias correction was also added to the observations. Also on this date the initialisation is not ideal (Figure 5.10) and the end results of the simulations do not fit the observations accurately, at least not in absolute values (Figure 5.10). When comparing the height profiles obtained using the two kind of models, the expectation is that the mixed layer would be higher and the potential temperature higher when applying the urban parametrisation instead of the original model, because the mixed layer is typically higher in urban areas (Lokoshchenko, 2014; Theeuwes et al., 2015). For the results on the 1st of June (Figure 5.10b), however, the mixed layer is higher when the original model is used than when the urban parametrisation of the model is used. It appears that the surface sensible heat release into the mixed layer is lower in the urban area. This might have resulted

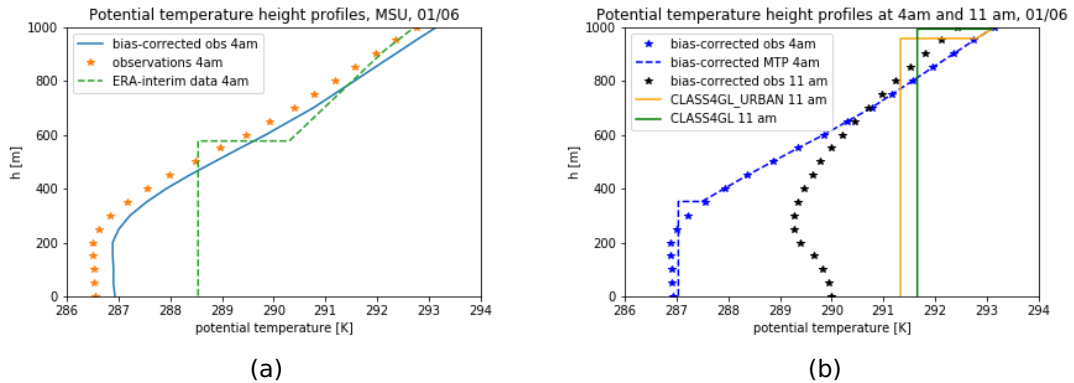


Figure 5.10: (a): The height profiles of potential temperature at 4am on 01/06/2015 obtained in MSU using the MTP device (orange), the ERA-interim data for MSU (green) and the bias-corrected observations (blue) that were used to initialise the model. (b): The potential temperature height profiles of the bias-corrected observations obtained in MSU using the MTP device that were used as initial data (blue). The initial profiles generated by the model (identical for MSU_ORIG_01 and MSU_URB_01, dashed blue lines), the observations at the end of the simulations (black; bias-corrected with ERA-interim data), and the height profile generated by MSU_ORIG_01 (green) and by MSU_URB_01 (orange) at the end of the simulations (11am) on the 1st of June.

from the enhanced heat storage in the urban areas that acts as an additional heat sink, hence making less energy available for the sensible heat release. The enhanced heat storage might have resulted from the high ground heat capacity in the urban area. It should also be noted that the model is initialized with soil and surface temperatures from ERA-Interim, which is too coarse in resolution to represent features on a scale of a single city. Beside this, June 1 2015 is a cloudy day. In turn, this could make the local surface-atmosphere feedbacks in terms of surface energy exchanges considered by the conceptual mixed-layer model less pronounced, so that the importance of other processes not explicitly represented by the model (such as local air circulation) become relatively more important.

Indicators of model performance

The change through time of the difference in potential temperature between a height of 1000m and the mixed layer as displayed in Figure 5.11 shows that the model underestimates the difference in potential temperature. The plot implies that at the end the model predicts that there is a smaller temperature change over height than is actually happening. So the model overestimates the potential temperature of the mixed layer. Because in the model the advection is turned off, the value at a height of 1000m remains unchanged over time. This means that if the difference in simulated potential temperature changes over time, this is caused by an increase or decrease in the potential temperature of the mixed layer. Figure 5.11 shows that the observed differences in potential temperature in the beginning is quite stable. This means that

the mixed layer is not changing, perhaps because the sun is still too weak. It could also be linked to cloud cover. If there is much cloud cover less radiation is transferred, so less energy is available. Around 7am the differences start to decrease strongly. This might reflect a change in cloud cover over time. When the clouds disappear more energy is available. In the model the cloud cover is kept constant, but this is not necessarily representative for reality. Changes in cloud cover through time can result in an over- or underestimation of the temperature difference over height.

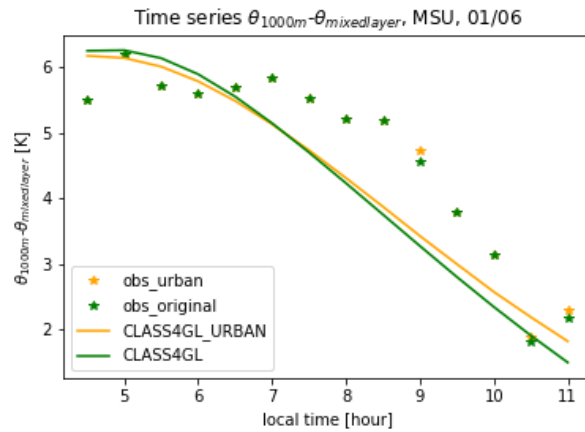


Figure 5.11: Time series of the difference in potential temperature between the height of 1000m and the mixed layer on the 1st of June at MSU for the observations (*) and simulations generated by MSU_ORIG_01 (green) and MSU_URB_01 (orange).

Table 5.3 and Figure 5.12 indicate that the urban parametrisation of the model outperforms the original model in predicting the potential temperature difference between a height of 1000 and the mixed layer over time. This is what was expected because MSU is located inside the city center of the megacity Moscow. An exception on this general pattern is the correlation, but the value for the original model is only 0.003 higher than that for the urban parametrisation of the model, and both models perform very well ($r > 0.91$). The bias indicates that both models underestimate the temperature differences in the observations. The scatterplots of Figure 5.12 that the lower values tend to be more underestimated than the higher values. This implies that the model predicts that the difference over height is lower than in reality. The simulated mixed-layer height is higher and warmer than in reality. The RMSE and MAE values are relatively high. This means that the average magnitude of the error is quite large and that there is quite some variation among the errors.

Table 5.3: The values for the different validation metrics when the model is initialised with bias-corrected MTP data for MSU from the 1st of June 2015. For each validation metric the performance of the urban parametrisation of the model (urban) as well as the performance of the original model are given. The values in red indicate which model has the best performance. 14 data points are used for these calculations.

01/06 MSU				
	MAE	RMSE	CORR	BIAS
urban	0.61 K	0.72 K	0.92	-0.40 K
original	0.67 K	0.79 K	0.92	-0.44 K

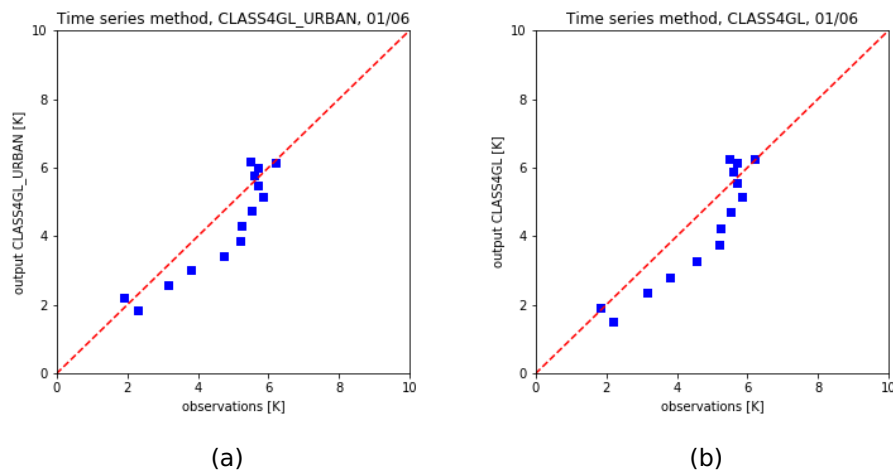


Figure 5.12: Scatterplots of the observations and the simulations of the differences in potential temperature between 1000m and the mixed layer for the MSU data on the 1st of June 2015. Every dot is a datapoint in time (every 30 min) of the differences in potential temperature between 1000m and the mixed layer for the MSU data on the 1st of June. (a) shows the results obtained with MSU_URB_01, while (b) shows the results obtained with MSU_ORIG_01.

Diurnal changes in the mixed layer features over time

Time series of the potential temperature, specific humidity and height (Figure 5.13b) reflect what would be expected: in the beginning the ABL is stable, the sun must still break through, and after a while, more specifically around 5.30am, the ABL becomes unstable, it increases, rises in temperature and decreases in specific humidity. These are characteristics one would expect in an urban area.

On the 1st of June 2015 the temperature of the soil (287.5K) is slightly higher than the mixed-layer temperature at initialisation (4am, 287.04K). One would expect a positive sensible heat flux to the atmosphere, but when looking at the height profiles and the energy balance (see Figure 5.13b) this is not observed. In the early morning the mixed-layer cools down and heat is transferred from the atmosphere to the ground or stored. One possible explanation could be that the temperature of the surface at

initialisation is taken from ERA interim (291.64K) and this value is higher than the temperature of the soil. As a result heat will be transferred from the atmosphere to the soil, at least for the original model. This is not the case for the urban parametrisation of the model, because ground flux is not taken into account here. In the urban parametrisation of the model, however, heat is stored in urban structures so less heat is transferred as sensible heat flux.

Surface energy balance

Figure 5.13b shows the changes in the different components of the energy balance over a diurnal cycle. The trends for both models are the same. In the beginning energy is transferred out of the system. In the urban parametrisation of the model, the sensible heat and latent heat are a bit flatter than the original model. This can be explained by the storage of heat, as a result of which some energy is not available for sensible or latent heat transfer. Figure 5.13a shows that the trend of both models is the same, but that the urban paramaterization of the model results in lower values for both the sensible as well as the latent heat flux. The urban parametrisation of the model suggest that a lot of energy is stored at this day, probably because this was a cloudy day. The sensible heat curve is located above the latent heat curve. This makes sense in an urban area because there is little vegetation and thus little heat transferred by evaporation. This pattern, however, differs from what observed on the 15th of June 2015, so this indicates variation from day to day. A possible reason for the differences between the two days is that the temperature of the atmosphere was colder on June 1st than on June 15th. As a result, the atmosphere can contain less water and was closer to the saturation point. This changes the fluxes from latent heat to sensible heat.

In Figure 5.14 the left and right part of the energy balance are plotted. As for the previous simulations the lines of the left and right side of the energy balance equation when using the urban parametrisation do not exactly match (see 5.2.1 for further explanations).

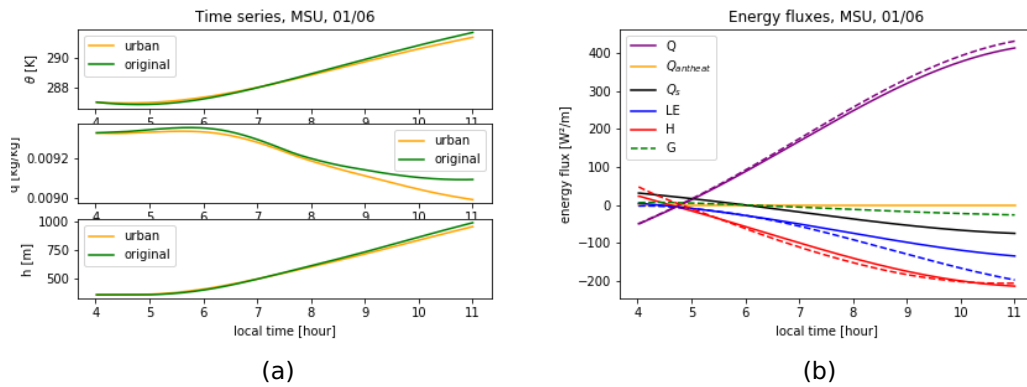


Figure 5.13: (a): The changes through a diurnal cycle of potential temperature (θ), specific humidity (q), and the mixed-layer height as generated by simulations MSU_ORIG_01 (dashed lines) and MSU_URB_01 (full lines). (b): The changes through a diurnal cycle of the different components of the energy balance from simulations MSU_ORIG_01 and MSU_URB_01. The dashed lines are the results of MSU_ORIG_15, while the full lines represent the results of MSU_URB_01. Q : net available radiative energy, $Q_{anthreat}$: anthropogenic heat; Q_s : storage heat; LE: latent heat flux; H: surface sensible heat flux; G: ground heat flux.

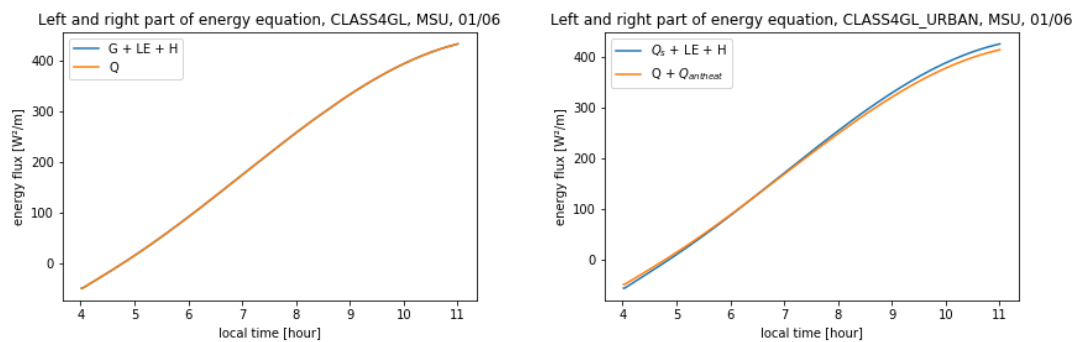


Figure 5.14: (a): The left part of the energy balance, which consists of the latent heat flux (LE), the sensible heat flux (H) and the ground heat flux (G), and the right part of the energy balance, which consists of the net radiation (Q) for the original model (MSU_ORIG_01). (b): The left part of the energy balance, which consists of the latent heat flux (LE), the sensible heat flux (H) and the storage energy (Q_s), and the right part of the energy balance, which consists of the net radiation (Q) and the anthropogenic heat ($Q_{anthreat}$) for CLASS4GL_urban (MSU_URB_01).

5.3 Perturbation experiment (batch 3)

The trends observed after the spin-up period are similar when using balloon soundings or bias-corrected MTP data for initialisation. The results of using balloon profiles of Rjazan on the 6th of August 1994 as initialisation can be found in Appendix I. Here the focus will be on the bias-corrected MTP data from MSU on the 15th of June 2015.

Figure 5.15 and Figure 5.16 show the results of the sensitivity analysis. The only set of parameters for which variation has an important impact on the results of the simulations is the relative coverage of buildings, vegetation and impervious surface.

Of this set of parameters, only changes in the relative cover of buildings (scenario 2) and changes in the relative cover of impervious surface (scenario 3; see 4.3.1) resulted in a distinct difference in mixed-layer evolution over time. The results of changing the other parameters can be found in Appendix J. Changing these other parameters only results in a small difference in the changes through a diurnal cycle of the mixed layer. The results show that mainly the amount of vegetation has an influence on the diurnal changes of the mixed layer. From Figure 5.15 and Figure 5.16 the conclusion can indeed be made that the fraction of vegetation versus total fraction of impervious surface (i.e. the sum of buildings and other impervious surfaces) has an important influence on the mixed-layer evolution. In either case, whether the fraction of buildings changes or the fraction of impervious surface changes, the effect is the same: when there is less vegetation the mixed-layer height increases, the sensible heat flux is higher, the potential temperature is higher, the latent heat flux is lower, and the specific humidity is lower. This is consistent with what can be found in the literature, namely that in general urban areas (which implies more buildings and impervious surfaces) are drier and warmer (Lokoshchenko, 2014; Varentsov et al., 2017).

It is noticeable that the roughness of the buildings (d) does not have a large influence on the diurnal evolution of the mixed layer. This suggests that the amount of impervious surface has a more important role than the features of the buildings itself. These results also imply that vegetation in an urban area can have a large influence on the diurnal evolution of the mixed layer and the consequences of it. The question remains whether most of the effect is linked to the presence of vegetation or whether a large part of the effect is linked to the energy storage by impervious surface. Further research is needed to fully explore this.

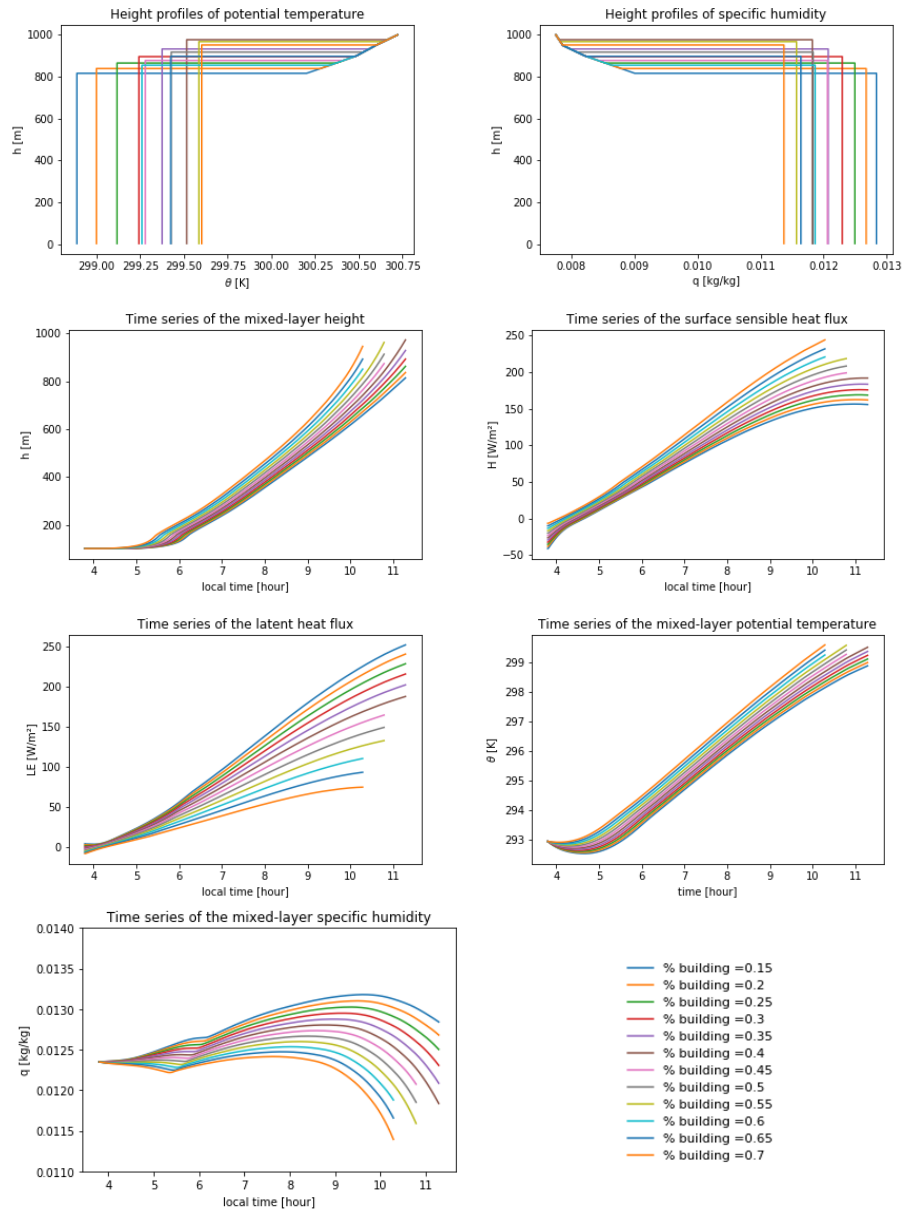


Figure 5.15: The height profiles and the time series of several variables are given for simulations with different values of percentage covered by buildings (keeping the fraction of impervious surface constant). θ : potential temperature; q : specific humidity; h : height; H : sensible heat flux; LE : latent heat flux.

5.3. PERTURBATION EXPERIMENT (BATCH 3)

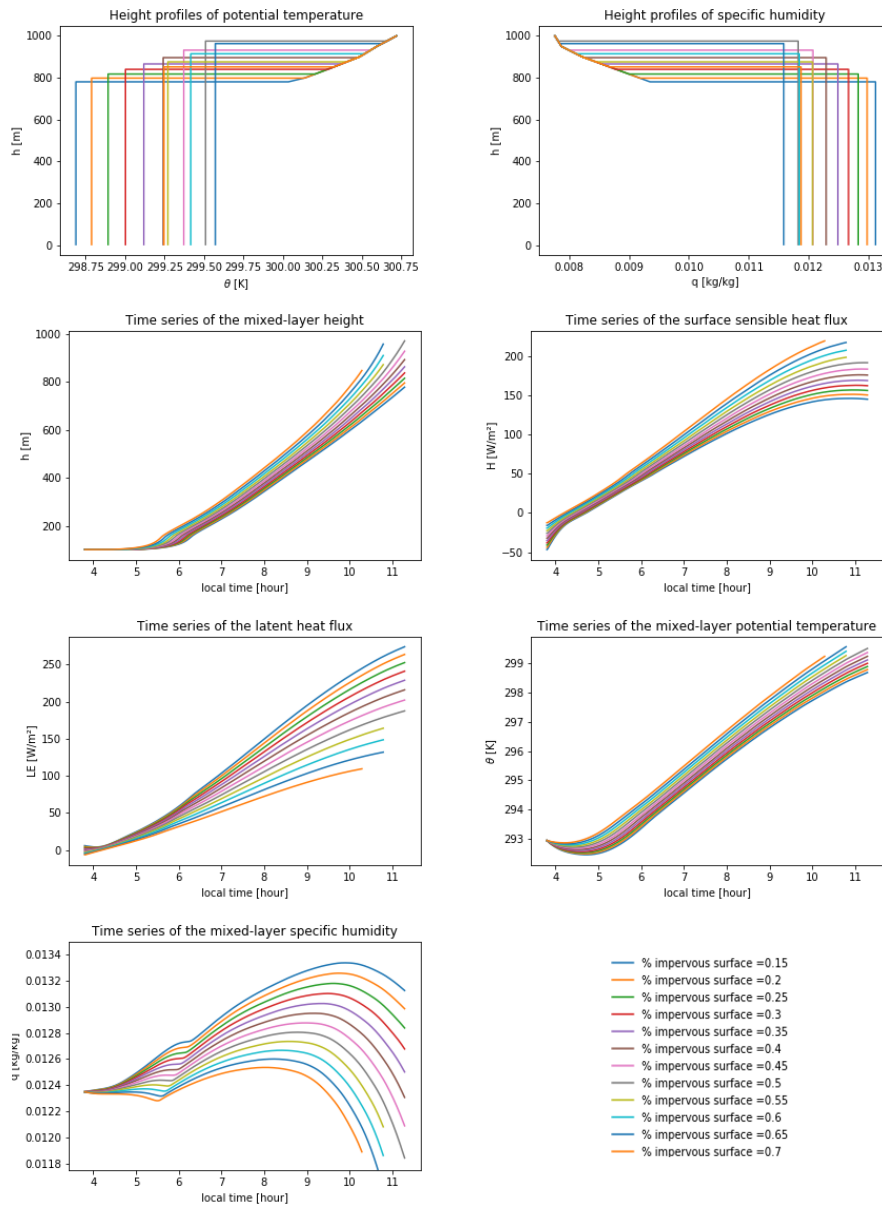


Figure 5.16: The height profiles and the time series of several variables are given for simulations with different values of percentage covered by impervious surface (keeping the fraction of buildings constant). θ : potential temperature; q : specific humidity; h : height; H : sensible heat flux; LE : latent heat flux.

CHAPTER 6

CONCLUSION

The aim of this thesis was to investigate how urban features impact the changes in the mixed layer during the course of the day. To that end, the ABL model CLASS was adjusted to take urban characteristics into account and use MTP data as initialisation. Then, data from Moscow was used to test the hypothesis that incorporating urban features in the framework CLASS4GL, which can simulate how feedbacks between land surface and atmospheric conditions lead to changes through a diurnal cycle of the mixed-layer features, improves the accuracy of the simulations with respect to the changes in height, potential temperature and specific humidity of the mixed layer during the course of the day. In addition, it was tested whether the use of high resolution MTP data as initialisation gives reliable prediction of the diurnal dynamics of the mixed layer. The first results are promising but more research is needed. From the first simulations outlined in this thesis the conclusion can be made that the performance of the model might depend, amongst others on the background weather conditions. CLASS4GL_urban in general outperforms the original CLASS4GL framework for urban areas, but the differences are not always large. Also the focus should be on the trends of the profile through time that the model generates and not on the absolute values. We can prudently conclude that CLASS4GL_urban provides added value to CLASS4GL when the goal is to understand climate development in urban areas. There is, however, a need for more research. Amongst others, the model needs to be validated with more datasets, ideally in settings in which as many as possible relevant parameters can be based on observations of sufficient resolution. Importantly, the results of this thesis also point to some inconsistencies that need further investigation, such as the implementation of the ground heat flux and the mismatch of the energy balance in CLASS4GL_urban. Once the model is validated and a general idea of the performance and drawbacks is obtained, its application could give additional insight into the main drivers of urban heatwaves. As such, this model could help inform the design of strategies to reduce the negative consequences of heatwaves.



CHAPTER 7

FUTURE RESEARCH

The previous chapter gave a first explorative analysis of the effect of urban characteristics on the ABL evolution with the CLASS model. More research and validation should happen to study its potential, and its usefulness to analyse the main drives during a heatwave in urban areas. I invested a lot of time in implementing the urban parametrisation of the model in CLASS and in adapting the model so that it is able to work with MTP data in addition to balloon sounding data. Because of this the time available to also engage in a thorough validation was limited. Right now the model still needs some more improvements and validation:

- First of all, only a few days have been looked at. Yet model performance depends a lot on the atmospheric conditions. So one may anticipate a lot of variation from day to day. Therefore, to be able to conclude if the urban parametrisation of the model provides added value it should be applied on many more days, and then the average error should be determined and compared between CLASS4GL_urban and CLASS4GL.
- The model was adapted so it can be initialised with MTP data. But the MTP data only go up to a height of 1000m. This means that the model is not able to run for an entire day, because it stops when the ABL becomes higher than 1000m. Some adjustments could be made to let the model run an entire day. For example the initialisation data could be linearly extrapolated before being bias-corrected and before they would be entered in the model.
- Also the initialisation is still not optimal. The specific humidity and wind values obtained from ERA-interim are, for instance, probably not representative for small scale urban areas. The method to calculate the initial height of the ABL can also be adjusted. For example, instead of basing it on the calculation of the Richardson bulk number exceeding a critical value $RiBc$ (Wouters et al., 2019). Searching for the maximal gradient of the potential temperature takes place could give a better match to the high-resolution mixed-layer fits.
- The method for validation can be further optimised. Currently, the average of the observations is taken based on the height of the mixed-layer as determined by the model. But when doing, this the assumption is made that the model

correctly predicts the mixed-layer height. This is not always the case. A solution can be to initialise the model with new observations every 30 minutes, and use the thus predicted height of the mixed layer at each time step.

- There are also data available for two other places in the megacity Moscow, more located in the suburban area. It could be interesting to simulate the diurnal evolution of the ABL based on these profiles and see if the characteristics are different for the different parts of the city. Depending on the wind direction, it would also be interesting to check whether downwind suburban areas are more influenced by atmosphere events in the center of Moscow.
- At this moment the parameters that define the LCZ 5 are obtained from literature, and for quite some parameters we need to rely on ERA-interim data, which have a low resolution. In future it will be important to try to replace as many of these input data by observations on the city of interest. Such data does certainly exist for quite a number of cities. Using observation based values for most parameters will likely lead to more accurate predictions of the actual values rather than just the trends over time.
- In this thesis LCZ 5 was used to describe Moscow. Ideally all the urban parameters should be defined by observations in stead of general values from literature, especially if the goal is to investigate the effects of urban characteristics on the temporal evolution of the mixed-layer features of that specific area.
- Here LCZ 5 is used without incorporating any information of the neighbourhood. Although when looking at Figure 2.3 Moscow is a heterogeneous city, thus by only taking LCZ 5 into account some important information could get lost. Some methods have already been developed to also include information of the neighbourhood, this could improve the accuracy (Verdonck et al., 2017).
- Currently the cloud cover during the day is kept constant in the model during the daily cycle. As suggested by the data on the first of June, this might lead to wrong predictions of the difference in potential temperature between a height of 1000m and the mixed layer over time. So adjustment of the model so that it can take changes in cloud cover through time (e.g. every hour) into account could improve the accuracy.
- A comparison of the diurnal changes of the mixed-layer features between the different LCZs could be made.
- Now the sensitivity analysis was only done qualitatively but doing more detailed experiments on what parameters have an influence on perturbation, e.g. by doing a more quantitative analysis could give additional insights.
- If the necessary data of a heatwave would be available for a megacity, the different drivers of such a heatwave could be investigated and which parameters

are most important in the evolution of the ABL under these specific conditions could be delineated.

- Some elements are not yet included in the model or were turned off in my analyses, such as air pollution (aerosols), large-scale advection. These could change the diurnal evolution of the ABL.
- In calculating the validation measures the spin-up period was also taken into account, while this should be left out because at these moments the model is by definition not yet accurate. But if I had done this for the data that were available, then not so many data points would be have been left to analyse.
- More research is needed on how the energy balance is implemented in the model. What are the consequences of leaving out the storage (probably this just implies that during daytime the surface sensible heat fluxes and latent heat fluxes will be overestimated) in the original model, using the hysteresis model and leaving out the ground flux in the urban parametrisation model. It is disturbing that the current runs of the urban parametrisation of the model results in (slight) deviations of the law of conservation of energy.



BIBLIOGRAPHY

- ATTEX, L. R. (2013). Mtp-5he. <http://attex.net/EN/mtp5.php>.
- Baccini, M., Biggeri, A., Accetta, G., Kosatsky, T., Katsouyanni, K., Analitis, A., Anderson, H. R., Bisanti, L., D'ippoliti, D., Danova, J., et al. (2008). Heat effects on mortality in 15 european cities. *Epidemiology*, 19:711–719.
- Bador, M., Terray, L., Boe, J., Somot, S., Alias, A., Gibelin, A.-L., and Dubuisson, B. (2017). Future summer mega-heatwave and record-breaking temperatures in a warmer france climate. *Environmental Research Letters*, 12:074025.
- Balchin, W. G. V. and Pye, N. (1947). A micro-climatological investigation of bath and the surrounding district. *Quarterly Journal of the Royal Meteorological Society*, 73:297–323.
- Barriopedro, D., Fischer, E. M., Luterbacher, J., Trigo, R. M., and García-Herrera, R. (2011). The hot summer of 2010: redrawing the temperature record map of europe. *Science*, 332:220–224.
- Boekee, J., Steeneveld, G.-J., and de Arellano, J. V.-G. (2018). Convective cloud cover above cities of contrasting morphology. Master's thesis, Wageningen university.
- Chai, T. and Draxler, R. R. (2014). Root mean square error (rmse) or mean absolute error (mae)?—arguments against avoiding rmse in the literature. *Geoscientific model development*, 7:1247–1250.
- Changnon, S. A. (1989). Midwestern drought conditions-1988. *Drought and Climate Change, Miscellaneous papers on the 1988 Drought and the issue of future climate change*, pages 17–40.
- Chapin, F. S., Matson, P. A., and Mooney, H. A. (2002). *Terrestrial Water and Energy Balance*. Springer.
- Cox, W. (2018). *Demographia World Urban Areas 14th Annual edition*. Wendell Cox Consultancy, Belleville, Illinois: Wendel Cox Consultancy, 14th edition.
- Dee, D. P., Uppala, S., Simmons, A., Berrisford, P., Poli, P., Kobayashi, S., Andrae, U., Balsameda, M., Balsamo, G., Bauer, d. P., et al. (2011). The era-interim reanalysis:

- Configuration and performance of the data assimilation system. *Quarterly Journal of the royal meteorological society*, 137:553–597.
- Droste, A. M., Steeneveld, G.-J., and Holtslag, A. A. (2018). Introducing the urban wind island effect. *Environmental research letters*, 13(9):094007.
- Dugord, P.-A., Lauf, S., Schuster, C., and Kleinschmit, B. (2014). Land use patterns, temperature distribution, and potential heat stress risk—the case study berlin, germany. *Computers, Environment and Urban Systems*, 48:86–98.
- Dupont, E., Menut, L., Carissimo, B., Pelon, J., and Flamant, P. (1999). Comparison between the atmospheric boundary layer in paris and its rural suburbs during the eclap experiment. *Atmospheric Environment*, 33:979–994.
- Durre, I., Vose, R. S., and Wuertz, D. B. (2006). Overview of the integrated global radiosonde archive. *Journal of Climate*, 19:53–68.
- Fischer, E. M. (2014). Climate science: Autopsy of two mega-heatwaves. *Nature Geoscience*, 7:332–333.
- Fischer, E. M., Oleson, K. W., and Lawrence, D. M. (2012). Contrasting urban and rural heat stress responses to climate change. *Geophysical research letters*, 39:419–420.
- Grimmond, C., Cleugh, H., and Oke, T. (1991). An objective urban heat storage model and its comparison with other schemes. *Atmospheric Environment. Part B. Urban Atmosphere*, 25:311–326.
- Grimmond, C. S. B., Blackett, M., Best, M., Barlow, J., Baik, J., Belcher, S., Bohnenstengel, S., Calmet, I., Chen, F., Dandou, A., et al. (2010). The international urban energy balance models comparison project: first results from phase 1. *Journal of applied meteorology and climatology*, 49:1268–1292.
- Hansen, M. C., Townshend, J. R., DeFries, R. S., and Carroll, M. (2005). Estimation of tree cover using modis data at global, continental and regional/local scales. *International Journal of Remote Sensing*, 26:4359–4380.
- Hoag, H. (2014). Russian summer tops ‘universal’ heatwave index. *Nature*, 16. doi:10.1038/nature.2014.16250.
- Kadygrov, E., Vorobevo, E., Kuznetsove, I., Folomeev, V., and E., M., editors (2009). *Application of Microwave Radiometry for Urban Heat Island Study*, Vols I and II, Moscow. PIERS.
- Kleerekoper, L., Van Esch, M., and Salcedo, T. B. (2012). How to make a city climate-proof, addressing the urban heat island effect. *Resources, Conservation and Recycling*, 64:30–38.

BIBLIOGRAPHY

- Liu, H. and Weng, Q. (2008). Seasonal variations in the relationship between landscape pattern and land surface temperature in indianapolis, usa. *Environmental Monitoring and Assessment*, 144:199–219.
- Lokoshchenko (2014). Urban ‘heat island’ in moscow. *Urban Climate*, 10:550–562.
- Lokoshchenko, M. A., Elansky, N. F., Belikov, I. B., Skorokhod, A. I., Semenova, N. V., Isaev, A. A., and Zvyagintsev, A. M. (2006). Some features of air pollution in moscow megapolis. *Proceedings of ICUC*, 6:104–107.
- Longxun, C., Wenqin, Z., Xiuji, Z., and Zijiang, Z. (2003). Characteristics of the heat island effect in shanghai and its possible mechanism. *Advances in Atmospheric Sciences*, 20:991–1001.
- Meehl, G. A. and Tebaldi, C. (2004). More intense, more frequent, and longer lasting heat waves in the 21st century. *Science*, 305:994–997.
- Miralles, D., Van Den Berg, M., Teuling, A., and De Jeu, R. (2012). Soil moisture-temperature coupling: A multiscale observational analysis. *Geophysical Research Letters*, 39:L21707. doi: 10.1029/2012GL053703.
- Miralles, D. G., Gentine, P., Seneviratne, S. I., and Teuling, A. J. (2019). Land-atmospheric feedbacks during droughts and heatwaves: state of the science and current challenges. *Annals of the New York Academy of Sciences*, 1436:19–35.
- Miralles, D. G., Teuling, A. J., Van Heerwaarden, C. C., and de Arellano, J. V.-G. (2014). Mega-heatwave temperatures due to combined soil desiccation and atmospheric heat accumulation. *Nature Geoscience*, 7:345.
- Moriwaki, R., WATANABE, K., and Morimoto, K. (2013). Urban dry island phenomenon and its impact on cloud base level. *Journal of JSCE*, 1:521–529.
- Murari, K. K., Ghosh, S., Patwardhan, A., Daly, E., and Salvi, K. (2015). Intensification of future severe heat waves in india and their effect on heat stress and mortality. *Regional Environmental Change*, 15:569–579.
- Näyhä, S. (2007). Heat mortality in finland in the 2000s. *International journal of circumpolar health*, 66:418–424.
- NOAA, N. C. f. E. I. (2010). State of the climate: Global hazards for august 2010. <https://www.ncdc.noaa.gov/sotc/global/201008>.
- Oke, T. R. (1982). The energetic basis of the urban heat island. *Quarterly Journal of the Royal Meteorological Society*, 108:1–24.
- Oke, T. R., Mills, G., and Voogt, J. (2017). *Urban climates*. Cambridge University Press.

- Oleson, K. (2012). Contrasts between urban and rural climate in ccsm4 cmip5 climate change scenarios. *Journal of Climate*, 25:1390–1412.
- Pielke, R. A. (2005). Land use and climate change. *Science*, 310:1625–1626.
- Pietersen, H. P., Vilà-Guerau de Arellano, J., Augustin, P., van de Boer, A., de Coster, O., Delbarre, H., Durand, P., Fourmentin, M., Gioli, B., Hartogensis, O., et al. (2015). Study of a prototypical convective boundary layer observed during bllast: contributions by large-scale forcings. *Atmospheric Chemistry and Physics*, 15:4241–4257.
- Population, R. (2019). Population of cities in russia (2019). <http://worldpopulationreview.com/countries/russia-population/cities/>.
- Robine, J.-M., Cheung, S. L. K., Le Roy, S., Van Oyen, H., Griffiths, C., Michel, J.-P., and Herrmann, F. R. (2008). Death toll exceeded 70,000 in europe during the summer of 2003. *Comptes rendus biologies*, 331:171–178.
- Russo, S., Sillmann, J., and Fischer, E. M. (2015). Top ten european heatwaves since 1950 and their occurrence in the coming decades. *Environmental Research Letters*, 10:124003. doi: <https://doi.org/10.1088/1748-9326/10/12/124003>.
- Samsonov, T. and Trigub, K. (2017). Towards computation of urban local climate zones (lcz) from openstreetmap data. In *Proceedings of the 14th International Conference on GeoComputation, Leeds, UK*, pages 4–7.
- Sánchez-Benítez, A., García-Herrera, R., Barriopedro, D., Sousa, P., and Trigo, R. (2018). June 2017: The earliest european summer mega-heatwave of reanalysis period. *Geophysical Research Letters*, 45:1955–1962.
- Seto, K. C., Güneralp, B., and Hutyrá, L. R. (2012). Global forecasts of urban expansion to 2030 and direct impacts on biodiversity and carbon pools. *Proceedings of the National Academy of Sciences*, 109:16083–16088.
- Sillmann, J., Thorarinsdottir, T., Keenlyside, N., Schaller, N., Alexander, L. V., Hegerl, G., Seneviratne, S. I., Vautard, R., Zhang, X., and Zwiers, F. W. (2017). Understanding, modeling and predicting weather and climate extremes: Challenges and opportunities. *Weather and climate extremes*, 18:65–74.
- Sisterson, D. L. and Dirks, R. A. (1978). Structure of the daytime urban moisture field. *Atmospheric Environment*, 12:1943–1949.
- Skamarock, W. C., Klemp, J. B., Dudhia, J., Gill, D. O., Barker, D. M., Duda, M. G., Huang, X.-Y., Wang, W., and Powers, J. G. (2008). A description of the advanced research wrf version 3, ncar technical note. *National Center for Atmospheric Research, Boulder, Colorado, USA*.

BIBLIOGRAPHY

- Sparks, N. and Toumi, R. (2015). Numerical simulations of daytime temperature and humidity crossover effects in london. *Boundary-layer meteorology*, 154:101–117.
- Stewart, I. D. and Oke, T. R. (2012). Local climate zones for urban temperature studies. *Bulletin of the American Meteorological Society*, 93:1879–1900.
- Tan, J., Zheng, Y., Tang, X., Guo, C., Li, L., Song, G., Zhen, X., Yuan, D., Kalkstein, A. J., Li, F., et al. (2010). The urban heat island and its impact on heat waves and human health in shanghai. *International journal of biometeorology*, 54:75–84.
- Taylor, R. (1990). Interpretation of the correlation coefficient: a basic review. *Journal of diagnostic medical sonography*, 6:35–39.
- Theeuwes, N. E., Steeneveld, G.-J., Ronda, R. J., Rotach, M. W., and Holtslag, A. A. (2015). Cool city mornings by urban heat. *Environmental Research Letters*, 10:114022. doi: <https://doi.org/10.1088/1748-9326/10/11/114022>.
- Tong, S., FitzGerald, G., Wang, X.-Y., Aitken, P., Tippet, V., Chen, D., Wang, X., and Guo, Y. (2015). Exploration of the health risk-based definition for heatwave: A multi-city study. *Environmental research*, 142:696–702.
- UN (2018). *World urbanization prospects: The 2018 revision*. United Nationsy.
- van Heerwaarden, C. and Teuling, A. J. (2014). Disentangling the response of forest and grassland energy exchange to heatwaves under idealized land-atmosphere coupling. *Biogeosciences*, 11:6159–6171.
- Van Heerwaarden, C. C., Vilà-Guerau de Arellano, J., Gounou, A., Guichard, F., and Couvreux, F. (2010). Understanding the daily cycle of evapotranspiration: A method to quantify the influence of forcings and feedbacks. *Journal of Hydrometeorology*, 11:1405–1422.
- Varentsov, M., Konstantinov, P., and Samsonov, T. (2017). Mesoscale modelling of the summer climate response of moscow metropolitan area to urban expansion. In *IOP Conference Series: Earth and Environmental Science*, volume 96, page 012009. IOP Publishing.
- Varentsov, M., Wouters, H., Platonov, V., and Konstantinov, P. (2018). Megacity-induced mesoclimatic effects in the lower atmosphere: A modeling study for multiple summers over moscow, russia. *Atmosphere*, 9:50.
- Verdonck, M.-L., Demuzere, M., Hooyberghs, H., Beck, C., Cyrus, J., Schneider, A., Dewulf, R., and Van Coillie, F. (2018). The potential of local climate zones maps as a heat stress assessment tool, supported by simulated air temperature data. *Landscape and urban planning*, 178:183–197.

- Verdonck, M.-L., Okujeni, A., van der Linden, S., Demuzere, M., De Wulf, R., and Van Coillie, F. (2017). Influence of neighbourhood information on 'local climate zone' mapping in heterogeneous cities. *International Journal of Applied Earth Observation and Geoinformation*, 62:102–113.
- Vilà-Guerau de Arellano, J., Heerwaarden, C. V., van Stratum, B., and Dries, K. V. D. (2015). *Atmospheric boundary layer: Integrating air chemistry and land interactions*. Cambridge University Press, Cambridge, UK.
- Voogt, J. A. and Oke, T. R. (2003). Thermal remote sensing of urban climates. *Remote sensing of environment*, 86:370–384.
- Ward, K., Lauf, S., Kleinschmit, B., and Endlicher, W. (2016). Heat waves and urban heat islands in europe: A review of relevant drivers. *Science of the Total Environment*, 569:527–539.
- Wilby, R. L. (2003). Past and projected trends in london's urban heat island. *Weather*, 58:251–260.
- Williams, J., Crowley, J., Fischer, H., Harder, H., Martinez, M., Petaja, T., Rinne, J., Back, J., Boy, M., Dal Maso, M., et al. (2011). The summertime boreal forest field measurement intensive (HUMPPA-COPEC-2010): an overview of meteorological and chemical influences. *Atmospheric Chemistry and Physics*, 11:10599–10618.
- Willmott, C. J. and Matsuura, K. (2005). Advantages of the mean absolute error (mae) over the root mean square error (rmse) in assessing average model performance. *Climate research*, 30:79–82.
- Wouters, H., De Ridder, K., Poelmans, L., Willems, P., Brouwers, J., Hosseinzadehtalaei, P., Tabari, H., Vanden Broucke, S., van Lipzig, N. P., and Demuzere, M. (2017). Heat stress increase under climate change twice as large in cities as in rural areas: A study for a densely populated midlatitude maritime region. *Geophysical Research Letters*, 44:8997–9007.
- Wouters, H., Petrova, I. Y., van Heerwaarden, C. C., de Arellano, J. V.-G., Teuling, A. J., Meulenbergh, V., Santanello, J. A., and Miralles, D. G. (2019). Atmospheric boundary layer dynamics from balloon soundings worldwide: Class4gl v1. 0. *Geoscientific Model Development*, 12:2139–2153.
- Wouters, H., Ridder, K. D., Demuzere, M., Lauwaet, D., and Van Lipzig, N. (2013). The diurnal evolution of the urban heat island of paris: a model-based case study during summer 2006. *Atmospheric Chemistry and Physics*, 13:8525–8541.
- Yushkov, V. (2014). What can be measured by the temperature profiler. *Russian Meteorology and Hydrology*, 39:838–846.

BIBLIOGRAPHY

Zhao, L., Oppenheimer, M., Zhu, Q., Baldwin, J. W., Ebi, K. L., Bou-Zeid, E., Guan, K., and Liu, X. (2018). Interactions between urban heat islands and heat waves. *Environmental research letters*, 13:034003.

APPENDIX A


















Built types	Definition	Land cover types	Definition
 <p>1. Compact high-rise</p>	Dense mix of tall buildings to tens of stories. Few or no trees. Land cover mostly paved. Concrete, steel, stone, and glass construction materials.	 <p>A. Dense trees</p>	Heavily wooded landscape of deciduous and/or evergreen trees. Land cover mostly pervious (low plants). Zone function is natural forest, tree cultivation, or urban park.
 <p>2. Compact midrise</p>	Dense mix of midrise buildings (3–9 stories). Few or no trees. Land cover mostly paved. Stone, brick, tile, and concrete construction materials.	 <p>B. Scattered trees</p>	Lightly wooded landscape of deciduous and/or evergreen trees. Land cover mostly pervious (low plants). Zone function is natural forest, tree cultivation, or urban park.
 <p>3. Compact low-rise</p>	Dense mix of low-rise buildings (1–3 stories). Few or no trees. Land cover mostly paved. Stone, brick, tile, and concrete construction materials.	 <p>C. Bush, scrub</p>	Open arrangement of bushes, shrubs, and short, woody trees. Land cover mostly pervious (bare soil or sand). Zone function is natural scrubland or agriculture.
 <p>4. Open high-rise</p>	Open arrangement of tall buildings to tens of stories. Abundance of pervious land cover (low plants, scattered trees). Concrete, steel, stone, and glass construction materials.	 <p>D. Low plants</p>	Featureless landscape of grass or herbaceous plants/crops. Few or no trees. Zone function is natural grassland, agriculture, or urban park.
 <p>5. Open midrise</p>	Open arrangement of midrise buildings (3–9 stories). Abundance of pervious land cover (low plants, scattered trees). Concrete, steel, stone, and glass construction materials.	 <p>E. Bare rock or paved</p>	Featureless landscape of rock or paved cover. Few or no trees or plants. Zone function is natural desert (rock) or urban transportation.
 <p>6. Open low-rise</p>	Open arrangement of low-rise buildings (1–3 stories). Abundance of pervious land cover (low plants, scattered trees). Wood, brick, stone, tile, and concrete construction materials.	 <p>F. Bare soil or sand</p>	Featureless landscape of soil or sand cover. Few or no trees or plants. Zone function is natural desert or agriculture.
 <p>7. Lightweight low-rise</p>	Dense mix of single-story buildings. Few or no trees. Land cover mostly hard-packed. Lightweight construction materials (e.g., wood, thatch, corrugated metal).	 <p>G. Water</p>	Large, open water bodies such as seas and lakes, or small bodies such as rivers, reservoirs, and lagoons.
 <p>8. Large low-rise</p>	Open arrangement of large low-rise buildings (1–3 stories). Few or no trees. Land cover mostly paved. Steel, concrete, metal, and stone construction materials.	VARIABLE LAND COVER PROPERTIES	
 <p>9. Sparsely built</p>	Sparse arrangement of small or medium-sized buildings in a natural setting. Abundance of pervious land cover (low plants, scattered trees).	b. bare trees	Leafless deciduous trees (e.g., winter). Increased sky view factor. Reduced albedo.
 <p>10. Heavy industry</p>	Low-rise and midrise industrial structures (towers, tanks, stacks). Few or no trees. Land cover mostly paved or hard-packed. Metal, steel, and concrete construction materials.	s. snow cover	Snow cover >10 cm in depth. Low admittance. High albedo.
		d. dry ground	Parched soil. Low admittance. Large Bowen ratio. Increased albedo.
		w. wet ground	Waterlogged soil. High admittance. Small Bowen ratio. Reduced albedo.

Figure A.1: An overview of the different Local Climate Zones (LCZs) (Stewart and Oke, 2012).



APPENDIX B



Figure B.1: An overview of the characteristics of LCZ 2, ‘compact mid-rise’ (Stewart and Oke, 2012), one of the key LCZs of Moscow.

LCZ

OPEN HIGH-RISE

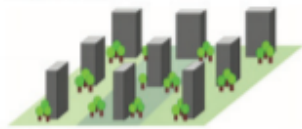
4

DEFINITION

Form: Tall buildings to tens of stories, set in open, geometric arrangement. Buildings typically uniform in height, width, and spacing. Sky view from ground level significantly reduced. Concrete, steel, and glass construction materials. Scattered trees and abundant plant cover. Moderate-low space heating/cooling demand. Moderate traffic flow. **Function:** Residential (apartment blocks, high-rise housing estates, multistorey tenements). **Location:** Periphery. Densely populated cities. **Correspondence:** Do2 (Ellefsen 1990/91).

ILLUSTRATION

High angle



Low level



PROPERTIES

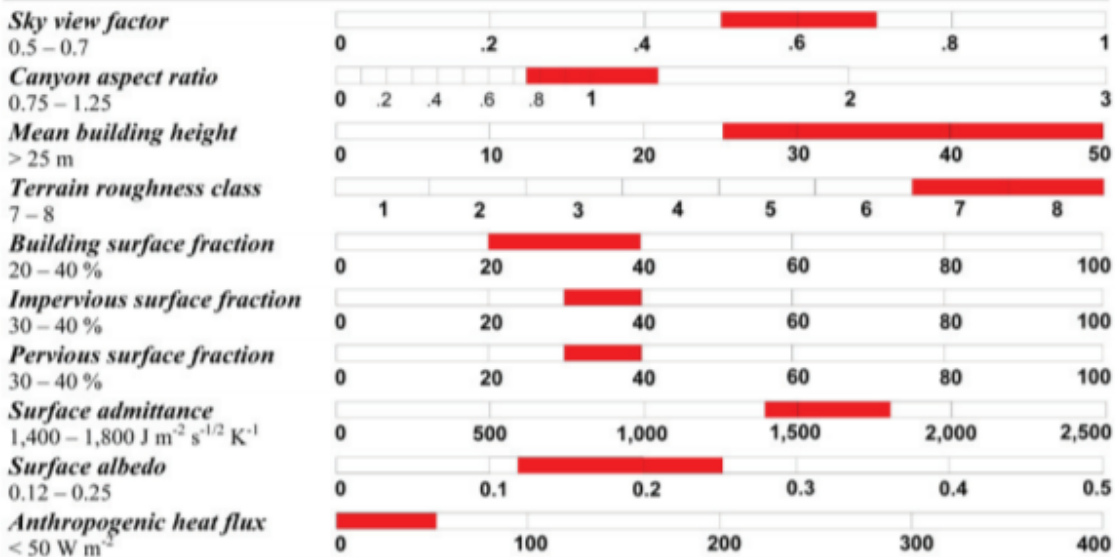


Figure B.2: An overview of the characteristics of LCZ 4, ‘open high-rise’ (Stewart and Oke, 2012), one of the key LCZs of Moscow.



Figure B.3: An overview of the characteristics of LCZ 5, ‘open mid-rise’ (Stewart and Oke, 2012), one of the key LCZs of Moscow.



APPENDIX C

Time (UTC)	Anthropogenic fluxes	UHI intensity
0	0.16	0
1	0.13	0.015
2	0.08	0.035
3	0.07	0.062
4	0.08	0.09
5	0.26	0.0188754
6	0.67	0.35
7	0.99	0.6
8	0.89	0.868521
9	0.79	0.968531
10	0.74	1
11	0.73	0.94
12	0.75	0.88
13	0.76	0.78
14	0.82	0.71
15	0.9	0.64
16	1	0.59
17	0.95	0.52
18	0.68	0.46
19	0.61	0.32
20	0.53	0.15
21	0.35	0.1
22	0.21	0.06
23	0.18	0.045

Table C.1: Factors used to include the diurnal variation of the UHI (Oke, 1982) and the anthropogenic fluxes of heat and moisture (Skamarock et al., 2008).



APPENDIX D

CODE

In Figure D.1 the different files which were adapted in this thesis are shown. Also a script was written to implement the bias-correction (see below). The code can be retrieved on request.

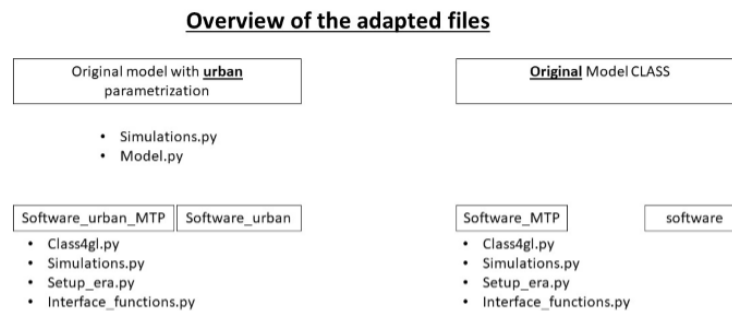


Figure D.1: An overview of the different files that were adapted or created in this thesis.

Bias-correction MTP data using data from ERA-interim

```
import pandas as pd
import numpy as np
import matplotlib.pyplot as plt
import yaml

from pandas import ExcelWriter
from pandas import ExcelFile

#01/06

ini_era_01 = pd.read_excel('ERA/profiles_ERANOAC_01_27730record_yaml_ini.xlsx')

#obs

obs = pd.read_excel('MTP_dtheta/input_MTP/MSU/01_06/01_06_MSU_4am.xls', header = None)
actual_T = obs.iloc[:,1].values
h_obs = obs.iloc[:,0].values

#manueel aanpassen actuelee temperatuur naar potentieel

q = 0

cp = 1005. # specific heat of dry air [J kg-1 K-1]
Rd = 287. # gas constant for dry air [J kg-1 K-1]
Rv = 461.5 # gas constant for moist air [J kg-1 K-1]

p = np.zeros(len(actual_T))
R = Rd*(1.-q)+ Rv*q
P0 = 100000
p[0] = P0

#rho op zeeniveau

rho = 1.293

for j in range(1,len(p)):

    p[j] = p[j-1] - rho*9.81*(h_obs[j]-h_obs[j-1])

#transform to potential temperature, both pressures are in Pa
```

```

theta = actual_T * (P0/p)**(R/cp)
#gem van 600-1000 = h nemen een het verschil optellen bij MTP
z_ = np.linspace(600,1000,9)
ERA_gem_01 = np.interp(z_,ini_era_01['z'].values,ini_era_01['theta'].values)
obs_gem_01 = theta[12::]
verschil_01 = np.mean(ERA_gem_01 - obs_gem_01)
obs_new_01 = theta+verschil_01
#wite to excel so can use as new input
theta_obs_new = theta + verschil_01
actual_new = theta_obs_new/((P0/p)**(R/cp))
df_prof = pd.DataFrame({'h':h_obs, 'actual T':actual_new})
writer_prof = ExcelWriter('new_input_MTP_01_06_dtheta.xlsx')
df_prof.to_excel(writer_prof,'Sheet1',index=False, header = False)
writer_prof.save()

#####
#####
#15/06
ini_era_15 = pd.read_excel('ERA/profiles_ERANOAC_15_27730record_yaml_ini.xlsx')
#obs
obs = pd.read_excel('MTP_dtheta/input_MTP/MSU/15_06/15_06_MSU_4am.xls', header = None)
actual_T = obs.iloc[:,1].values
h_obs = obs.iloc[:,0].values
#manueel aanpassen actuelee temperatuur naar potentieel
q = 0
cp    = 1005.      # specific heat of dry air [J kg-1 K-1]
Rd    = 287.      # gas constant for dry air [J kg-1 K-1]
Rv    = 461.5     # gas constant for moist air [J kg-1 K-1]
p = np.zeros(len(actual_T))
R = Rd*(1.-q) + Rv*q
P0 = 100000

```

```

p[0] = P0
#rho op zeeniveau
rho = 1.293
for j in range(1,len(p)):
    p[j] = p[j-1] - rho*9.81*(h_obs[j]-h_obs[j-1])

#transform to potential temperature, both pressures are in Pa
theta = actual_T * (P0/p)**(R/cp)

z_ = np.linspace(600,1000,9)
ERA_gem_15 = np.interp(z_,ini_era_15['z'].values,ini_era_15['theta'].values)
obs_gem_15 = theta[12::]
verschil_15 = np.mean(ERA_gem_15 - obs_gem_15)
obs_new_15 = theta+verschil_15
#
#wite to excel so can use as new input
theta_obs_new = theta + verschil_15
actual_new = theta_obs_new/((P0/p)**(R/cp))
df_prof = pd.DataFrame({'h':h_obs,'actual T': actual_new})
writer_prof = ExcelWriter('new_input_MTP_15_06_dtheta.xlsx')
df_prof.to_excel(writer_prof,'Sheet1',index=False,header = False)
writer_prof.save()

```

APPENDIX E

VALIDATION AND SCATTER

PLOTS

Here the figures are shown on of the height profile validation method, (method (1), section 4.3.2). Also the scatterplots are displayed, this for RJA_ORIG, RJA_URB, SUH_ORIG, SUH_URB.

E.1 RJA_ORIG

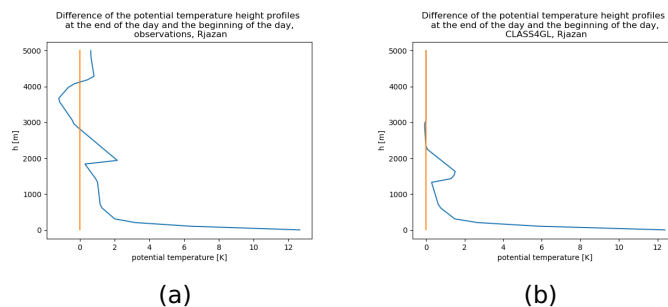


Figure E.1: This is the result when the potential temperature height profile at the beginning of the day is subtracted from the potential temperature profile at the end of the day (around 2.30pm). This for the observations (a) and results obtained using CLASS4GL (b) of Rjazan. The orange line indicates where the difference is zero. If the blue line is located left of the orange line than the initial potential temperature height profile has higher values than the potential temperature height profiles at the end of the day.

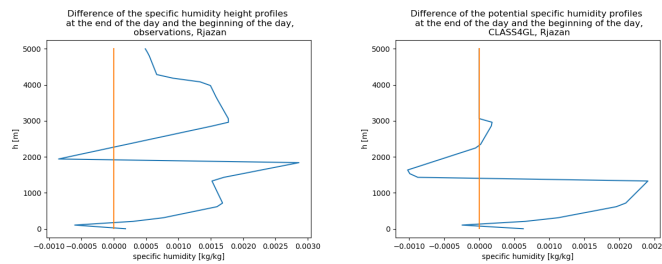
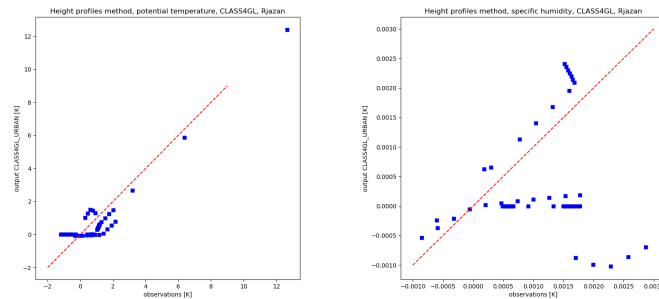


Figure E.2: This is the result when the specific moisture height profile at the beginning of the day is subtracted from the specific humidity profile at the end of the day (around 2.30pm). This for the observations (a) and results obtained using CLASS4GL (b) of Rjazan. The orange line indicates where the difference is zero. If the blue line is located left of the orange line than the initial specific moisture height profile has higher values than the specific humidity height profiles at the end of the day.



(a) Scatterplots of the observations and the simulations using CLASS4GL of the differences in the potential temperature height profiles at the end of the day and the beginning of the day for data of Rjazan on the 6th of August 1994. Every dot is a datapoint over height of the differences in potential temperature at the end and the beginning of the day.

(b) Scatterplots of the observations and the simulations using CLASS4GL of the differences in the specific humidity height profiles at the end of the day and the beginning of the day for data of Rjazan on the 6th of August 1994. Every dot is a datapoint over height of the differences in specific humidity at the end and the beginning of the day.

Figure E.3

E.2 RJA_URB

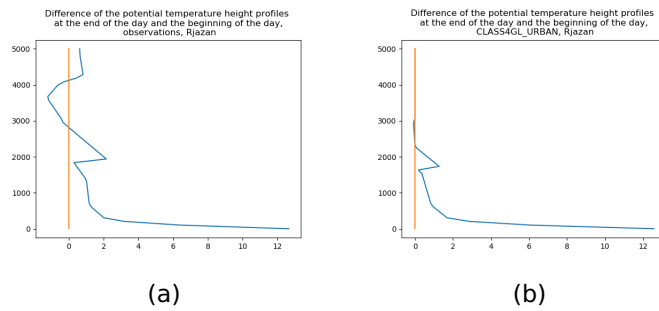


Figure E.4: This is the result when the potential temperature height profile at the beginning of the day is subtracted from the potential temperature profile at the end of the day (around 2.30pm). This for the observations (a) and results obtained using CLASS4GL_URBAN (b) of Rjazan. The orange line indicates where the difference is zero. If the blue line is located left of the orange line than the initial potential temperature height profile has higher values than the potential temperature height profiles at the end of the day.

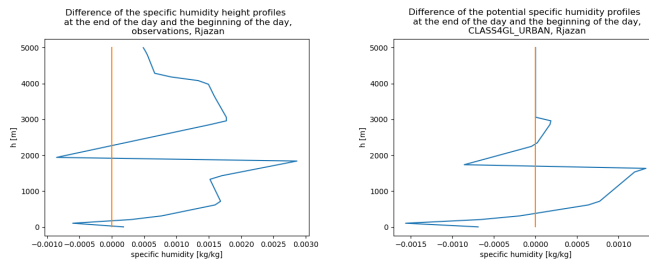
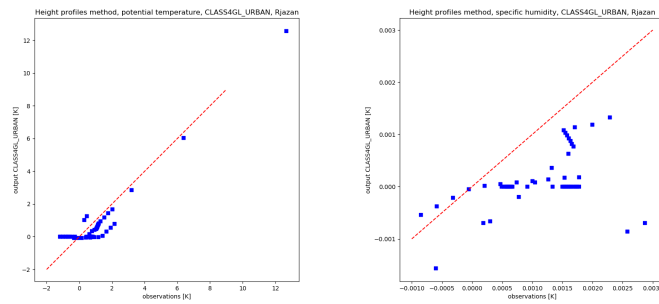


Figure E.5: This is the result when the specific moisture height profile at the beginning of the day is subtracted from the specific humidity profile at the end of the day (around 2.30pm). This for the observations (a) and results obtained using CLASS4GL_URBAN (b) of Rjazan. The orange line indicates where the difference is zero. If the blue line is located left of the orange line than the initial specific moisture height profile has higher values than the specific humidity height profiles at the end of the day.



(a) Scatterplots of the observations and the simulations using CLASS4GL_URBAN of the differences in the potential temperature height profiles at the end of the day and the beginning of the day for data of Rjazan on the 6th of August 1994. Every dot is a datapoint over height of the differences in potential temperature at the end and the beginning of the day.

(b) Scatterplots of the observations and the simulations using CLASS4GL_URBAN of the differences in the specific humidity height profiles at the end of the day and the beginning of the day for data of Rjazan on the 6th of August 1994. Every dot is a datapoint over height of the differences in specific humidity at the end and the beginning of the day.

Figure E.6

E.3 SUH_ORIG

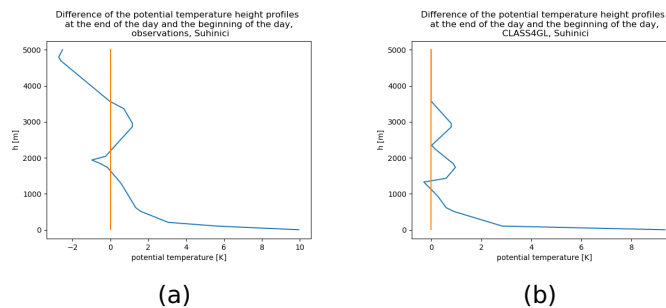


Figure E.7: This is the result when the potential temperature height profile at the beginning of the day is subtracted from the potential temperature profile at the end of the day (around 2.30pm). This for the observations (a) and results obtained using CLASS4GL (b) of Suhinici. The orange line indicates where the difference is zero. If the blue line is located left of the orange line than the initial potential temperature height profile has higher values than the potential temperature height profiles at the end of the day.

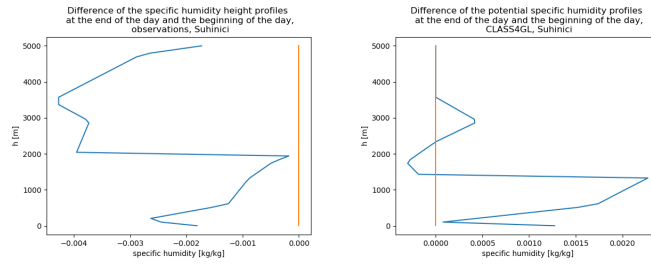
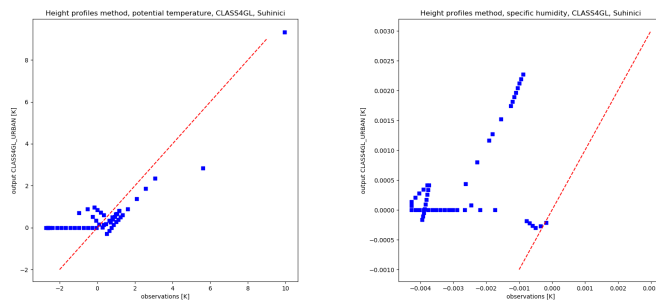


Figure E.8: This is the result when the specific moisture height profile at the beginning of the day is subtracted from the specific humidity profile at the end of the day (around 2.30pm). This for the observations (a) and results obtained using CLASS4GL (b) of Suhinici. The orange line indicates where the difference is zero. If the blue line is located left of the orange line than the initial specific moisture height profile has higher values than the specific humidity height profiles at the end of the day.



(a) Scatterplots of the observations and the simulations using CLASS4GL of the differences in the potential temperature height profiles at the end of the day and the beginning of the day for data of Suhinici on the 6th of August 1994. Every dot is a datapoint over height of the differences in potential temperature at the end and the beginning of the day.

(b) Scatterplots of the observations and the simulations using CLASS4GL of the differences in the specific humidity height profiles at the end of the day and the beginning of the day for data of Suhinici on the 6th of August 1994. Every dot is a datapoint over height of the differences in specific humidity at the end and the beginning of the day.

Figure E.9

E.4 SUH_URB

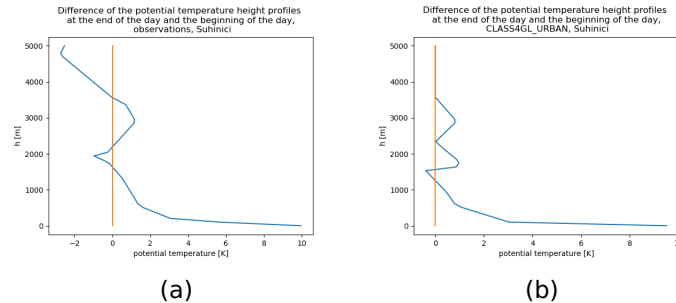


Figure E.10: This is the result when the potential temperature height profile at the beginning of the day is subtracted from the potential temperature profile at the end of the day (around 2.30pm). This for the observations (a) and results obtained using CLASS4GL_URBAN (b) of Suhinici. The orange line indicates where the difference is zero. If the blue line is located left of the orange line than the initial potential temperature height profile has higher values than the potential temperature height profiles at the end of the day.

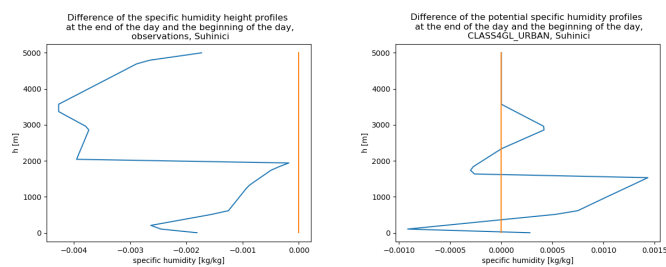
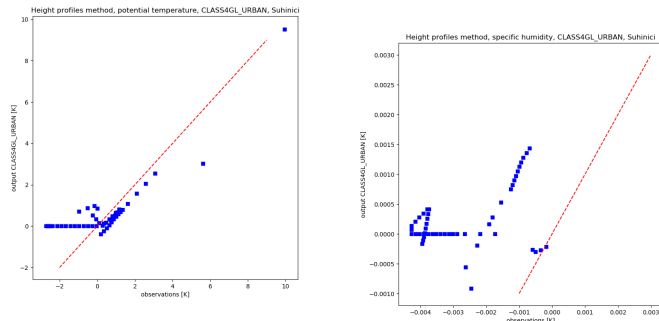


Figure E.11: This is the result when the specific moisture height profile at the beginning of the day is subtracted from the specific humidity profile at the end of the day (around 2.30pm). This for the observations (a) and results obtained using CLASS4GL_URBAN (b) of Suhinici. The orange line indicates where the difference is zero. If the blue line is located left of the orange line than the initial specific moisture height profile has higher values than the specific humidity height profiles at the end of the day.



(a) Scatterplots of the observations and the simulations using CLASS4GL_URBAN of the differences in the potential temperature height profiles at the end of the day and the beginning of the day for data of Suhinici on the 6th of August 1994. Every dot is a datapoint over height of the differences in potential temperature at the end and the beginning of the day.

(b) Scatterplots of the observations and the simulations using CLASS4GL_URBAN of the differences in the specific humidity height profiles at the end of the day and the beginning of the day for data of Suhinici on the 6th of August 1994. Every dot is a datapoint over height of the differences in specific humidity at the end and the beginning of the day.

Figure E.12

APPENDIX F

TIME SERIES ALL SCENARIOS

WHEN USING BALLOON

PROFILES AS INITIALISATION

DATA

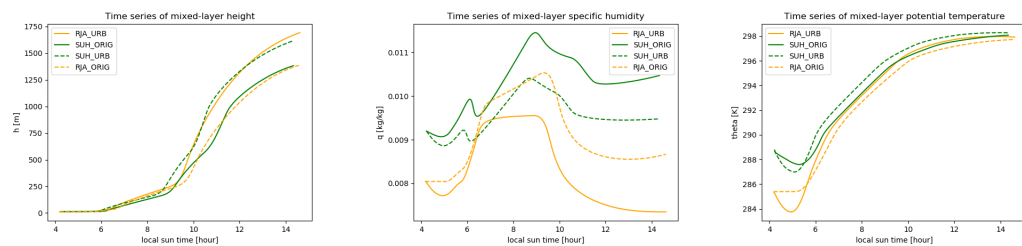


Figure F.1: Time series of the mixed-layer height (h), specific humidity (q) and potential temperature (θ) for RJA_ORIG (dashed orange line), RJA_URB (full orange line), SUH_ORIG (full green line) and SUH_URB (dashed green line). CLASS4GL_URBAN for Rjazan (RJA_URB, orange) and by the original model for Suhinici (SUH_ORIG, green).

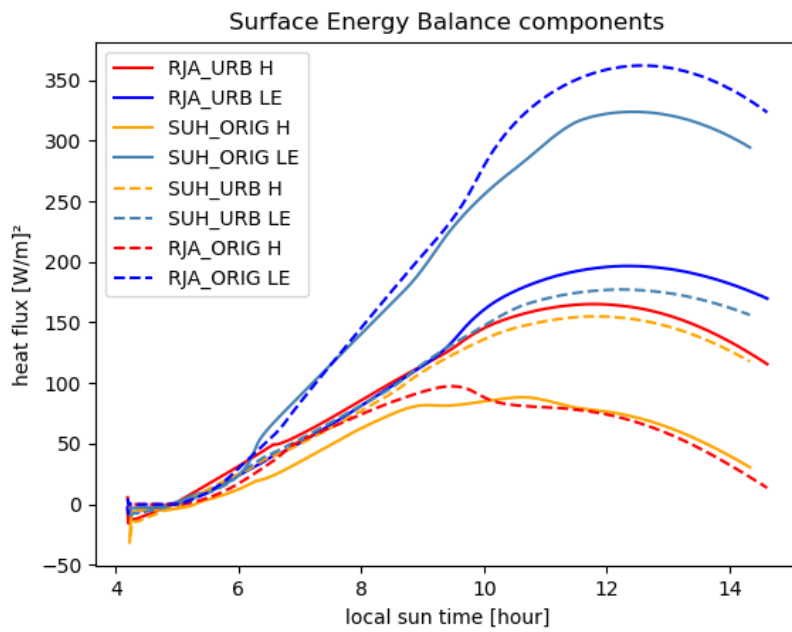


Figure F.2: Time series of the surface sensible heat flux (H, red or orange) and latent heat flux (LE, blue or light blue) for RJA_ORIG (dashed red and blue lines), RJA_URB (full red and blue lines), SUH_ORIG (full orange and light blue lines) and SUH_URB (dashed orange and light blue lines).

APPENDIX G

COMPARISON MTP DATA AND BIAS-CORRECTED MTP DATA

In Table G the values of the validation metrics are given when the MTP data is used as initialisation. When comparing these values with the values of Table 5.2 and Table 5.3 it can be noticed that the values are slightly better when the MTP data is bias-corrected with ERA-interim data.

Table G.1: The values for the different validation metrics when the model is initialised with bias-corrected MTP data for MSU from the 1st and the 15th of June 2015. For each validation metric the performance of the urban parameterization of the model (urban) as well as the performance of the original model are given. The values in red indicate which model has the best performance.

01/06 MSU				
	MAE	RMSE	CORR	BIAS
urban	0.68 K	0.79 K	0.88	-0.48 K
original	0.75	0.87 K	0.90	-0.53 K
15/06 MSU				
	MAE	RMSE	CORR	BIAS
urban	0.47 K	0.60 K	0.97	0.17 K
original	0.96 K	1.08 K	0.96	0.88 K



APPENDIX H

HEIGHT PROFILES OF POTENTIAL TEMPERATURE AND SPECIFIC HUMIDITY USING THE BIAS-CORRECTED MTP DATA AS INITIALISATION

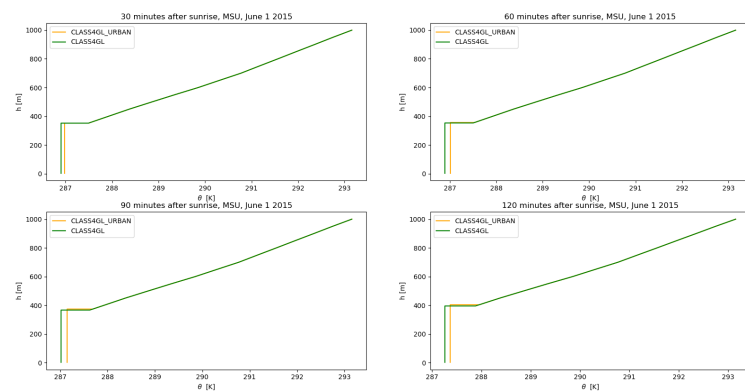


Figure H.1: Potential temperature height profiles 30min, 60min, 90min and 120 min after sunrise on June 1, 2015 in MSU. These height profiles are obtained using CLASS4GL_URBAN (orange) and CLASS4GL (green).

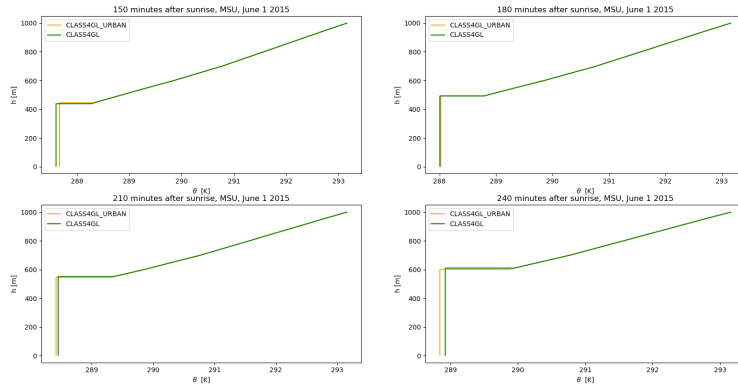


Figure H.2: Potential temperature height profiles 150min, 180min, 210min and 240 min after sunrise on June 1, 2015 in MSU. These height profiles are obtained using CLASS4GL_URBAN (orange) and CLASS4GL (green).

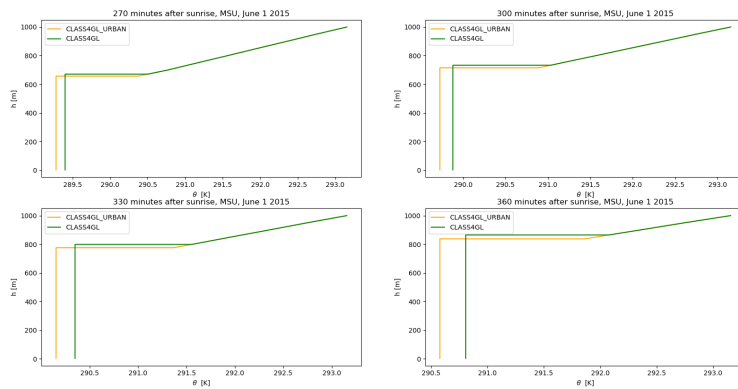


Figure H.3: Potential temperature height profiles 270min, 300min, 330min and 360 min after sunrise on June 1, 2015 in MSU. These height profiles are obtained using CLASS4GL_URBAN (orange) and CLASS4GL (green).

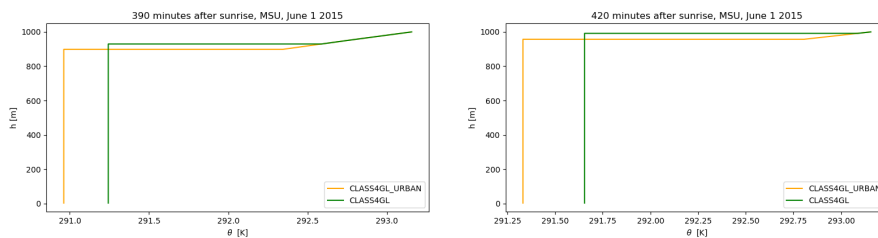


Figure H.4: Potential temperature height profiles 390min and 420min after sunrise on June 1, 2015 in MSU. These height profiles are obtained using CLASS4GL_URBAN (orange) and CLASS4GL (green).

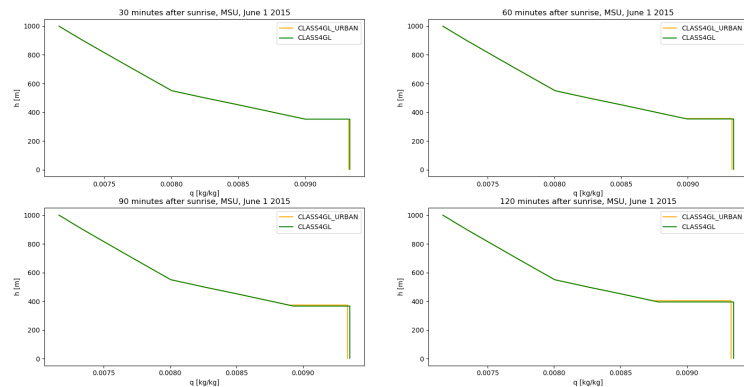


Figure H.5: Specific humidity height profiles 30min, 60min, 90min and 120 min after sunrise on June 1, 2015 in MSU. These height profiles are obtained using CLASS4GL_URBAN (orange) and CLASS4GL (green).

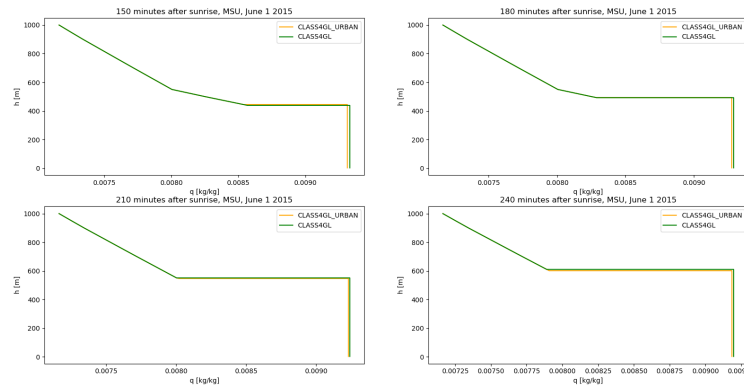


Figure H.6: Specific humidity height profiles 150min, 180min, 210min and 240 min after sunrise on June 1, 2015 in MSU. These height profiles are obtained using CLASS4GL_URBAN (orange) and CLASS4GL (green).

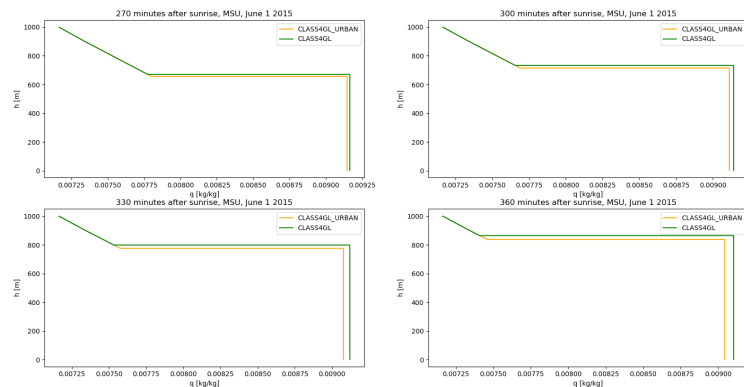


Figure H.7: Specific humidity height profiles 270min, 300min, 330min and 360 min after sunrise on June 1, 2015 in MSU. These height profiles are obtained using CLASS4GL_URBAN (orange) and CLASS4GL (green).

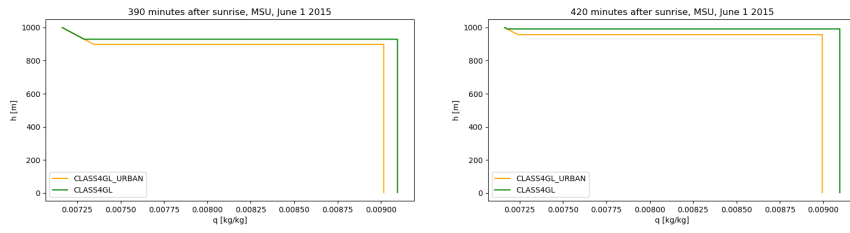


Figure H.8: Specific humidity height profiles 390min and 420min after sunrise on June 1, 2015 in MSU. These height profiles are obtained using CLASS4GL_URBAN (orange) and CLASS4GL (green).

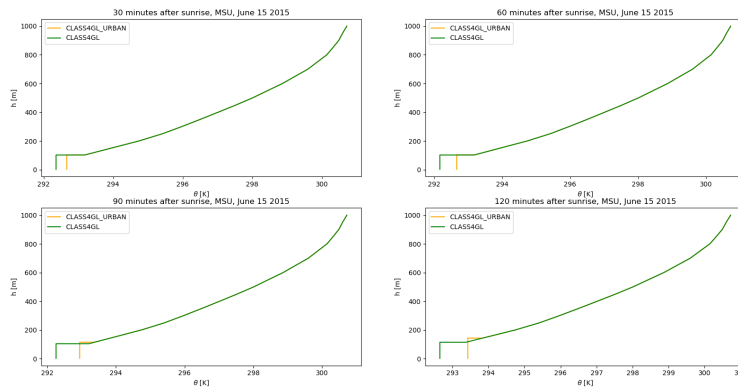


Figure H.9: Potential temperature height profiles 30min, 60min, 90min and 120 min after sunrise on June 15, 2015 in MSU. These height profiles are obtained using CLASS4GL_URBAN (orange) and CLASS4GL (green).

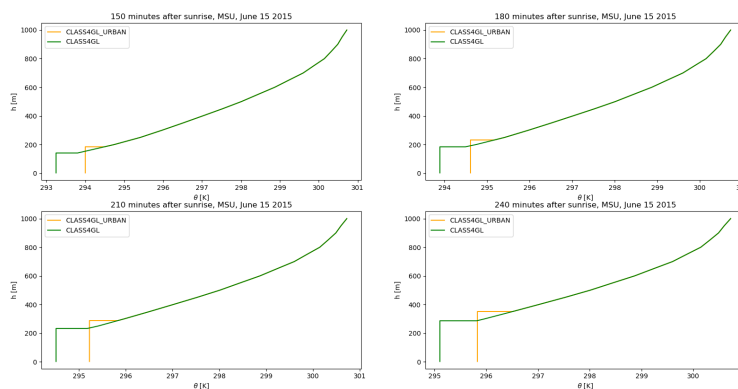


Figure H.10: Potential temperature height profiles 150min, 180min, 210min and 240 min after sunrise on June 15, 2015 in MSU. These height profiles are obtained using CLASS4GL_URBAN (orange) and CLASS4GL (green).

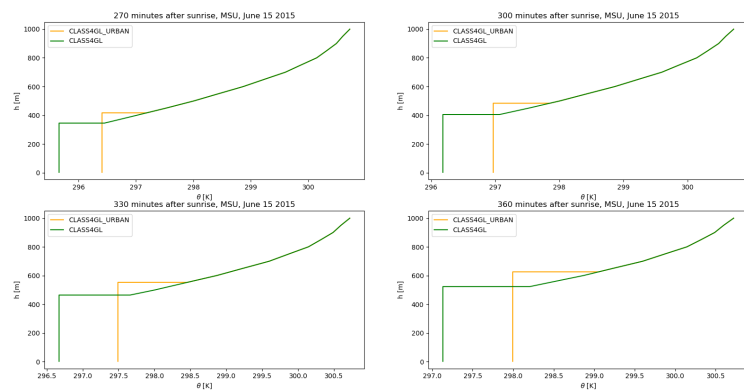


Figure H.11: Potential temperature height profiles 270min, 300min, 330min and 360 min after sunrise on June 15, 2015 in MSU. These height profiles are obtained using CLASS4GL_URBAN (orange) and CLASS4GL (green).

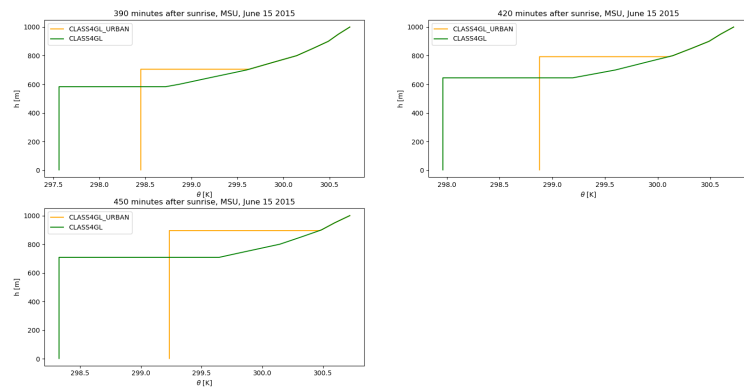


Figure H.12: Potential temperature height profiles 390min, 420min, 450min and 480min after sunrise on June 15, 2015 in MSU. These height profiles are obtained using CLASS4GL_URBAN (orange) and CLASS4GL (green).

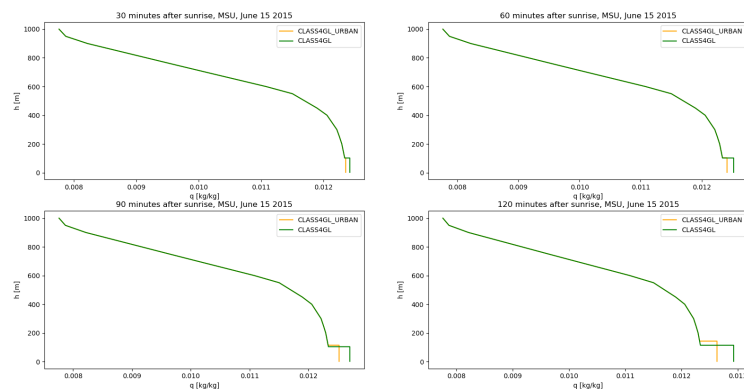


Figure H.13: Specific humidity height profiles 30min, 60min, 90min and 120 min after sunrise on June 15, 2015 in MSU. These height profiles are obtained using CLASS4GL_URBAN (orange) and CLASS4GL (green).

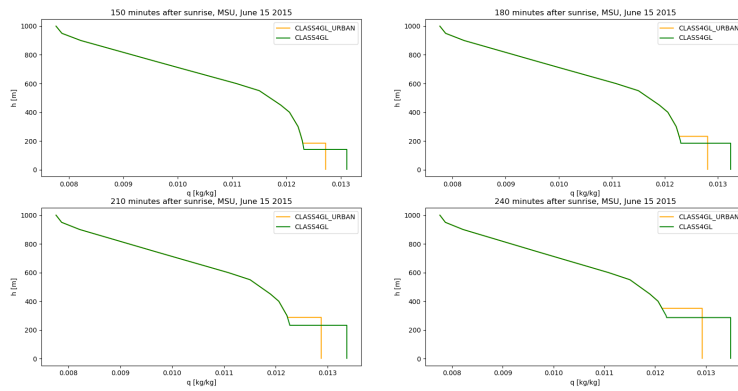


Figure H.14: Specific humidity height profiles 150min, 180min, 210min and 240 min after sunrise on June 15, 2015 in MSU. These height profiles are obtained using CLASS4GL_URBAN (orange) and CLASS4GL (green).

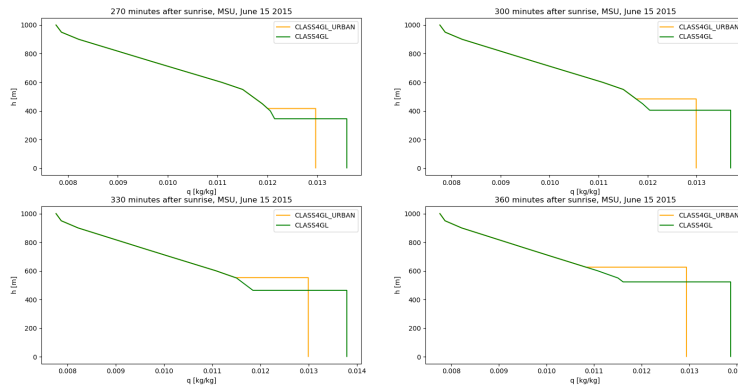


Figure H.15: Specific humidity height profiles 270min, 300min, 330min and 360 min after sunrise on June 15, 2015 in MSU. These height profiles are obtained using CLASS4GL_URBAN (orange) and CLASS4GL (green).

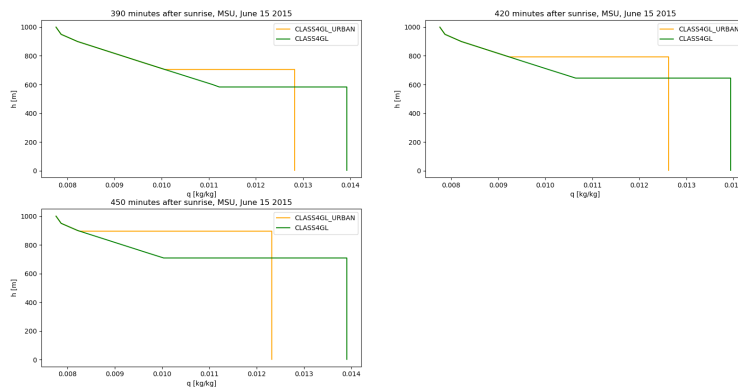


Figure H.16: Specific humidity height profiles 390min, 420min, 450min and 480min after sunrise on June 15, 2015 in MSU. These height profiles are obtained using CLASS4GL_URBAN (orange) and CLASS4GL (green).

APPENDIX I

PERTURBATION EXPERIMENT

USING BALLOON PROFILES OF

RJAZAN AS INITIALISATION

DATA

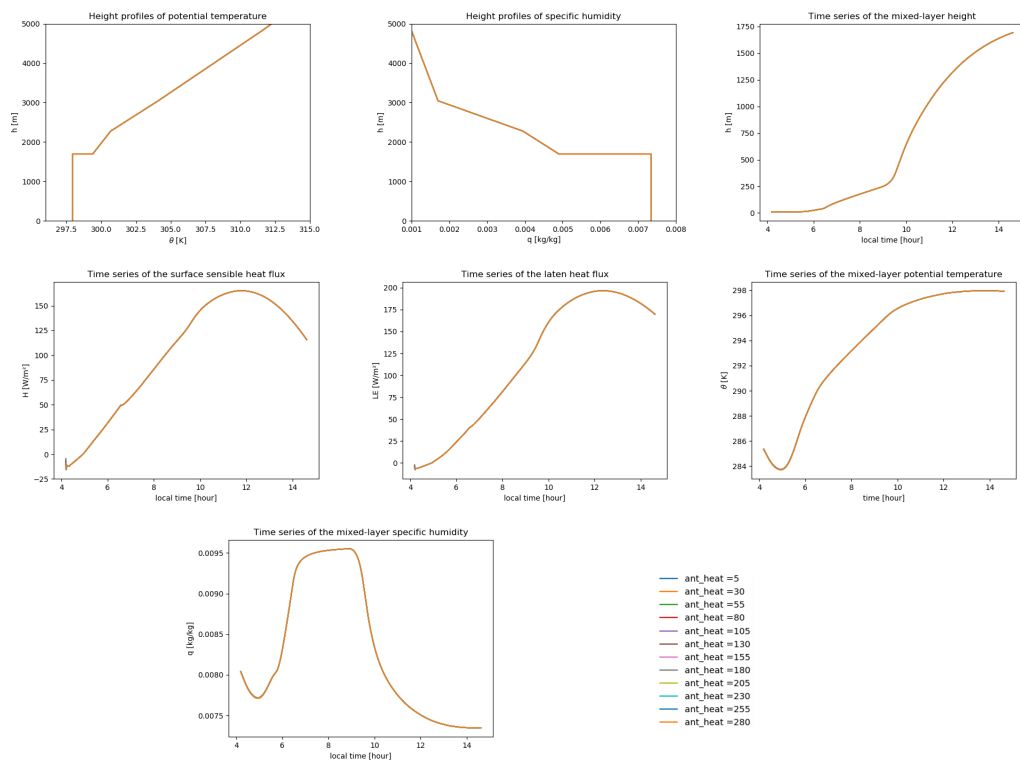


Figure I.1: The height profiles and the time series of several variables are given for simulations with different values of the anthropogenic heat flux ($Q_{anthheat}$). θ : potential temperature; q : specific humidity; h : height; H : sensible heat flux; LE : latent heat flux.

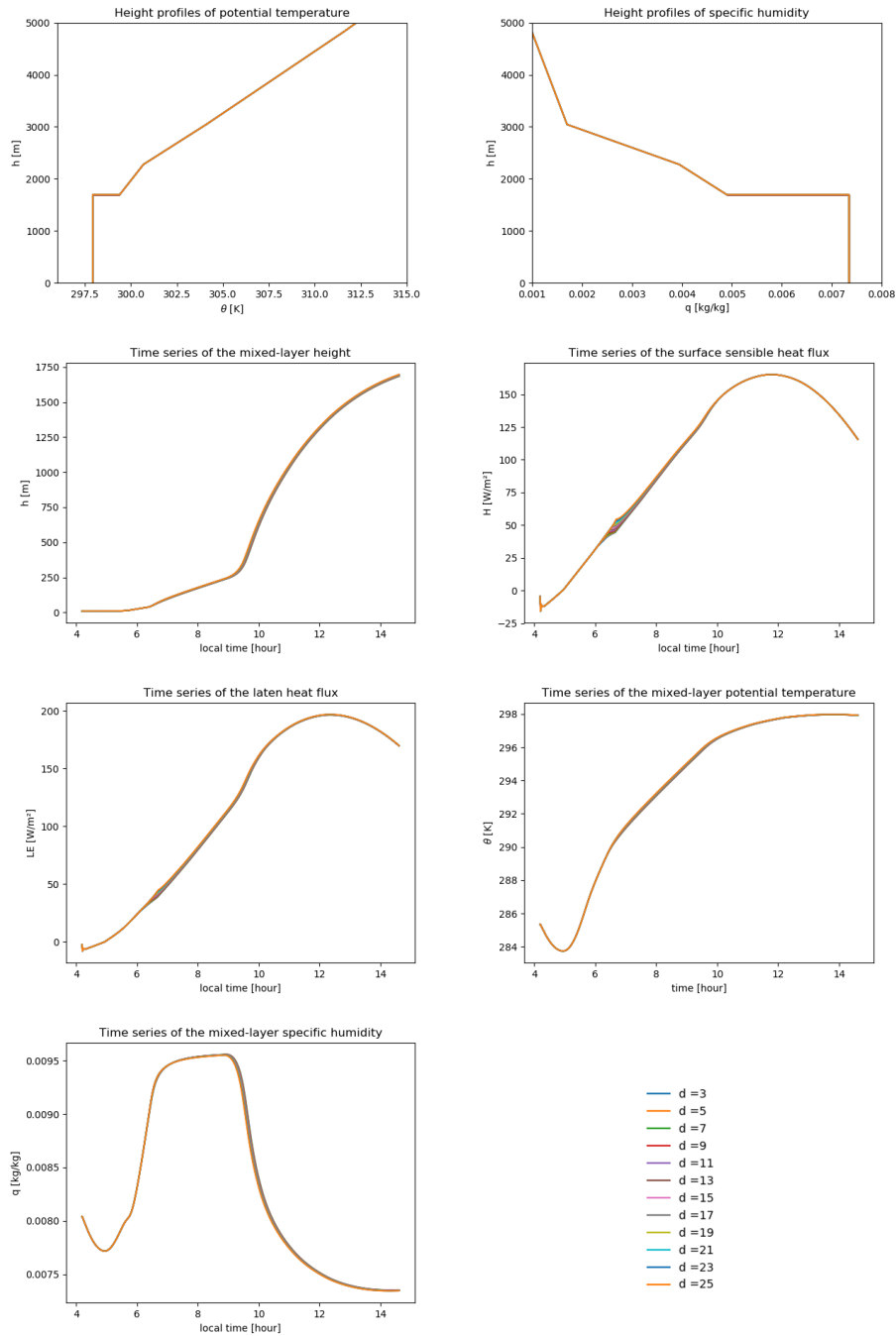


Figure I.2: The height profiles and the time series of several variables are given for simulations with different values of the roughness length (d). θ : potential temperature; q : specific humidity; h : height; H : sensible heat flux; LE : latent heat flux.

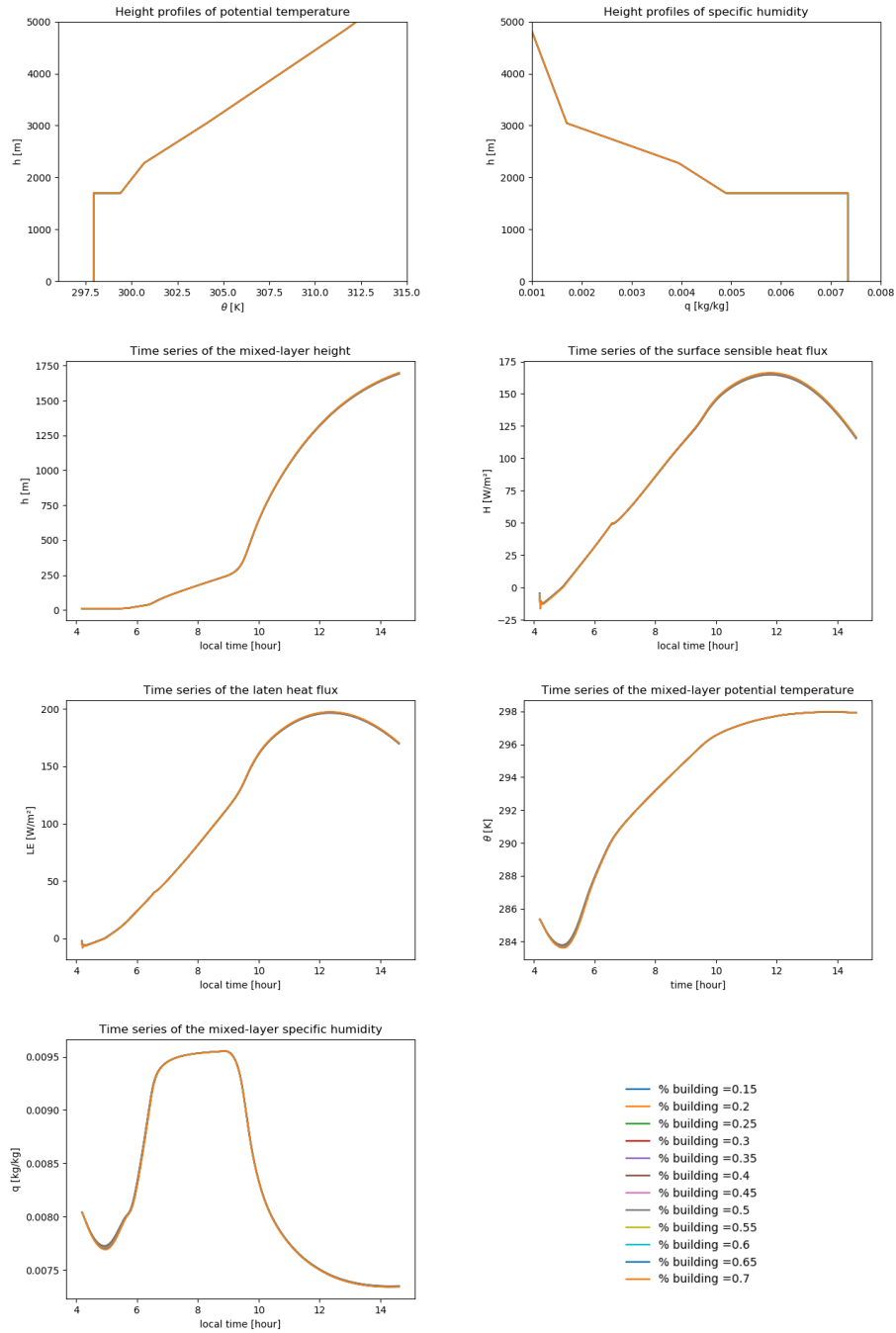


Figure I.3: The height profiles and the time series of several variables are given for simulations with different values of percentage covered by buildings (keeping the fraction of vegetation constant). θ : potential temperature; q : specific humidity; h : height; H : sensible heat flux; LE : latent heat flux.

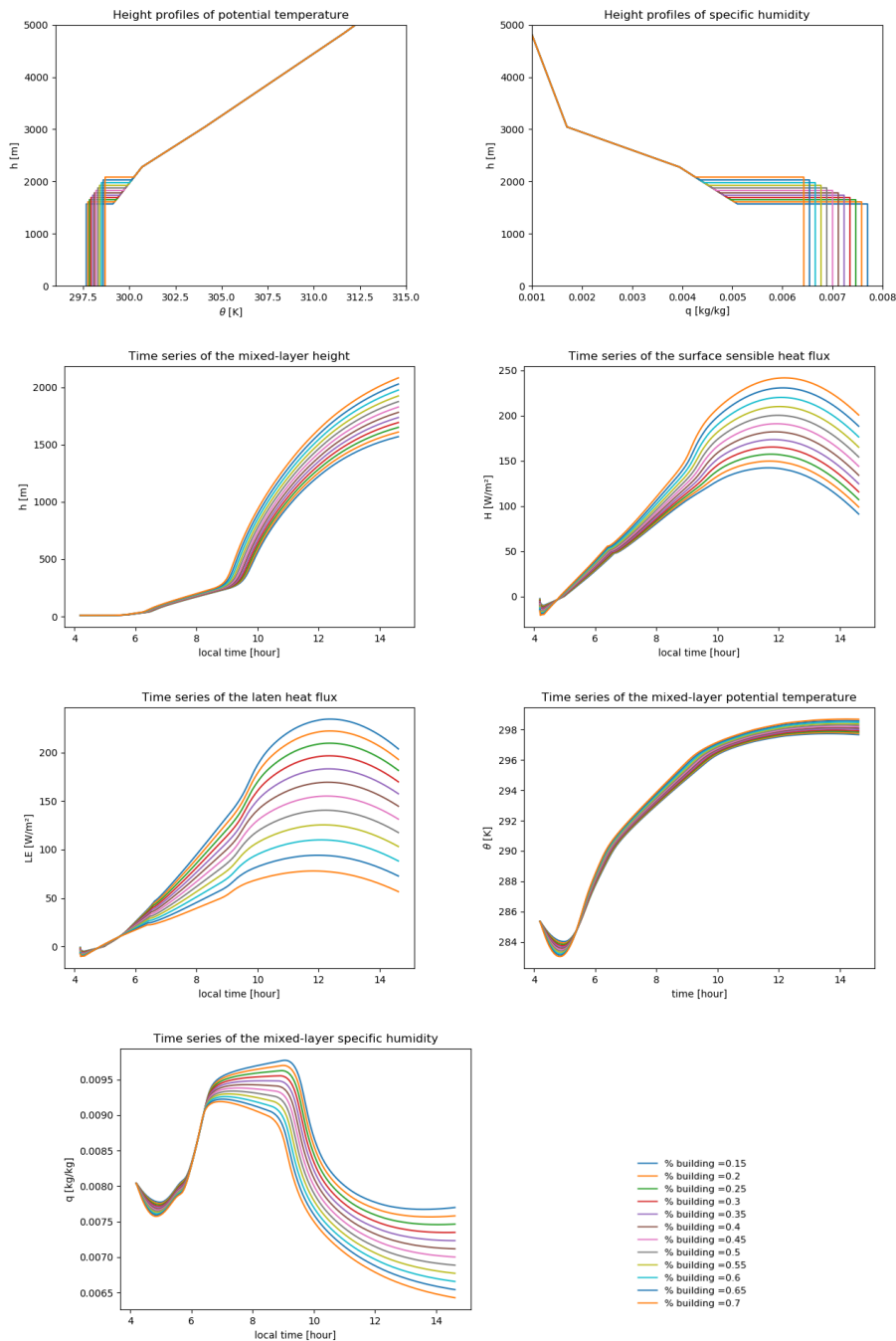


Figure I.4: The height profiles and the time series of several variables are given for simulations with different values of percentage covered by buildings (keeping the fraction of impervious surface constant). θ : potential temperature; q : specific humidity; h : height; H : sensible heat flux; LE : latent heat flux.

APPENDIX J

OTHER PERTURBATION

EXPERIMENTS USING

BIAS-CORRECTED MTP DATA ON

JUNE 15 2015 AS

INITIALISATION DATA

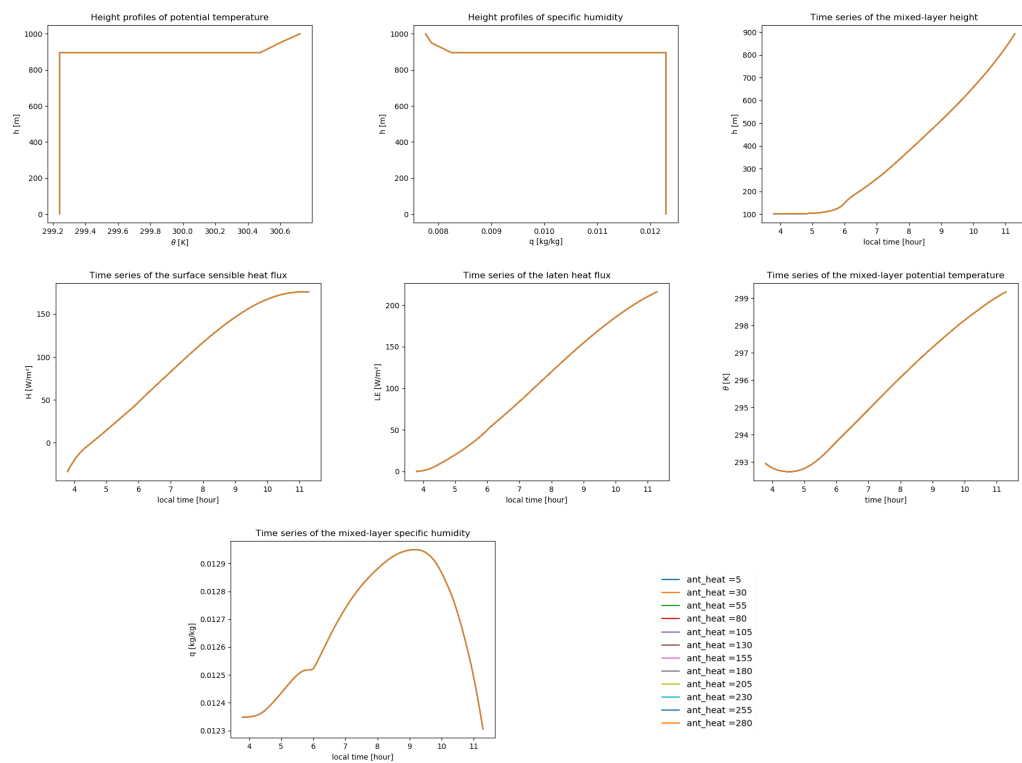


Figure J.1: The height profiles and the time series of several variables are given for simulations with different values of the anthropogenic heat flux ($Q_{anthheat}$). θ : potential temperature; q : specific humidity; h : height; H : sensible heat flux; LE : latent heat flux.

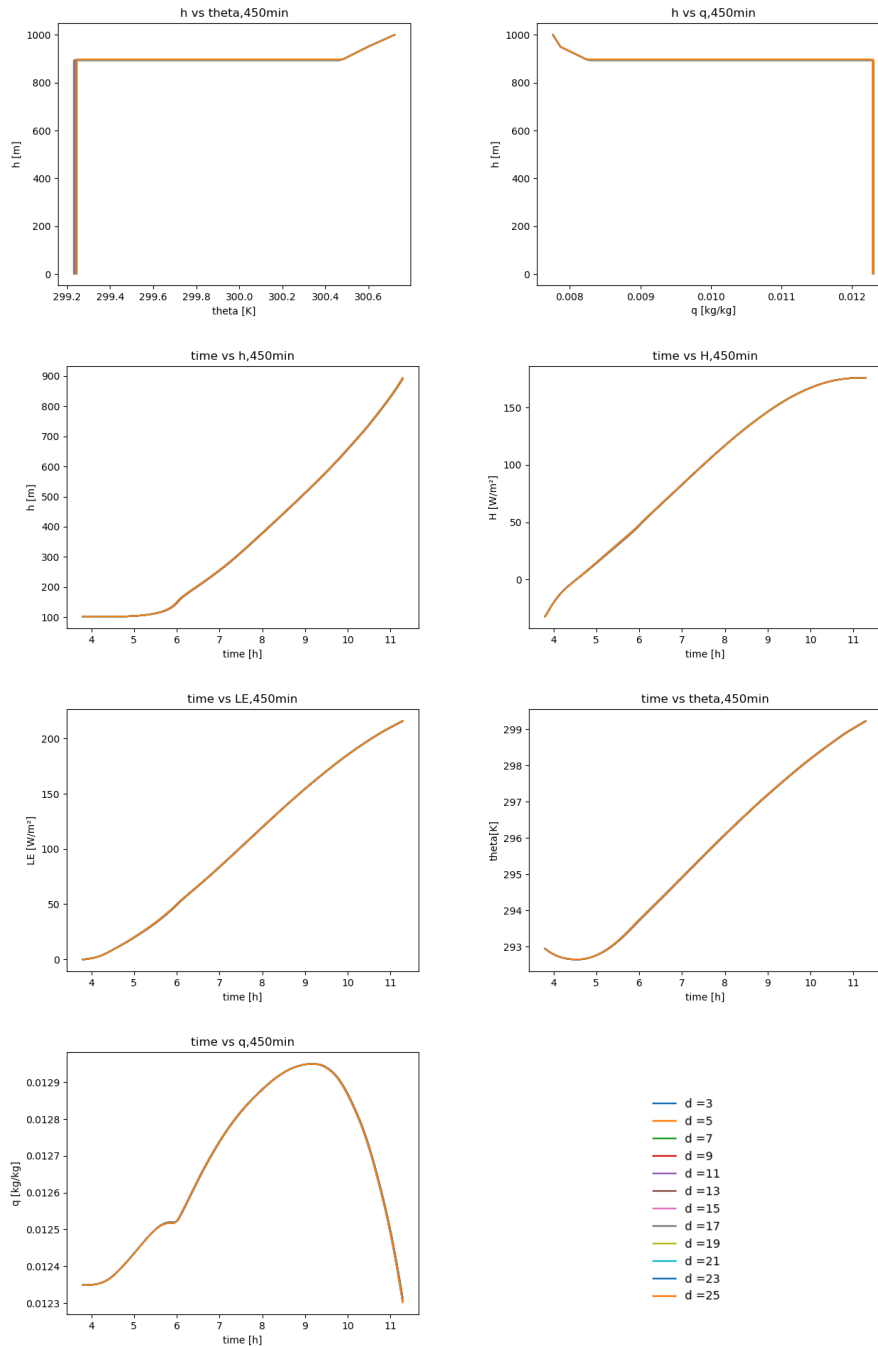


Figure J.2: The height profiles and the time series of several variables are given for simulations with different values of the roughness length (d). θ : potential temperature; q : specific humidity; h : height; H : sensible heat flux; LE : latent heat flux.

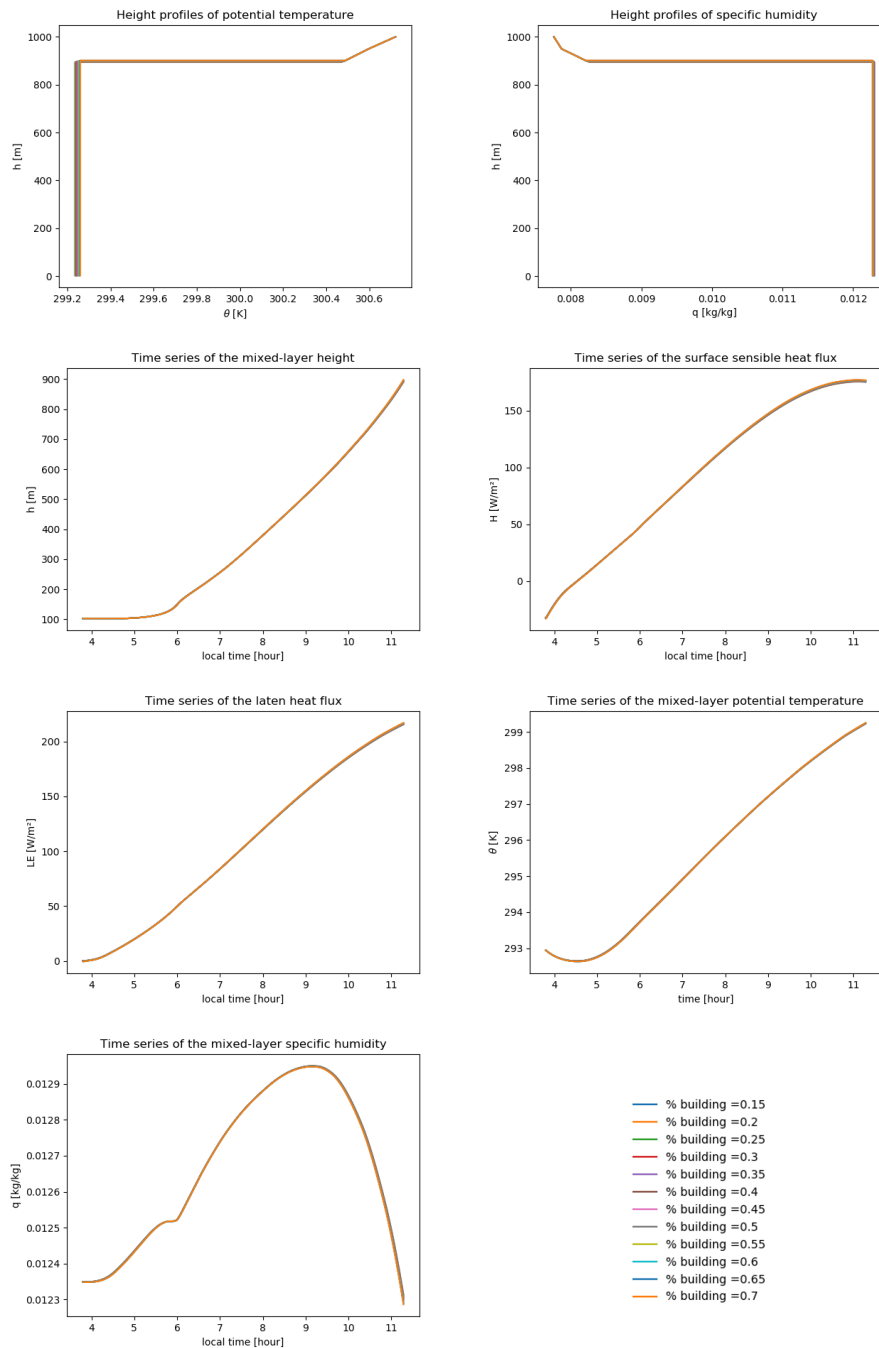


Figure J.3: The height profiles and the time series of several variables are given for simulations with different values of percentage covered by buildings (keeping the fraction of vegetation constant). θ : potential temperature; q : specific humidity; h : height; H : sensible heat flux; LE : latent heat flux.